Dynamics of coupled quantum systems

Ohanesjan, V.

Citation

Ohanesjan, V. (2024, February 7). *Dynamics of coupled quantum systems*. *Casimir PhD Series*. Retrieved from https://hdl.handle.net/1887/3716227

Dynamics of Coupled Quantum Systems

Proefschrift

ter verkrijging van
de graad van doctor aan de Universiteit Leiden,
op gezag van rector magnificus prof.dr.ir. H. Bijl,
volgens besluit van het college voor promoties
te verdedigen op woensdag 7 februari 2024
klokke 13:45 uur

door

Vladimir Ohanesjan
geboren te Prilep, Macedonië
in 1991

Promotor:	Prof.dr. K.E. Schalm
Copromotor:	Prof.dr. J. Zaanen
Promotiecommissie:	Dr. M. Schiró (Collège de France, Paris, France)
	Prof.dr. S. Vandoren (Universiteit Utrecht)
	Prof.dr. J. Aarts
	Prof.dr. A. Achúcarro
	Dr. V. Cheianov

Cover: Abstract impression of two interacting Sachdev-Ye-Kitaev systems, produced with AI assistance.

To my love, Renata.

Contents

1 | Introduction

1.1. Two roads to thermal equilibrium

Soon after the discovery of quantum mechanics, it was realized that the probability-preserving unitary evolution of the wave function clashed with the entropy production needed to explain thermalization. The straightforward resolution was to make the notion of an environmental heat bath, or more general any environment, a more principled one. So-called open quantum systems indeed thermalize beautifully though they sidestep many subtle issues intrinsic to quantum mechanics. Thermalization in these systems is not much different from Boltzmann's original fully classical picture of chaotic mixing due to microscopic collisions.[1]

This all changed rather abruptly with the numerical findings of Rigol, Dunjko, and Olshanii. Simulating the unitary time evolution of a finite number of bosonic quantum excitations, they surprisingly found that the density matrix of this system rapidly becomes nearly indistinguishable from a thermal density matrix [1]. Mathematically this could not be the exact thermal density matrix, but the difference was exponentially small. It turned out that this rapid near-indistinguishability of a unitarily evolved many-body density matrix from a thermal one was already predicted independently by Deutsch [2] and Srednicki [3], who coined it the *Eigenstate Thermalization Hypothesis* (ETH). In the simplest of terms, their result boils down to the sleight of hand that in a quantum system the system itself can act as a heat bath due to its parametrically larger Hilbert space.[2] Physically what ETH really emphasizes is that a specific quantum aspect — entanglement — does not only play an important role in thermalization but can actually *overpower* the semi-classical Boltzmann point of view.

This poses a deeper question. Given a dynamical many-body system, there are now two drastically different ways for this system to approach equilibrium.

---

[1]Recall that even in classical physics there is an inherent paradox between thermalization and Liouville's theorem that the volume of phase-space is preserved under classical Hamiltonian evolution. The extreme sensitivity to initial conditions inherent in chaotic systems resolves this paradox. In quantum systems, it is the connection with the heat-bath that allows an initially fully determined initial state to mix and be considered an ensemble average.

[2]A system of N particles has a $6N$-dimensional classical phase space, but a $\sim e^N$-dimensional quantum Hilbert space.

Though not so much voiced in the literature [4], this has triggered a consistently recurring debate on whether a system thermalizes classically (Boltzmann) or quantum-mechanically (ETH) and what determines this (see e.g. [5] for an attempt to unify the descriptions). Nearly non-interacting theories (dilute gases) clearly ought to be an example of the former. By contrast strongly interacting theories or more precisely densely entangled theories should exhibit ETH. But where is the boundary?

This is not only a philosophical question. Experiments on cold atoms have already passed the threshold of the number of constituents where ETH should apply and it has conclusively been seen [6, 7, 8, 9, 10, 11]. These same experiments have also provided a controlled avenue into non-equilibrium phenomena. Far-from-equilibrium physics is often cast aside in introductory physics. The intuition is that the extreme sensitivity to initial conditions in any rapid change makes it intractable, non-universal and therefore not interesting. Certainly, this last statement does not hold water: there is an enormous amount of interesting far-from-equilibrium physics (see e.g. [12]).

This thesis will explore these questions by studying the time evolution of quantum systems after a rapid change: a so-called quench, with focus on the early-time non-equilibrium behavior and the transition to late-time classical thermalization. With this method, we probed the differences in the early stage of thermalization between systems with a chaotic spectrum like the Mixed Field Ising, ones that additionally display exponential out-of-time-ordered correlation growth, as is the case with the Sachdev-Ye-Kitaev model, and quantum integrable systems. This deep dive into the early time evolution of those systems provided us with enlightening intuition that proved crucial for discerning between quantum and classical features that are intertwined during the evolution of a quantum system far from equilibrium. It also helped us solve the paradox of temperature rise in a hotter system when coupled to a colder bath, which was initially identified in [13] based on the energy increase of the hotter system. Interestingly enough, similar behavior shows up in other physical systems during the early stages of their thermalization. For example, it was reported in studies of evaporative black hole formation [14] which, on the gravity side, is explained by the averaged null energy condition [15] and in this thesis was related to the von Neumann and relative entropy of the quantum system, which paves a way for a future holographic connection in the same spirit as [16]. Another case in point is when the systems under consideration are charged, chaotic, and strongly entangled, e.g. charged SYKs whose energy and charge transport, on the road to thermalization, display features subtly related to the linear in T resistivity of strange metals [17, 18]. While it might seem unusual, it is in accord with other results that use SYK chains as toy models for studying high T_c superconductors [19, 20].

1.2. Quantum thermodynamics and quenches

The role of entanglement or strong quantum rather than classical correlations is more readily encoded in the density matrix of the quantum system than its wavefunction. Given a basis $|\alpha\rangle$ of states in the Hilbert space, a generic state $|\psi\rangle = c_\alpha |\alpha\rangle$ that is normalized $\sum_\alpha c_\alpha c_\alpha^\dagger = 1$ corresponds to the density matrix

$$\rho = |\psi\rangle\langle\psi| = \sum_{\alpha,\beta} c_\alpha c_\beta^\dagger |\alpha\rangle\langle\beta| \tag{1.1}$$

The density matrix can also describe an ensemble of quantum states which is the basis of quantum thermodynamics. For example, if the system can be found in the $i-$th vector state from the set $\{|\psi_i\rangle\}$ with a probability p_i, its state is given by the following density matrix:

$$\rho = \sum_i p_i |\psi_i\rangle\langle\psi_i| \tag{1.2}$$

As the density matrix consists of a bra and a ket, it can also be seen as an operator. From the Schrödinger equation we directly see that it evolves with time as

$$\rho(t) = \hat{U}_t \rho \hat{U}_t^\dagger \ , \quad \hat{U}_t = e^{-i\hat{H}t/\hbar} \tag{1.3}$$

The expectation value of an observable $\hat{O}$ is computed as a trace of the state times the observable:

$$O = \mathrm{Tr}\left(\rho\hat{O}\right). \tag{1.4}$$

Density matrices are positive operators with trace one ($\mathrm{Tr}(\rho) = \sum_i p_i = 1$), which asserts conservation of probability. As a positive operator, it has a spectral decomposition:

$$\rho = \sum_i \lambda_i |i\rangle\langle i|, \quad \langle i|i\rangle = 1, \quad \lambda_i \leq 1 \tag{1.5}$$

where the vectors $|i\rangle$ are ortho-normal, and λ_i are real, non-negative eigenvalues of ρ. The quantum systems that can be described by a single vector $|\psi\rangle \in \mathcal{H}$ with the equivalent density matrix representation $\rho = |\psi\rangle\langle\psi|$ are known as pure states. A system represented by an ensemble, i.e. a mixture of pure states $\rho = \sum_i p_i |\psi_i\rangle\langle\psi_i|$ is accordingly named a mixed state. For the density matrix of a pure state it holds that $\mathrm{Tr}\,\rho^2 = 1$, whereas a mixed state has $\mathrm{Tr}\,\rho^2 < 1$.

Another important difference between those two types of states is their von Neumann entropy:

$$S_{\mathrm{vN}} = -\,\mathrm{Tr}\left(\rho\ln\rho\right) = -\sum_i \lambda_i \ln \lambda_i, \tag{1.6}$$

where the last expression is obtained from the spectral decomposition of the density matrix. Now, combining (1.6) and (1.5) we immediately deduce that pure states ($\lambda = 1$) have vanishing von Neumann entropy, wheres for mixed states ($\lambda_i < 1$) S_{vN} is a positive quantity.

A quintessential mixed state is the density operator that describes a thermal quantum system at inverse temperature $\beta = 1/T$. Classical systems with constant temperature are described by the canonical ensemble, likewise, quantum thermal states are represented by an ensemble of the Hamiltonian's eigenstates $\{|n\rangle\}$ with probabilities $e^{-\beta E_n}/Z_\beta$:

$$\rho_\beta = \frac{1}{Z_\beta} \sum_n e^{-\beta E_n} |n\rangle\langle n| \equiv \frac{1}{Z_\beta} e^{-\beta \hat{H}}, \quad Z_\beta = \text{Tr}\left(e^{-\beta \hat{H}}\right). \tag{1.7}$$

Here, Z_β is the partition function and the free energy of the system is obtained through the well-known relation $F_\beta = -\frac{1}{\beta} \ln Z_\beta$. It is easy to check this is a mixed state, since $\text{Tr}\left(\rho_\beta^2\right) = \sum_n e^{-2\beta E_n}/Z_\beta^2 < 1$. It has von Neumann entropy:

$$S_\beta = -\frac{1}{Z_\beta} \sum_n e^{-\beta E_n} \ln\left(e^{-\beta E_n}/Z_\beta\right) = \beta \sum_n E_n e^{-\beta E_n} - \ln Z_\beta = \beta(E_\beta - F_\beta). \tag{1.8}$$

It is important to note that the von Neuman entropy of a Gibbs state at inverse temperature β is identical to the thermal entropy of a thermal system with internal energy equal to the energy of the state $E_\beta = \text{Tr}\left(\rho_\beta \hat{H}\right)$ and free energy F_β. This is the connection with classical thermodynamics.

Another quantity, important for the discussions in this thesis, is the relative entropy between two density matrices $\rho, \tilde{\rho} \in \mathcal{B}(\mathcal{H})$:

$$D\left(\rho||\tilde{\rho}\right) = \text{Tr}\,\rho\left(\ln \rho - \ln \tilde{\rho}\right) \geq 0. \tag{1.9}$$

which is often used in both quantum information processing [21] and quantum thermodynamics [22] to distinguish between two quantum states and as a measure of the irreversibility of a thermodynamic process [23]. In Chapter 2 and Chapter 3 we use the relative entropy as a measure of how different a certain state is from a corresponding thermal state with the same energy $D(\rho||\rho_\beta)$.

The full potential of the density matrix approach comes to light when studying composite quantum systems, as a descriptive tool for the subsystems. Imagine a system in a state ρ_{AB} that is composed of two subsystems A and B. If we are only interested in, or have access to, the subsystem A, we can study it through its reduced density matrix ρ_A, obtained by tracing out B:

$$\rho_A = \text{Tr}_B\left(\rho_{AB}\right) \tag{1.10}$$

Naturally, for two non-interacting systems the full density matrix is a tensor product state $\rho_{AB} = \rho_A \otimes \rho_B$, and the reduced density matrix is equal to the individual state (e.g. $\text{Tr}_B(\rho_{AB}) = \rho_A \, \text{Tr}_B(\rho_B) = \rho_A$), where we used that density operators are trace 1. In general, for interacting subsystems, the full state is not a tensor product and the reduced density matrix encodes information about the correlations between the two subsystems which are reflected in their von Neumann entropies (e.g. $S_A = -\text{Tr}(\rho_A \ln \rho_A)$). The simplest example is the entangled state between two quantum spins $|\psi\rangle = \frac{1}{\sqrt{2}}\left(|\uparrow\downarrow\rangle - |\downarrow\uparrow\rangle\right)$. Tracing over the second spin one finds that the reduced density matrix $\rho_A = \frac{1}{2}(|\uparrow\rangle\langle\uparrow| + |\downarrow\rangle\langle\downarrow|)$ has von Neumann entropy $S_{\rho_A} = \ln(2)$. This is why sometimes S_{vN} is called entanglement entropy. However, one has to be extremely careful with this nomenclature, for, as we've seen above, the von Neumann entropy also captures the thermal entropy of the system and there is no practical way of distinguishing those two contributions. Only at zero temperature, in the absence of the thermal contribution according to the third law of thermodynamics, is the von Neumann entropy proportional to the entanglement between the subsystems.

Such composite systems are the focus of this thesis. More precisely we consider situations where initially ($t < 0$) both subsystems A and B do not interact and are governed by their respective Hamiltonians $\hat{H}_A$ and $\hat{H}_B$. Additionally, we shall assume that each of them has fully been made to relax to independently to thermal equilibrium at temperature T_A and T_B, respectively, and the whole system is in a decoupled state $\rho_0 = \rho_{T_A} \otimes \rho_{T_B}$. Then, at time $t = 0$ we quench the system by instantaneously turning on an interaction between A and B, modeled with the Hamiltonian H_{int}, and for times ($t \geq 0$) the evolution of the combined system is governed with the following Hamiltonian:

$$\hat{H} = \hat{H}_A + \hat{H}_B + \hat{H}_{int} \tag{1.11}$$

Using concepts introduced in this section we study what happens to each subsystem after the quench. Analyzing the interplay between thermal fluxes, correlations, charged currents, and the exchange of information between A and B we strive to explain the post-quench non-equilibrium dynamics, the time-scale for the transition between quantum and conventional hydrodynamic behavior and propose experimental applications of the discovered quantum features.

1.3. Quantum Chaos "Quantum chaology"

In the introduction we pointed out the difference between the thermalization mechanisms in classical systems and quantum systems. Classical Boltzmannian thermalization relies on the assumption of chaos; thermalization in closed quantum systems on eigenstate thermalization. Nevertheless, some notion of mixing or information scrambling as it has been recently called, must also occur in quantum

systems. For quantum systems, there are two notions of chaos. One is defined by the early time evolution of quantum systems that display exponential growth of an observable known as out-of-time-correlator (OTOC) Section 1.3.1, analogously to exponentially divergent trajectories in classical phase space. The other definition is based on some of the Hamiltonian's spectral properties, and their relation to random matrices, as exposed in Section 1.3.2 which is significant for understanding the late-time evolution of quantum systems and especially their thermalization, in light of the Eigenstate Thermalization Hypothesis (ETH). The natural time-scale associated with the two viewpoints distinguishes them, but also provides a window on a unifying viewpoint [5]. We shall not pursue this question directly, but for this thesis it is useful to know the underlying thoughts concepts and concepts in more detail and we briefly review them here.

1.3.1. Exponential growth of OTOC

The defining feature of classically chaotic dynamics is the exponential sensitivity of the system on the initial conditions. Namely, an infinitesimal change in $\delta q^j(0)$ can result in exponentially diverging trajectories (1.12), known as the butterfly effect. For a Hamiltonian systems, where dynamics is encoded in Poisson brackets, this is defined by:

$$|\{q^i(t), p^j(0)\}_c| = \left|\frac{\partial q^i(t)}{\partial q^j(0)}\right| \approx \left|\frac{\delta q^i(t)}{\delta q^j(0)}\right| \sim e^{\lambda t} \tag{1.12}$$

The rate of exponential growth is determined by the Lyapunov coefficient λ, which is a property of the system. Going to quantum systems, this Poisson bracket can be generalized to a commutator to construct an observable $C(t)$ such that it captures the early time chaotic behavior from the correlations between two reasonably local Hermitian operators V and W, on which one has a free choice as long as they're not conserved charges and are simple [24].

$$C(t) = -\operatorname{Tr}\left(\rho^{1/2}[V(t), W(0)]\rho^{1/2}[V(t), W(0)]\right) =$$

$$= 2\operatorname{Tr}\left(V(t)\rho^{1/2}V(t)W\rho^{1/2}W\right) - \operatorname{OTOC}\left(t - \frac{i\beta}{4}\right) - \operatorname{OTOC}\left(t + \frac{i\beta}{4}\right) \tag{1.13a}$$

$$\operatorname{OTOC}(t) = \operatorname{Tr}\left(\rho^{1/4}V(t)\rho^{1/4}W\rho^{1/4}V(t)\rho^{1/2}W\right) \tag{1.13b}$$

Here ρ is the thermal density matrix of the system. To avoid confusion with quantum interference, one has squared the amplitude [24] and obtains an estimator of the effect an initial perturbation $W(0)$ has on a measurement of $V(t)$ at a time t. The choice of the particular regularization ($\rho^{1/4} = \left(e^{-\beta H}/Z\right)^{1/4}$) in the $OTOC(t)$ was initially proposed on the basis of hermiticity [25], and later

was proven to have an even more profound reasoning as it most closely reflects physical microscopic chaos [26]. In systems with a small parameter $\epsilon \ll 1$, the communtator-squared $C(t) \sim \epsilon^2 e^{2\lambda t}$ will have exponential growth in time with an exponent λ, which is usually used as an indication of chaotic behavior. In known systems $\epsilon = \hbar$ or $\epsilon = 1/N$ with N the number of (field theory) degrees of freedom. Different from classical physics, this exponential growth continues up until the scrambling time $t_* \sim \beta \log 1/\epsilon$, It was shown in [25] that, under some physically motivated assumptions, the rate at which a given system can scramble information is bounded from above:

$$\lambda \leq \frac{2\pi k_B}{\hbar \beta}. \tag{1.14}$$

Systems that saturate this bound are known as "fast scramblers" and the Sachdev-Ye-Kitaev model, which we shall review shortly, is one of them and is the main protagonist of this thesis.

1.3.2. Spectral Chaos

The other definition of quantum chaos is inspired by similarities between the spectral properties of Random Matrices (RM) and certain Hamiltonians. We know that for large classical systems the exact knowledge of the position and momentum of each degree of freedom, even if theoretically possible, is practically intractable so we study those systems using statistical mechanics. Similarly, for quantum systems, where the Hilbert space scales exponentially with the degrees of freedom, the exact determination of each eigenstate and corresponding eigenvalue is unfeasible, and of limited usefulness, hence one studies their statistical properties. The origins of this idea are in Wigner's research on large nuclei, and then it advanced into one of the most useful approaches in understanding many-body quantum systems. This development was substantiated by the fact that in the middle of the spectrum, spectral properties (e.g. nearest neighbor spacing, spectral form factor) of many-body Hamiltonians effectively resemble those of random matrices. To better understand this line of reasoning, we introduce some relevant concepts of Random Matrix Theory (RMT) [27, 28, 4] and will comment on how they relate to chaotic quantum systems.

We are interested in square $N \times N$ matrices $\mathcal{H}$ drawn from a probability distribution function $P(\mathcal{H})$. Broadly speaking, there are three different Gaussian ensembles based on the invariance properties of the probability (1.15a). One of them is the Gaussian Orthogonal Ensemble (GOE), named due to its invariance under orthogonal transformation, which samples real matrices and is used for modeling Hamiltonians with time-reversal symmetry. Next is the Gaussian Unitary Ensemble (GUE) which samples Hermitian matrices that can represent a generic Hamiltonian without time reversal or rotational symmetry. The third class is the

Gaussian symplectic ensemble (GSE) which is useful for studying Hamiltonians with time-reversal symmetry but broken rotational symmetry. Each of the Gaussian ensembles (1.15b) is denoted by their Dyson index $\beta = 1$, $\beta = 2$, and $\beta = 4$ respectively [29, 30, 31], which counts the number of real degrees of freedom per matrix element.

$$P(\mathcal{H})d\mathcal{H} = P(\mathcal{H}')d\mathcal{H}' \quad ; \quad \mathcal{H}' = \mathcal{W}^{-1}\mathcal{H}\mathcal{W} \tag{1.15a}$$

$$P_\beta(\mathcal{H}) = \frac{1}{Z_\beta}\exp\left\{-\beta\frac{N}{4}\operatorname{Tr}\mathcal{H}^2\right\} \tag{1.15b}$$

Where Z_β is an ensemble-dependent normalization constant. Using the Gaussian PDFs (1.15b) one can derive the joint probability distribution of the eigenvalues $\{\lambda\} = \{\lambda_1, \lambda_2 \dots \lambda_N\}$:

$$P_\beta(\{\lambda\}) = \frac{1}{Z_\beta}\exp\left\{-\beta\frac{N}{4}\sum_i \lambda_i^2 + \beta\sum_{i<j}\log\left|\lambda_i - \lambda_j\right|\right\}, \tag{1.16}$$

which is a useful object for studying their spectral properties. We note here that the logarithmic term acts as a repulsive potential between two eigenstates, effectively preventing coincident eigenstates which is the mathematical explanation behind the famous level repulsion in quantum mechanics. Integrating (1.16) over all but one eigenvalue the density of states can be derived [27], which in the limit $N \to \infty$ simplifies to the Wigner semicircle distribution:

$$\rho(\lambda) = \lim_{N\to\infty}\int P(\lambda, \lambda_2, \dots \lambda_N)\prod_{i=2}^N d\lambda_i = \begin{cases} \frac{1}{\pi}\sqrt{1-\lambda^2} & |\lambda| \le 1 \\ 0 & |\lambda| > 1 \end{cases}. \tag{1.17}$$

Another important spectral property is the distribution of the normalized level spacing between two adjacent eigenstates $s = (\lambda_n - \lambda_{n-1})/\langle s\rangle$, where $\langle s\rangle = \langle\lambda_n - \lambda_{n-1}\rangle$. In the limit $N \to \infty$ its probability distribution — first surmised by Wigner — can be analytically computed [32].

$$P_\beta(s) = \begin{cases} \dfrac{\pi}{2}se^{-\frac{s^2\pi}{4}} & \beta = 1 \\[2mm] \dfrac{32}{\pi^2}s^2e^{-\frac{s^2 4}{\pi}} & \beta = 2 \\[2mm] \dfrac{2^{18}}{3^6\pi^3}s^4e^{-\frac{s^2 64}{9\pi}} & \beta = 4 \end{cases} \tag{1.18}$$

The turnover between the polynomial rise at low s and the exponential decay at large s shows the level repulsion between states whose eigenvalues are closer together than the average.

As mentioned before, large nuclei were the initial testing ground for the RMT applicability of to quantum many-body systems, however, the connection between random matrix theory and quantum chaos was made by Bohigas, Giannoni and Schmidt [33]. Studying the spectrum of a quantum particle in a Sinai billiard potential, they discovered that in the semi-classical limit, the nearest neighbor statistics match the GOE ($\beta = 1$) Wigner surmise . This observation led them to conjecture that this is more general: the nearest neighbor statistics of quantum systems with a classically chaotic counterpart can be described with RMT. Afterward, this conjecture has also been used the other way around, namely as a diagnosis of quantum chaos even for systems that don't have good classical analogs, like quantum chains, and lattice fermions [34, 35]. The corollary of this conjecture was made by Berry and Tabor, who observed that in quantum systems that are non-chaotic in the classical limit the statistic of s exhibits Poisson statistics instead of Wigner-Dyson statistics [36]. [3]

It is this connection between chaos and RMT that underlies the novel quantum mechanism of eigenstate thermalization. When talking about quantum thermalization, we specifically refer to the thermalization of observables. More precisely, if we prepare a system, with a Hamiltonian $\hat{H}$, in a nonstationary state $|\psi\rangle$, with well-defined mean energy $\langle\psi|\hat{H}|\psi\rangle = E$, an observable $\hat{O} = \sum_i O_i |i\rangle\langle i|$ thermalizes if, under the time evolution of the system, it relaxes to the microcanonical expectation value:

$$\lim_{t\to\infty} \langle\psi(t)|\hat{O}|\psi(t)\rangle = \sum_{n\in\{E-\Delta E, E+\Delta E\}} \langle n|\hat{O}|n\rangle = \langle\hat{O}\rangle_{\text{microcan.},E}, \qquad (1.19)$$

and remains close to it, meaning temporal fluctuations around the microcanonical value are negligible. If the quantum system is isolated and evolves unitarily with Hamiltonian $\hat{H}$, the puzzle is how to square this expectation with the exact expression in terms of energy eigenstates $|\psi(0)\rangle = \sum_n c_n |n\rangle$.

$$\langle\psi(t)|\hat{O}|\psi(t)\rangle = \sum_n |c_n|^2 O_{nn} + \sum_{n\neq m} c_m^* c_n e^{i(E_m-E_n)t} O_{mn} \qquad (1.20)$$

For an arbitrary quantum system, there is no real reason to expect the second term to be small. If the Hamiltonian is a random matrix, however, its eigenstates are practically random orthogonal vectors in any arbitrary basis ($\overline{\langle m|i\rangle\langle j|n\rangle} = \delta_{mn}\delta_{ij}1/d$) [38], where the overline denotes averaging over the random eigenstates $|n\rangle$ and $|m\rangle$, and d is the dimension of the Hilbert space. In this case, the off-

---

[3]Neither the Bohigas-Gianonni-Schmidt nor the Berry-Tabor conjecture are strictly true. Counterexamples are known to both, see the previous sentence and [37, 4].

diagonal terms disappear $\overline{O_{mn}} = 0$, the diagonal ones are state-independent:

$$\overline{O_{nn}} = \sum_i O_i \overline{\langle n|i \rangle \langle i|n \rangle} = \frac{1}{d} \sum_i O_i \equiv \overline{O}, \tag{1.21}$$

$$\overline{O_{nn}^2} = \sum_{ij} O_i O_j \langle i|j \rangle \overline{\langle n|i \rangle \langle j|n \rangle} = \sum_i O_i^2 \overline{\langle n|i \rangle \langle i|n \rangle} = \frac{1}{d} \sum_i O_i^2 \equiv \overline{O^2}, \tag{1.22}$$

and each of the fluctuations is suppressed by the dimension of the Hilbert space [4]. From those results, one can deduce the form of the matrix elements in the basis of a random Hamiltonian, to a leading order in $1/d$, and such that they not only capture the average value but the fluctuations too:

$$O_{mn}^{\text{RMT}} \approx \bar{O} \delta_{mn} + \sqrt{\frac{\overline{O^2}}{d}} R_{mn}. \tag{1.23}$$

More precisely, the fluctuations are encoded in the second term where R_{mn} is a zero mean and unit variance random variable that depends on the ensemble of the random matrix.

The natural suppression of the variance in an RMT inspired the idea that the evolution of an isolated quantum system can mimic thermalization. Of course, in real systems, we know that the Hamiltonian has more structure compared to a random matrix, hence the diagonal and off-diagonal elements have to contain information on the energy of the system and the relaxation time. The generalization of RMT, needed to describe real physical systems, was suggested by Deutsch [2] and Srednicki [3] and is known as the Eigenstate Thermalization Hypothesis (ETH):

$$O_{mn} = O(\overline{E}) \delta_{mn} + e^{-\frac{S(\overline{E})}{2}} f_O(\overline{E}, \omega) R_{mn} . \tag{1.24}$$

Here $\overline{E} = (E_m + E_n)/2$ and $\omega = E_n - E_m$ are the average energy and energy difference between the two energy levels, $S(E)$ is the thermodynamic entropy and R_{mn} a random number, same as before. The important difference with RMT is that the diagonal term in ETH is equal to the expectation value in the microcanonical ensemble at energy $\overline{E}$, the entropy $S(E)$ also has the appropriate energy dependence and is not just the dimension of the Hilbert space, and a final important requirement is that $O(\overline{E})$ and $f_O(\overline{E}, \omega)$ are smooth functions of their arguments.

Due to the exponential growth of the Hilbert space with the number of degrees of freedom, many quantum systems in isolation have a regime where they exhibit ETH as the physics of their very large N-body Hamiltonian becomes closer and closer to a random one [4]. This mathematical exponential growth is the reflection of the physically new quantum feature of entanglement. In these settings the

scrambling and information loss driving thermalization is therefore of a physically different origin than classical chaos, even though in the abstract it still resides in the impracticality of tracing every bit of information with infinite precision.

1.4. Theoretical Models

We present a brief overview of the theoretical models studied in this thesis. One of the main models we shall use in this thesis to study the dynamics of relaxation and thermalization in an isolated quantum system is the Sachdev Ye Kitaev model (SYK) [39, 40]. This is a strongly interacting quantum mechanical system of N Majorana fermions with all-to-all random couplings. which is exactly solvable in the IR limit when $N \to \infty$. The strongly coupled IR fixed point has an emergent reparametrization symmetry where the effective dynamic is described by the Schwarzian action. The SYK model can be argued to be the ideal (solvable) representative of many-body quantum systems. It displays maximally chaotic behavior, as defined in Section 1.3.1, with an exponentially growing OTOC and a Lyapunov coefficient that, in the deep IR, saturates the bound (1.14), but at its heart it also obeys ETH [41]. These properties are precisely what makes the SYK an interesting playground for studying quantum chaos, quantum gravity and information scrambling. Moreover, as we will briefly describe for completeness in Section 1.5, these properties are also typical for 2D dilaton gravities which describe the near horizon physics of extremal black hole [42, 43, 44]. And a version of SYK built on charged Dirac fermions instead of Majoranas [45, 46, 47] has proved to be a useful toy model for studying strange metals and high-temperature superconductivity [19, 48].

The other model we shall study is the Transverse Field Ising model (TI), which is a set of Pauli matrices on a 1D chain, a well-known model in the study of quantum thermalization [49, 50]. On one hand, it is also solvable: using the Jordan-Wigner (1.46) and Bogoliubov (1.51) transformations can be shown it is equivalent to free fermions (1.52) (Section 1.4.2). On the other hand, it is representative of systems with a second-order quantum phase transition. The quantum phase transition occurs for an infinite chain at zero temperature $T = 0$ when the transverse magnetic field equals the hopping strength $h_x = J$. At this quantum critical point, the system becomes strongly entangled and it has distinct dynamics even at finite temperatures and finite system sizes.

The last considered model is a generalization of the TI known as the Mixed Field Ising (MFI) Section (1.4.3), a fruitful playground for, among others, studying quantum thermalization, quantum chaos and information scrambling [51, 52, 53, 54]. Its usefulness comes from the ability, simply by tuning its parameters, to describe different phenomena which range from quantum criticality, through a phase with quantum chaotic level statistics, all the way to a classical Ising model.

This will prove very useful in understanding possible differences between classical and quantum thermalization in Chapter 3.

1.4.1. SYK

The Sachdev-Ye-Kitaev model (SYK) is a quantum mechanical model of N all-to-all interacting fermions with random independent couplings drawn from a Gaussian distribution with zero mean and standard deviation. The latter sets the energy scale of the model. There are two main types of SYK models, based on the type of fermions. One is the Majorana SYK (mSYK), where the fermions are Majorana fields $\{\psi_i, \psi_j\} = \delta_{ij}$, which is usually used for studying fast scramblers, quantum chaos, and black holes through its duality with 2D dilaton gravity. As we shall see, it is the model where energy dynamics alone dominates. The other type is the complex SYK (cSYK) whose constituents are charged Dirac fermions $\{c_i^\dagger, c_j\} = \delta_{ij}$. This type of model includes a conserved $U(1)$-current naturally used for studying phenomena in strongly correlated electron systems. The usefulness of either type of SYK model lies in the formal solvability of its Schwinger-Dyson equations —i.e. the full quantum evolution equations — in the large N-limit. Here we briefly review the derivation of these Schwinger-Dyson equations and its solution for the mSYK, directly from the disorder-averaged partition function. The same result can be obtained by diagrammatic expansion, for which we refer the reader to [55, 56].

We start from the path integral representation of SYK partition function [57]:

$$Z_m = \int \mathcal{D}[\psi] \exp\left\{ i \int dt \left(\frac{i}{2} \sum_j \psi_j \partial_t \psi_j + \sum_{j_1,j_2,j_3,j_4=1}^{N} J_{j_1 j_2 j_3 j_4} \psi_{j_1} \psi_{j_2} \psi_{j_3} \psi_{j_4} \right) \right\},$$

$$\tag{1.25}$$

A key part of the SYK model is that the couplings are independent random variables drawn from a Gaussian distribution (1.26) :

$$P(J) = \frac{1}{\sigma_J \sqrt{2\pi}} \exp\left\{ -\frac{1}{2\sigma_J^2} \sum_{j_1 < j_2 \cdots < j_4} J_{j_1 j_2 j_3 j_4}^2 \right\} \quad ; \quad \sigma_J = \frac{3! J^2}{N^3}, \tag{1.26a}$$

$$\langle J_{j_1 j_2 j_3 j_4} \rangle_J \equiv \int \mathcal{D}J \, J_{j_1 j_2 j_3 j_4} P(J) = 0 \quad ; \quad \langle J_{j_1 j_2 j_3 j_4} J_{j_1' j_2' j_3' j_4'} \rangle_J = \sigma^2 \delta_{j_1 j_1'} \delta_{j_2 j_2'} \delta_{j_3 j_3'} \delta_{j_4 j_4'},$$

$$\tag{1.26b}$$

The physical observables are defined to be the ones that follow after averaging over the ensemble of different couplings (quenched disorder) Formally this has to be done through the replica trick, but for replica diagonal solutions which are the

ones of interest[4], one can just naively include the averaging in the path-integral directly

$$\langle Z_m \rangle_{\text{SYK}} = \int \mathcal{D}J P(J) \int \mathcal{D}[\psi] \exp\left\{ i \int dt S_m \right\} \tag{1.27}$$

$$= K' \int \mathcal{D}[\psi] \exp\left\{ i \int dt \left(\frac{i}{2} \sum_j \psi_j \partial_t \psi_j + \right. \right. \tag{1.28}$$

$$\left. \left. + i\frac{\sigma_J^2}{2 \cdot 4!} \int dt \int dt' \sum_{j_1,j_2,j_3,j_4=1}^N \psi_{j_1} \psi'_{j_1} \psi_{j_2} \psi'_{j_2} \psi_{j_3} \psi'_{j_3} \psi_{j_4} \psi'_{j_4} \right) \right\} \tag{1.29}$$

where $\psi' \equiv \psi(t')$. One introduces the bilinear field

$$\tilde{G}(t,t') = -\frac{i}{N} \sum_i^N \psi_i(t)\psi_i(t') \tag{1.30}$$

through a Lagrange multiplier $\Sigma(t,t')$ (1.32), that imposes this identity

$$1 = \int \mathcal{D}\tilde{G} \int \mathcal{D}\tilde{\Sigma} \exp\left\{ i^2 \frac{N}{2} \int dt \int dt' \tilde{\Sigma}(t,t') \left(\tilde{G}(t',t) + \frac{i}{N} \sum_i^N \psi_i(t')\psi_i(t) \right) \right\} \tag{1.31}$$

Inserting this identity into the path integral and after integrating out the Majorana fields, one can write the dynamics of the model in terms of the bilinear fields:

$$\langle Z_m \rangle_{\text{SYK}} = \int \mathcal{D}\tilde{G} \int \mathcal{D}\tilde{\Sigma} \exp\left\{ -\frac{N}{2} \left[-\text{Tr}\log\left(-i(i\partial_t \delta_{tt'} - \tilde{\Sigma}(t,t')) \right) + \right. \right. \tag{1.32}$$

$$\left. \left. + \int dt \int dt' \left(\tilde{\Sigma}(t,t') + \frac{J^2}{4}\tilde{G}^3(t',t) \right) \tilde{G}(t',t) \right] \right\}. \tag{1.33}$$

Upon using the redefinition $\sigma_J^2 = 3!J^2/N^3$, we notice that in the limit $N \gg 1$, $1/N$ is a small parameter, analogously to $\hbar$, and the path integral is dominated by the saddle point solution. This can be obtained by varying the action with respect to $\tilde{G}$ and $\tilde{\Sigma}$:

$$\frac{\delta S[\tilde{G}, \tilde{\Sigma}]}{\delta \tilde{\Sigma}(t,t')} = 0 \quad \Rightarrow \quad \Sigma(t,t') = i\partial_t \delta_{tt'} - G^{-1}(t,t') \tag{1.34a}$$

$$\frac{\delta S[\tilde{G}, \tilde{\Sigma}]}{\delta \tilde{G}(t',t)} = 0 \quad \Rightarrow \quad \Sigma(t,t') = -\frac{\sigma_J^2 N^3}{3!} G^3(t',t) \tag{1.34b}$$

---

[4]See [58, 59] for a discussion of replica symmetry breaking in SYK models.

We adopted the notation from [55] where the tilded expressions $\tilde{G}$ and $\tilde{\Sigma}$ label the dynamic fields whereas G, Σ without tildes are the classical solutions of the Schwinger-Dyson equations (1.34) These Schwinger-Dyson equations — or when computed on the doubled time Schwinger-Keldysh contour the Kadanoff-Baym equations, can be solved numerically to study non-equilibrium dynamics in an SYK system [57] as we shall do in Chapter 5. The equilibrium properties, however, can be solved analytically at low temperatures, which are where the power of the SYK model lies. Wick rotating the SD equations to periodic Euclidean time $t = -i\tau = -i(\tau + \beta)$, the first term on the RHS of (1.34a) can be neglected at low temperatures $\beta J \gg 1$ equivalent to the strong coupling regime. This leads to an emergent time reparametrization symmetry $\tau \to f(\tau), \partial_\tau f(\tau) > 0$:

$$G(\tau, \tau') \to [\partial_\tau f(\tau) \partial'_\tau f(\tau')]^\Delta G(f(\tau), f(\tau')), \tag{1.35a}$$

$$\Sigma(\tau, \tau') \to [\partial_\tau f(\tau) \partial'_\tau f(\tau')]^{3\Delta} \Sigma(f(\tau), f(\tau')). \tag{1.35b}$$

This indicates that in the deep IR the fermions develop an anomalous conformal dimension $\Delta = \frac{1}{4}$ which yields a scaling solution at zero temperature $\beta \to \infty$:

$$G_c(\tau) = \frac{1}{(4\pi)^{1/4}} \frac{\text{sgn}(\tau)}{|J\tau|^{2\Delta}}. \tag{1.36}$$

The conformal propagator at inverse temperature β can be promptly obtained from the reparametrization $\tau \to \tan \frac{\pi \tau}{\beta}$ and the symmetry transformation (1.35a):

$$G_c^\beta(\tau) = \frac{\pi^{1/4}}{\sqrt{2\beta J}} \frac{\text{sgn}\left(\sin \frac{\pi \tau}{\beta}\right)}{|\sin \frac{\pi \tau}{\beta}|^{2\Delta}}, \quad \tau \in \left[-\beta/2, \beta/2\right) \tag{1.37}$$

It is important to note here that these solutions spontaneously break the emergent reparametrization symmetry (1.35a) down to the $SL(2, \mathbb{R})$ group. This is because the scaling solutions (1.37), are invariant only under the reparametrization $\tau \to \frac{a\tau + b}{c\tau + d}$ where $ad - bc = 1$. Additionally, the full reparametrization symmetry is also explicitly broken by $i\partial_\tau \delta_{\tau, \tau'}$, which cannot be neglected once we move away from the deep IR. For this reason, the reparametrization modes are pseudo-Nambu-Goldstone bosons (also known as "soft-mode") with dynamics approximately described by the Schwarzian action:

$$S_{\text{Sch}} = -N\frac{C}{J} \int d\tau \text{Sch}[f, \tau] \quad ; \quad \text{Sch}[f, \tau] = \left(\frac{f'''}{f'} - \frac{3}{2}\left(\frac{f''}{f'}\right)^2\right) \tag{1.38}$$

In a similar fashion, the leading contributions ($\sim 1/N$) to the (Euclidean time-

ordered) four-point function (1.39) can also be determined.

$$\mathcal{F}(\tau_1, \tau_2, \tau_3, \tau_4) = \frac{1}{N^2} \sum_{ij}^{N} \langle \mathcal{T} \psi_i(\tau_1) \psi_i(\tau_2) \psi_j(\tau_3) \psi_j(\tau_4) \rangle - G(\tau_1, \tau_2) G(\tau_3, \tau_4)$$

(1.39)

We won't go into the details of this computation but encourage the reader to study this beautiful derivation in [55]. However, we note that the OTOC of the SYK can be computed from the four-point function (1.39), by analytically continuing to Lorentzian time, and behaves as

$$
\begin{aligned}
\text{OTOC}(t) \approx & G(\beta/2)G(\beta/2) + \mathcal{F}(\frac{\beta}{4} + it, -\frac{\beta}{4} + it, 0, -\frac{\beta}{2}) \\
= & \frac{\sqrt{\pi}}{2\beta J} \left(1 - C \frac{\beta J}{N} e^{\kappa t} \right), \quad \beta \ll t \ll \beta \log \frac{N}{\beta J}
\end{aligned}
$$

(1.40)

This expression is valid in the range of small but non-zero temperatures $\frac{N}{J} \gg \beta \gg \frac{1}{J}$ ($\frac{J}{N} \ll T \ll J$) where $\mathcal{F}$ has two leading contributions, one coming from excitations of the soft-mode, as described by the Schwarzian action (1.38), and the other is related to fluctuations around the conformal action. One not only sees the exponential growth characterized by the Lyapunov coefficient:

$$\kappa \approx \frac{2\pi}{\beta}(1 - \# \frac{1}{\beta J}),$$

(1.41)

it is also immediately obvious that in the IR ($\beta J \to \infty$) the SYK saturates the maximal chaos bound (1.14) and is a "fast scrambler".

1.4.2. Transverse Field Ising Chain

The one-dimensional transverse field Ising model (TI) consists of N spins acted on by Pauli operators $\hat{\sigma}_i^x \equiv \hat{X}_i$ and $\hat{\sigma}_i^z \equiv \hat{Z}_i$ residing on each site i; see Appendix 4.C.3.[5] The dynamics of the model is given by the TI Hamiltonian:

$$H_{\text{TI}} = -J \sum_{i=1}^{N} \hat{Z}_i \hat{Z}_{i+1} - h_x \sum_{i=1}^{N} \hat{X}_i,$$

(1.42)

where $J > 0$ is a dimensionful nearest-neighbor interaction constant, and h_x is the strength of the transverse field. In this thesis, the microscopic scale, set by the interaction constant, is fixed $J = 1$, Consequently, the ground state of the TI Hamiltonian depends only on h_x, which is used to tune the system across the quantum critical point at $h_x = 1$.

---

[5]There are many reviews; we shall use [50].

Let us first consider the phase with dominant nearest-neighbor interaction $h_x < 1$. At the extreme case of $h_x = 0$, the Hamiltonian is diagonalized by the eigenstates of $\hat{Z}_i$ ($\hat{Z}_i \left|\uparrow\right\rangle_i = \left|\uparrow\right\rangle_i$ and $\hat{Z}_i \left|\downarrow\right\rangle_i = -\left|\downarrow\right\rangle_i$). Due to the exact Z_2 symmetry of H_{TI} ($Z_i \to -Z_i, X_i \to X_i$) the ground state is degenerate with all spins either up or down:

$$\left|\uparrow\right\rangle = \prod_i^N \left|\uparrow\right\rangle_i \quad ; \quad \left|\downarrow\right\rangle = \prod_i^N \left|\downarrow\right\rangle_i \equiv \prod_i^N \hat{X}_i \left|\uparrow\right\rangle . \tag{1.43}$$

Systems with small fields $h_x \ll 1$ have a ground-state (labeled here as $\left|0_f\right\rangle$) with a small fraction of spins aligned in the opposite direction, but the global Z_2 symmetry preserves the degeneracy for any small h_x.[6] This symmetry is thus spontaneously broken and the normalized order parameter $\hat{m} = \frac{1}{N} \sum_i^N \hat{Z}_i$ is non-vanishing: $\left\langle 0_f \middle| \hat{m} \middle| 0_f \right\rangle \sim \pm 1$. Hence this phase is known as the ordered (ferromagnetic) phase.

The other limit of the model is at large fields $h_x \gg 1$ with ground state $\left|0_p\right\rangle$ that, to leading order in $1/h_x$, is given by the eigenstate of $\hat{X}_i$ with positive eigenvalue ($\hat{X}_i \left|\rightarrow\right\rangle_i = \left|\rightarrow\right\rangle_i$, and $\hat{X}_i \left|\rightarrow\right\rangle_i = -\left|\rightarrow\right\rangle_i$):

$$\left|0_p\right\rangle = \prod_i^N \left|\rightarrow\right\rangle_i , \tag{1.44}$$

$$\left|\rightarrow\right\rangle_i = \frac{1}{\sqrt{2}} \left(\left|\uparrow\right\rangle_i + \left|\downarrow\right\rangle_i \right) \quad ; \quad \left|\leftarrow\right\rangle_i = \frac{1}{\sqrt{2}} \left(\left|\uparrow\right\rangle_i - \left|\downarrow\right\rangle_i \right) \tag{1.45}$$

In this phase, the symmetry remains unbroken and the order parameter vanishes $\left\langle 0_p \middle| \hat{m} \middle| 0_p \right\rangle \sim 0$, so this is the disordered (paramagnetic) phase.

The usefulness of the TI model results from the observation that it can also be exactly solved by finding a basis in which the Hamiltonian is diagonal [50, 60]. Firstly, using the Jordan-Wigner transformation and the ladder operators ($\hat{\sigma}^\pm$), defined in Appendix 4.C.3, one can transform the spin-$\frac{1}{2}$ operators to spinless fermions:

$$c_i = \left(\prod_{j<i} \hat{Z}_j \right) \hat{\sigma}_i^+ \quad ; \quad c_i^\dagger = \left(\prod_{j<i} \hat{Z}_j \right) \hat{\sigma}_i^- \tag{1.46}$$

$$\{\hat{c}_i, \hat{c}_j^\dagger\} = \delta_{ij}, \quad \{\hat{c}_i, \hat{c}_j\} = \{\hat{c}_i^\dagger, \hat{c}_j^\dagger\} = 0, \tag{1.47}$$

---

[6]The global Z_2 symmetry may be broken by boundary conditions, but we shall not consider that here.

which, upon rotation of the spin axis by 90°, constitute a basis in which the TI Hamiltonian (1.42) reads

$$H_{TI} = -J \sum_i^N \left(\hat{c}_i^\dagger \hat{c}_{i+1} + \hat{c}_{i+1}^\dagger \hat{c}_i + \hat{c}_{i+1} \hat{c}_i + \hat{c}_i^\dagger \hat{c}_{i+1}^\dagger - 2\frac{h_x}{J} \hat{c}_i^\dagger \hat{c}_i \right). \tag{1.48}$$

This form of the TI Hamiltonian does not have a conserved fermion number, due to the $\hat{c}_{i+1} \hat{c}_i$ and $\hat{c}_i^\dagger \hat{c}_{i+1}^\dagger$ terms. However, it is quadratic in operators suggesting it can be diagonalized. Indeed, the Fourier transformation:

$$\hat{c}_k = \frac{1}{\sqrt{N}} \sum_i^N \hat{c}_j e^{-ikaj}, \tag{1.49}$$

brings the Hamiltonian (1.48) to :

$$H_{TI} = J \sum_k^N \left(2 \left(\frac{h_x}{J} - \cos(ka) \right) \hat{c}_k^\dagger \hat{c}_k + i \sin(ka) \left(\hat{c}_{-k} \hat{c}_k + \hat{c}_{-k}^\dagger \hat{c}_k^\dagger \right) - \frac{h_x}{J} \right). \tag{1.50}$$

From here, one can use the Bogoliubov transformation (1.51):

$$\gamma_k = u_k c_k - i v_k c_{-k}^\dagger, \tag{1.51a}$$

$$u_k = \cos\left(\frac{\theta_k}{2} \right), \quad v_k = \sin\left(\frac{\theta_k}{2} \right) \quad ; \quad \tan \theta_k = \frac{\sin(ka)}{\cos(ka) - \frac{h_x}{J}}, \tag{1.51b}$$

$$u_k^2 + v_k^2 = 1, \quad u_{-k} = u_k, \quad v_{-k} = -v_k, \quad u_k, v_k \in \mathbb{R}, \tag{1.51c}$$

which map the $\hat{c}_i^{(\dagger)}$ operators to a new set of fermions (γ_k) that satisfy the cannonical fermionic relations $\{\hat{\gamma}_k, \hat{\gamma}_{k'}^\dagger\} = \delta_{kk'}, \{\hat{\gamma}_k, \hat{\gamma}_k'\} = \{\hat{\gamma}_k^\dagger, \hat{\gamma}_k'^\dagger\} = 0$. In this basis, the Hamiltonian has a conserved fermionic number and is manifestly solvable, since it represents a set of N free fermions with dispersion relation ε_k:

$$H_{\text{TI}} = \sum_k^N \varepsilon_k \left(\hat{\gamma}_k \hat{\gamma}_k - \frac{1}{2} \right) \tag{1.52}$$

$$\varepsilon_k = 2J \sqrt{1 + \frac{h_x^2}{J^2} - 2\frac{h_x}{J} \cos(k)} . \tag{1.53}$$

1.4.3. Mixed Field Ising Chain

The Mixed Field Ising model (MFI) is a simple generalization of the Transverse Field Ising model with dynamics is governed by the following Hamiltonian:

$$H_{\text{MFI}} = -J \sum_{i=1}^N \hat{Z}_i \hat{Z}_{i+1} - h_x \sum_{i=1}^N \hat{X}_i - h_z \sum_{i=1}^N \hat{Z}_i. \tag{1.54}$$

This model has a few different manifestations, dependent on the point in the parameter space (h_x, h_z), which make it a rich playground for the theoretical testing of new hypotheses. For $h_z = 0$ this model reduces to the TI model (1.4.2), and for $h_x = 0$ reduces to the regular Ising model. We used the latter in Chapter 3 as a representative case of classical systems. The prominence of this model is that it is an archetype of quantum-chaotic behavior. At a particular point in the parameter space $h_x = -1.05$ and $h_z = 0.5$ it has the RMT-like spectral statistics [61]. Even though this point is not an isolated instance of chaotic behavior, sometimes it is referred to as "strong-chaoticity" [52], since, by varying (h_x, h_z), the spectral statistics of the model continuously transform between Wigner-Dyson distribution at $h_x = -1.05$ and $h_z = 0.5$ and Poisson distribution at an integrable point $h_x = 0$ or $h_z = 0$ in the parameter space. This smooth interpolation between chaotic and integrable regimes is what makes this model particularly convenient as a theoretical toy model.

1.5. Holographic duality

Though holographic duality itself is not part of the research presented in this thesis, the studies using holography to understand the dynamics of quantum black holes through its duality with non-gravitational quantum systems did provide a large motivating factor. For that reason we do briefly review it here.

The specific version of holography of relevance is the conjectured holographic duality of the SYK model with a 2D anti-de-Sitter (AdS) dilaton gravity [40, 55]. Below we outline how these pure two-dimensional dilaton gravities are described by the same Schwarzian action Eq.(1.38) in the IR limit and thus also exhibit maximal chaotic behavior with the Lyapunov coefficient saturating the bound Although it is much more difficult to find a gravitational theory and prove their duality in the full RG flow, the equivalence in the IR behavior of both theories has been an encouraging aspect in the quest for understanding their connection. There has been vast excitement around this duality because, for the first time, we have an exactly solvable field theory that can probe the realms of quantum gravity. Moreover, the far-reaching impact is far reaching since, as we'll demonstrate below, these 2D gravities appear as a universal behavior in the near-horizon limit of extremal black holes. Using an extension of this universal sector of the duality with the newly developed double-holographic paradigm [62, 63, 64, 65], that studies dualities between 1D field theories and 2D gravity with matter that's then dual to a 3D gravity, results from the SYK model have proven useful in understanding the process of black hole evaporation while preserving unitarity of the underlying physical process. In particular for the first time a tractable computation was able to reproduce the Page curve describing the evolution of the entanglement entropy between the black hole and its Hawking radiation. The

holographically dual description of this process in terms of the SYK physics is that of quenched cooling, and this is what motivated us to study the latter.[7]

First, we introduce pure AdS_2 in Euclidean signature and with radius set to unity. The particular choice of signature is useful for latter consideration of correlation functions in the dual boundary theory. In the Euclidean case, AdS_2 is simply a hyperbolic disk that is fully covered by both Poincaré:

$$ds^2 = \frac{dt^2 + dz^2}{z^2}, \tag{1.55}$$

and Rindler coordinates:

$$ds^2 = d\rho^2 + \sinh^2 \rho \, d\varphi^2. \tag{1.56}$$

In order to regularize the infinite volume of this space one cuts off the AdS_2 space along some curve $(t(\tau), z(\tau))$ close to the boundary, with a local affine parameter (the "time" on this boundary curve) in the interval $\tau \in [0, \beta)$. The physical length of this boundary curve goes to infinity in the limit $\epsilon \to 0$:

$$ds_b = \sqrt{\frac{ds^2}{d\tau^2}} d\tau = \sqrt{\frac{dt'^2 + dz'^2}{z^2}} = \frac{d\tau}{\epsilon} . \int ds_b \qquad = \int_0^\beta \frac{d\tau}{\epsilon} = \frac{d\beta}{\epsilon}, \tag{1.57}$$

Due to the isometry of Euclidean AdS_2, curves with the following $SL(2, \mathbb{R})/\mathbb{Z}_2$ reparametrisation describe the same geometry.

$$\tilde{t}(\tau) = \frac{at(\tau) + b}{ct(\tau) + d} \quad ; \quad ad - bc = 1, \quad a, b, c, d \in \mathbb{R} \tag{1.58}$$

Already here we notice the first possible hint of a duality with SYK as the dynamics in the AdS_2 space with cutoff is captured by a one-dimensional curve $t(\tau)$ with the same symmetry as the IR limit of the SYK model in Section 1.4.1.

In the same way that the full SYK model starts with weakly interacting fermions in the IR that flow to the strongly interacting theory in the IR, it is also useful to start from a full model defined in the UV on the holographic side. This UV will clearly *not* be the same UV as the SYK model, but it will serve as an anchor for studying the resulting AdS_2 IR. We will use electromagnetically charged AdS_4 Reissner-Nordström black holes to demonstrate how AdS_2 appears. These AdS_4 RN black holes are described by the metric

$$ds^2 = \frac{(r - r_+)(r - r_-)}{r^2} dt^2 + \frac{r^2}{(r - r_+)(r - r_-)} dr^2 + r^2 d\Omega^2 \tag{1.59a}$$

$$r_\pm = l_p Q + l_p^2 E \pm \sqrt{2l_p^3 QE + l_p^4 E^2} \quad ; \quad F_{rt} = \frac{Q}{r^2}, \tag{1.59b}$$

---

[7]In earlier papers this was called evaporative cooling. However, the actual process is prompted by an instantaneous change and hence a quench in the language of non-equilibrium physics.

where $l_P = \sqrt{G}$ is the Planck length, M and Q are the mass and charge of the black hole and $r_\pm$ the two horizons that coincide at extremality $E = 0$. The near-horizon geometry is obtained by taking $r \to r_+$, $l_P \to 0$ while keeping the variable z constant:

$$z = \frac{Q^2 l_P^2}{r - r_+}. \tag{1.60}$$

Expressing the the RN metric (1.59) in the new coordinate z (1.60), the near-horizon geometry of extremal black holes factorizes into an AdS_2 and a 2D sphere:

$$ds^2 \approx Q^2 l_P^2 \left(\frac{-dt^2 + dz^2}{z^2} + d\Omega^2 \right). \tag{1.61}$$

While this is the ground state of the extremal RN black hole, excitations above it are described by two-dimensional dilaton gravities, Φ being the dilaton field. This follows from its derivation from the Einstein-Hilbert action:

$$I = -\frac{1}{16\pi l_P^2} \int dx^4 \sqrt{-g} \left(R_g - \frac{l_P^2}{4} F_{\mu\nu} F^{\mu\nu} \right), \tag{1.62}$$

and focusing only on static, spherically symmetric field configurations [42, 66, 56] of the form:

$$ds^2 = h_{ij}(r,t) dx^i dx^j + \Phi^2(r,t) d\Omega^2. \tag{1.63}$$

One obtains, after reduction over the two-sphere, an effective 2D theory:

$$I = -\frac{1}{4l_P^2} \int dx^2 \sqrt{-h} \left(\Phi^2 R_h + 2(\boldsymbol{\nabla}\Phi)^2 + 2 - \frac{2Q^2 l_P^2}{\Phi^2} \right). \tag{1.64}$$

This is a special case of a class of 2D dilaton gravity models with an arbitrary scalar potential U, studied extensively in [42].

$$I = \frac{1}{16\pi G_N} \int dx^2 \sqrt{-h} \left(\Phi^2 R_h + \lambda(\boldsymbol{\nabla}\Phi)^2 - U\left(\Phi^2\right) \right). \tag{1.65}$$

Returning to the specific model (1.64), one can remove the dilaton kinetic term with a Weyl transformation [42]:

$$I = -\frac{1}{4l_P^2} \int dx^2 \sqrt{-h} \left(\Phi^2 R_h + 2 - \frac{2Q^2 l_P^2}{\Phi^2} \right). \tag{1.66}$$

and readily obtain the saddle point solution,

$$\delta_\Phi I|_{\phi_0} = 0 \Rightarrow R_h = -2\frac{Q^2 l_P^2}{\phi_0^4} \tag{1.67}$$

which is an AdS$_2$-like space with radius $L = \phi_0^2/(|Q|l_P)$. The remaining variation $\delta_{h_{ij}} I_{h_{ij,0}} = 0$ has the AdS$_4$ RN black hole as solution but also just the near-horizon AdS$_2$ limit of the extremal RN black hole (1.61), in which case $\Phi(x,r) = \phi_0$.

Without proof we will state that the fluctuations around this solution with non-trivial dependency on the coordinates on the two-sphere are all energetically costly and the low lying excitations are given by small fluctuations of the dilaton field around its AdS$_2$ saddle point:

$$\Phi^2 = \phi_0^2 + \phi(x^0, x^1), \quad \phi(x^0, x^1) \ll \phi_0^2. \tag{1.68}$$

Substituting this ansatz in (1.66) and expanding to second order in ϕ/ϕ_0^2 the following action is obtained:

$$I \approx -\frac{1}{2l_P^2} \int dx^2 \sqrt{-h} - \frac{\Phi_0^2}{4l_P^2} \left[\int dx^2 \sqrt{-h} \left(R_h + \frac{2}{L^2} \right) + 2 \int_{\partial\text{AdS}} \mathcal{K} \right]$$
$$- \frac{1}{4l_P^2} \left[\int dx^2 \sqrt{-h} \phi \left(R_h + \frac{2}{L^2} \right) + 2 \int_{\partial\text{AdS}} \phi_b \mathcal{K} \right], \tag{1.69}$$

where we have restored the proper AdS$_2$ boundary terms proportional to trace of the extrinsic curvature $\mathcal{K}$ [66]. In this action, the first term is proportional to the volume of the AdS$_2$ space, the second represents the ordinary 2D Einstein gravity, and the last one (1.70), known as the Jackiw-Teitelboim (JT) gravity [67, 68], is the subject of our interest since it gives rise to a non-trivial dynamics.

$$I_{JT} = -\frac{1}{4l_P^2} \left[\int dx^2 \sqrt{-h} \phi \left(R_h + \frac{2}{L^2} \right) + 2 \int_{\partial\text{AdS}} \phi_b \mathcal{K} \right], \tag{1.70}$$

If one derives the equation of motion for the dilaton ϕ, with a boundary condition given by ϕ_b, the bulk term in the JT gravity manifestly sets the spacetime to an (asymptotically) AdS$_2$ with constant scalar curvature $R_h = -2$. When we restrict the analysis to a nearly-AdS geometry the last term encodes the dynamics of the cutoff curve $(t(\tau), z(\tau))$, which after proper treatment of the arising infinities [69, 43, 55] is described by the Schwarzian action to leading order in ϵ:

$$I_b \approx -\frac{\phi_r}{8\pi G} \int_0^\beta d\tau \text{Sch}[t(\tau), \tau], \tag{1.71}$$

where $\phi_r(\tau)$ is renormalized boundary dilaton ($\phi_r(\tau)/\epsilon \approx \phi_b$). The Schwarzian action is obtained under the assumption that the dilaton is constant at the boundary $\phi_r(\tau) = \phi_r$, a more detailed treatment, leading to the same result, can be found in [56, 66] and citations therein. With the knowledge that the dynamics of the cutoff modes in fact comprise the full low energy, this proves the duality with the IR action of the reparametrization modes in the SYK (1.38): they are both described by the Schwarzian action. It is a beautiful example of IR universality in that the two wildly differing UVs flow to the same fixed point in the IR.

At last, to establish the connection in the chaotic behavior, the introduction of matter fields $\xi(t, z)$ is required on top of the empty dilaton gravity. We consider a minimally coupled free theory in the cut-off AdS$_2$ background,

$$I_m = \frac{1}{2} \int dx^2 \sqrt{-h} \left[\partial^a \xi \partial_a \xi + m^2 \xi^2 \right] . \qquad (1.72)$$

Its saddle point solution is completely determined by its boundary value $\xi_r(t)$ defined as

$$\xi(t, z) = z^{1-\Delta} \xi_r(t) + \cdots \quad ; \quad \Delta = \frac{1}{2} + \sqrt{\frac{1}{4} + m^2}. \qquad (1.73)$$

The AdS/CFT dictionary tells us that, in the dual field theory, there is an operator $V(\tau)$ with conformal dimension Δ that is conjugate to $\xi_r(\tau)$. Introducing a second free field $\chi(t, z)$, with the same action (1.72), that is conjugate to another operator $W(\tau)$ with the same conformal dimension Δ, one can show [70, 43] that the leading behavior of the OTOC of those operators arises from the fluctuations of the boundary shape and is given by:

$$\text{OTOC}(t) \approx \left(\frac{\pi}{\beta}\right)^2 \left(1 - 2\Delta^2 \frac{\beta G}{\phi_r} e^{\frac{2\pi t}{\beta}}\right), \quad \beta \ll t \ll \beta \log \frac{\phi_r}{\beta G}. \qquad (1.74)$$

From the exponential growth of the second term in (1.74) with a Lyapunov coefficient $\lambda = 2\pi/\beta$ that saturates the bound (1.14) we conclude that the 2D dilaton gravity exhibits a maximally chaotic behavior that coincides with the SYK (1.13) as it should.

1.6. Thesis outline

This thesis studies the non-equilibrium dynamics of composite quantum systems following the quench described in the introduction at early times specifically. The time scales of interest are well before the validity of ETH and even hydrodynamics, so the analysis is based on the evolution of energy, the von Neumann and relative entropies, as well as the information spread between different parts of

the system. This was initially motivated by an observation in numerical simulations of a peculiar early-time energy increase in the hotter of two quench-coupled systems. This thesis not only provides a detailed explanation of this quantum phenomenon but also explores how it can be used for experimentally measuring quantum correlations, both as a feature for detecting a lab realization of an SYK system as well as the implications it has on the formation of black holes. Those results have been published in three different papers [71, 72, 73] plus one yet unpublished manuscript. Before elaborating on them we provided a brief overview of each of the four chapters.

In the first Chapter 2, we introduce this paradoxical early time rise in energy in the hotter of the two baths and the quantum thermodynamic approach to studying post-quench dynamics. To understand the essence of this phenomenon, without the interference of model-dependent peculiarities, we use the 1D free fermion model as a case study. Conveniently, in the time regime of interest, we obtain analytical expressions for the energy and for the von Neumann entropies, which is an additional benefit of this model. In addition to the theoretical study, we have suggested an experimentally realizable quench protocol that can measure entanglement between two subsystems using the energy increase and its relation to von Neumann entropy. In this quench, one starts with two originally independent systems of free fermions A and B initially prepared in quantum thermal states at temperatures T_A and T_B. At low temperatures, when quenched, the increasing entanglement contribution to the von Neumann entropy is dominant over the decreasing thermal one. As a consequence the von Neumann entropy of each subsystem increases for a certain period after the subsystems are coupled. If in this period one decouples the subsystems there is an energy transfer to the system in the amount set by the von Neumann entropy accumulated during the joint evolution of A and B. This energy transfer appears as work produced by the quench to decouple the reservoirs. Once A and B are disconnected, the information about their mutual correlations – von Neumann entropy – is stored in the energy increment of each reservoir which allows a direct readout of quantum correlations by measuring the energy of the subsystems. While this thesis doesn't cover the details on the feasibility of the experimental realization and subtleties when the temperature of either subsystem approaches $T \to 0$, interested readers are advised to consult [71].

Next, in Chapter 3 we study the post-quench quantum dynamics of both strongly correlated SYK systems and weakly correlated mixed field Ising chains. As previously mentioned, the quantum thermodynamic relations require exact knowledge of the time evolution of energy and the von Neumann and relative entropies. For those systems these cannot be obtained analytically, therefore, we resort to exact diagonalization. While this approach is limited to finite sized systems, it allows us to study their evolution at an arbitrary time-scale allowing us to distinguish two qualitatively different behaviours. Namely, the early time polynomial increase of

energy in both sub-systems is followed by a conventional classical-like evaporation with the energy of the hotter/colder system exponentially decreasing/increasing. At the transition time t_m the energy of the hotter system peaks, a feature known as the energy bump. We show that even in the quantum regime the origin of this energy bump is not due to thermal flux from the hot to the cold, contrary to what has been reported before [13]. Instead the early-time energy increase of the hotter subsystem is not related to a temperature increase but results from the potential energy gained by coupling the two systems. The size of the energy increase is set by the entropy gain and lasts until correlations between the subsystems saturate. When the systems of interests are SYK dots we have numerically found that the energy bump appears regardless of the initial temperature difference, which isn't surprising, given the ultra quantum nature of this system.[8] To answer the question "Why we haven't seen this phenomenon in everyday life?", we use the MFI model which has classical, integrable, chaotic and critical regimes. At the critical point, same as with SYK, the energy bump always appears, but moving even slightly away from criticality there is a distinct temperature T_c such that, when the hotter system is initiated above $T_A > T_c$, its energy decreases from the very beginning in full agreement with our (classical) intuition. If MFI is tuned to the classical regime this distinct temperature vanishes $T_c = 0$ and classical dynamics is recovered at any initial configuration.

In order to better understand the numerical results for the SYK and MFI models we analyze in Chapter 4 their properties with a perturbative time expansion of each subsystem's energy. We derive the coefficients up to the third order and focus on situations where both subsystems are initialized in a thermal state. In this case the first and third coefficients vanish and the second coefficient captures the relation between the appearance of the early time energy increase in the hotter subsystem and before-quench thermodynamic states. More precisely, the bump appears whenever the second coefficient is larger than zero. Using this approach we have shown that, for two quench-coupled SYKs, the existence of the quantum regime isn't conditioned on the temperature difference. since the second coefficient of each subsystem depends only on its own parameters and they're always positive. Consequently, the early time energy increase will always appear, as we've suspected from the numerical results. However, if the systems under consideration are MFI models, the second coefficient has two competing contributions. One is always positive, similar to the SYK case, and depends only on the analyzed subsystem, whereas the other is negative and depends on the initial parameters of both, hence, the bump persists as long as the former term is dominant over the former. Both terms have the same magnitude at the critical temperature T_c, after which the second term dominates resulting in the bump disappearance, for any temperature $T \geq T_c$. Here, using the perturbative

---

[8]This is intrinsically linked to the ANEC inequality when modeling evaporative black hole formation with SYK dots [14, 15].

analytical expressions, we were able to compute the critical temperature as a function of quantities evaluated in the initial thermal state and prove it matches with results obtained from numerical time evolution.

In the last Chapter 5 we study the post-quench dynamics, using the same protocol of coupling two initially independent subsystems, but now for charged SYKs. Furthermore, the first hot system is a SYK_4 dot, but unlike before, the second is a much larger disordered Fermi liquid heat bath modeled by an SYK_2 at zero temperature and chemical potential. This project was motivated by efforts to engineer an experimental realization of the SYK model and the fragility upon measurement of the non-Fermi liquid SYK_4 phase. By studying the time evolution of the SYK's spectral properties we demonstrated that, while the non-Fermi liquid phase eventually breaks under the influence of the bath, it is preserved right after the quench and we were able to estimate the transition timescale, which matches with results obtained from extrapolation of equilibrium studies. In early post-quench times, before the non-FL/Fermi liquid transition, we discovered that the charged current undergoes a power-law increase and reaches maximum before exponentially relaxing, resembling the energy behavior analyzed in the three previous chapters. The half-life of the current is inversely proportional to the coupling between the system and the bath and it increases with temperature. Investigating this temperature dependence of the half-life we have found that at low temperatures its temperature dependence behaves as $t_{1/2} \sim T$ when the hot system is a non-Fermi liquid SYK_4 dot. However, when the hot system is a disordered regular Fermi liquid SYK_2 system, at the same chemical potential, the half-life scales as $t_{1/2} \sim T^2$. Based on this result, we proposed measuring the half-life of the discharging current in the quench-coupling protocol, as a feasible experimental setup for detecting the fragile non-Fermi liquid SYK phase and differentiating it from a disordered Fermi-liquid phase.

2 | Dynamics of quenched Fermi gas after a local quench

2.1. Introduction

Entanglement entropy is a measure of non-classical correlations in quantum composite systems. It is commonly defined as the von Neumann entropy of a subpart of a quantum composite system described by a pure quantum state [21]. Consideration of the later one requires zero temperature limit. Despite entanglement being an inherent characteristic of quantumness, the entanglement entropy itself is not easy to measure directly because of its nonlocal nature. Still, a few proposals are suggesting that the entanglement entropy can be related to the particle number fluctuations in free fermion systems [74, 75, 76, 77] and elicited from the low-energy states population dynamics in quantum many-body systems [78, 79]. A recent experiment reports that the entanglement entropy can be measured by an interference of two clones of a many-body state in ultra-cold atoms [80].

However, one may ask if there are generic consequences of quantum correlations between the subparts of a given system that are known to exist above zero temperature. This question may be answered in the framework of quantum thermodynamics – a rapidly developing field that relates general properties of quantum systems, such as work, heat, and entropy, irrespective of their microscopic nature [22]. Within this approach, the classical thermodynamic entities are extended to their quantum counterparts. In quantum thermodynamics, the energy of the evolving quantum state is usually expressed in terms of thermal free energy and entropy production – a measure of the irreversibility of a quantum process defined as the relative entropy between an actual state of the system and a reference state [22, 81]. The latter is usually chosen as a thermal state of the system taken at the same time as the evolving one. This method has proven to be quite fruitful for thermodynamic analysis of quantum composite systems. In particular, it was shown that entanglement in quantum composite systems can be converted to work or heat [82, 23, 83, 84]. The conversion of quantum correlations to heat arises naturally for quantum systems in a form of decoherence due to interactions with environment [85, 86] and governs a borderline between quantum and

classical worlds [87, 88]. On the other hand, the conversion of quantum correlations to work is actively studied as it paves the way to quantum thermal engines potentially superior to their classical analogs [89, 90, 91].

In this paper, we are interested in the way how quantum correlations may be converted to energy for quantum thermal states. We consider two arbitrary quantum systems, each of them initially in thermal equilibrium, coupled and then jointly evolving until decoupling. The coupling and decoupling process is controlled by a chosen quench protocol. We show that the energy acquired during the joint evolution by a subpart of a quantum composite system can be related to its entropies only, namely, the von Neumann entropy and the relative entropy between the evolved state of the subsystem and its initial thermal state. The von Neumann entropy accumulated during the joint evolution of the two systems sets the lower bound on the energy change. We apply this inherently quantum description to a quench-coupled system of non-interacting fermions. The composite free Fermi systems are particularly attractive since they allow to directly access the entanglement entropy between its subparts when coupled [76, 77]. For temperatures much lower than the Fermi energy in the system, the quantum correlations between the two subparts of the system, given by the change in the von Neumann entropy, are transferred to the subsystem's energy. This energy increment originates from the external work produced by the quench to erase the correlations between the subsystems at the moment of decoupling. The von Neumann entropy accumulated during the joint evolution of the two subsystems can be directly read out from the energy increment.

2.2. Entropy to energy relation in quantum thermodynamics

We consider two isolated quantum systems A and B, initially both in thermal equilibrium, that are instantaneously coupled by an arbitrary interaction V_{AB}. The general time-dependent Hamiltonian is

$$H(t) = H_A + H_B + g(t)V_{AB}, \tag{2.1}$$

where the function $g(t)$ defines a quench protocol that turns on/off the interaction at a given time. The initial state of the full system is given by the product of two thermal density matrices

$$\rho_0 = \rho_A \otimes \rho_B, \tag{2.2}$$

$$\rho_\alpha = \frac{1}{Z_\alpha} \sum_{n_\alpha} e^{-E_{n_\alpha}/T_\alpha} |n_\alpha\rangle\langle n_\alpha| = \frac{e^{-H_\alpha/T_\alpha}}{Z_\alpha}, \quad \alpha = A, B. \tag{2.3}$$

Here $|n_\alpha\rangle$ is an eigenstate of the Hamiltonian H_α with an eigenenergy E_{n_α}, T_α is the initial temperature, and $Z_\alpha = \text{Tr}_\alpha e^{-H_\alpha/T_\alpha}$ is the partition function for $\alpha = A, B$. Below we focus on the properties of the system A for brevity and use the units $\hbar = k_\text{B} = 1$ everywhere.

Once the two systems are coupled they become correlated. A natural measure to study the correlations between A and B is the von Neumann entropy. The von Neumann entropy for the system A is

$$S_\text{vN}(t) = -\text{Tr}_A \, \rho_A(t) \ln \rho_A(t), \tag{2.4}$$

where $\rho_A(t) = \text{Tr}_B \, \rho(t)$ is the reduced density matrix. Here we are not limiting ourselves to the unitary evolution of the full density matrix $\rho(t)$. For example, it can be drawn from the Lindblad master equation in case the system (2.1) is dissipative.

Let us introduce the relative entropy, which is often used in both quantum information processing [21] and quantum thermodynamics [22] to distinguish two quantum states. For our purpose, we define the relative entropy between the evolved state $\rho_A(t)$ of the system A from its initial thermal state ρ_A:

$$S\left(\rho_A(t)||\rho_A\right) = \text{Tr}_A \, \rho_A(t) \left(\ln \rho_A(t) - \ln \rho_A\right) \geq 0. \tag{2.5}$$

As we shall use shortly, the relative entropy is defined as non-negative [21].

Now, we substitute the von Neumann entropy (2.4) into Eq. (2.5). Using that the initial state of A is a thermal state at temperature T_A, we relate the expectation value of the Hamiltonian H_A to the combination of the von Neumann and relative entropy

$$\text{Tr}_A \, \rho_A(t) H_A = \mathcal{F}_A + T_A \left(S_\text{vN}(t) + S(\rho_A(t)||\rho_A)\right). \tag{2.6}$$

Here $\mathcal{F}_A = -T_A \ln Z_A$ is the initial thermal free energy of the system A. Subtracting the initial energy value $\text{Tr}_A \, \rho_A H_A = \mathcal{F}_A + T_A S_\text{vN}(0)$ from Eq. (2.6), we derive

$$\Delta E_A(t) = T_A \left(\Delta S_\text{vN}(t) + S(\rho_A(t)||\rho_A)\right), \tag{2.7}$$

where $\Delta E_A(t) = \text{Tr}_A \, \rho_A(t) H_A - \text{Tr}_A \, \rho_A H_A$ and $\Delta S_\text{vN}(t) = S_\text{vN}(t) - S_\text{vN}(0)$. The relation (2.7) combines the first and the second law of thermodynamics for a subpart of an arbitrary quantum composite system. Being a thermodynamic statement, Eq. (2.7) should be understood as the equation of the energy-to-entropy balance after the process is over. In contrast with the previous studies, see e.g. Refs. [82, 23, 83, 86], we relate the energy of the system A to its entropy properties solely. At low temperatures, the energy change is set by the amount

of correlations with the other subpart of the full system, that emerge when the coupling is switched-on, and by its deviation from the initial state.

When the two systems are coupled, it is not possible to completely isolate them from each other to determine the actual energy shift in A or B. However, one can count whether the energy of the system changes if A and B are decoupled later on. Since the relative entropy is non-negative, the von Neumann entropy provides the lower bound on the overall energy shift:

$$\Delta E_A \geq T_A \Delta S_{\text{vN}}. \tag{2.8}$$

The inequality (2.8) is a generic thermodynamic property of quantum composite systems and yield quite intriguing consequences at low temperatures. Indeed, turning on the interaction between the subparts of a quantum composite system induces quantum correlations. Ergo, their von Neumann entropy increases in absence of thermal imbalance between the subsystems. According to Eq. (2.8), it necessarily leads to the energy increment when the systems are decoupled ($\Delta E_A > 0$). This prompts the question: can one directly detect quantum correlations between the subparts of a quantum composite system by measuring the resulting energy increment? Putting this in perspective, we explain the physics of this effect by taking the thermodynamic point of view on the quench-coupling/decoupling protocol in a free fermion system.

2.3. The case study: free fermions

The possibility of detection quantum correlations and entanglement entropy, in particular, is widely discussed for the free Fermi systems [75, 76, 74, 77]. In light of this, free fermions seem as a natural framework to proceed with our thermodynamic consideration.

Consider for systems A and B two isolated spinless fermionic reservoirs at temperatures T_A and T_B. At time $t = 0$ we instantaneously couple the reservoirs together and then disconnect them at $t = t_0$. The coupling/decoupling process is controlled by the quench protocol $g(t) = \theta(t) - \theta(t - t_0)$ in the Hamiltonian (2.1). The Hamiltonian (2.1) reads

$$H_A = \sum_p \xi_p a_p^\dagger a_p, \tag{2.9}$$

$$H_B = \sum_{p'} \xi_{p'} b_{p'}^\dagger b_{p'}, \tag{2.10}$$

$$V_{AB} = \lambda \delta(x) a^\dagger(x) b(x) + h.c., \tag{2.11}$$

where A and B are coupled locally. Here $a, a^\dagger$ and $b, b^\dagger$ are the fermionic operators, ξ_p is the corresponding dispersion, and λ is the coupling constant. Note that

$[V_{AB}, H_A] \neq 0$ and $[V_{AB}, H_B] \neq 0$. Below we put both reservoirs at the same chemical potential to avoid electric currents.

The chosen quench protocol leads to the non-conservation of energy in our model. It immediately follows from the general form of the Hamiltonian (2.1) that the energy can be added to the system at the moment of turning on/off the interaction between A and B:

$$\frac{d\langle H(t)\rangle}{dt} = g'(t)\langle V_{AB}(t)\rangle = \delta(t)\langle V_{AB}(0)\rangle - \delta(t - t_0)\langle V_{AB}(t_0)\rangle. \qquad (2.12)$$

The origin of this effect is quite simple. The quench can produce work to couple and decouple the reservoirs.

When A and B are coupled at $t = 0$ they become correlated and, hence, one can not measure their energy separately until the systems are disconnected at $t = t_0$. To evaluate the overall energy shift in the reservoir A after decoupling from B, we compute the corresponding energy flux

$$\frac{d\langle H_A(t)\rangle}{dt} = i\langle[H, H_A]\rangle = -ig(t)\sum_{pp'}\xi_p(\lambda\langle a_p^\dagger b_{p'}\rangle - h.c.). \qquad (2.13)$$

The correlation functions that define the energy flux (2.13) satisfy the equation

$$\lambda\frac{d\langle a_p^\dagger b_{p'}\rangle}{dt} = i\lambda(\xi_p - \xi_{p'})\langle a_p^\dagger b_{p'}\rangle - ig(t)|\lambda|^2\sum_q(\langle a_p^\dagger a_q\rangle - \langle b_q^\dagger b_{p'}\rangle). \qquad (2.14)$$

The exact solution of Eq. (2.14) requires notion of the correlation functions $\langle a_p^\dagger a_q\rangle$ and $\langle b_q^\dagger b_{p'}\rangle$, the momenta-diagonal components of which are dynamic occupation numbers $n_\alpha(\xi_p, t)$ of fermions $\alpha = a, b$ with momentum p at time t. We solve Eq. (2.14) perturbatively in the lowest order in λ implying the equilibrium occupation numbers of the initial state of the system. Indeed, since there are no inter-momenta couplings before the quench, we use diagonal correlations $\langle a_p^\dagger a_q\rangle = \delta_{pq}\langle a_p^\dagger a_p\rangle = \delta_{pq}n_A(\xi_p)$ and $\langle b_q^\dagger b_{p'}\rangle = \delta_{qp'}\langle b_{p'}^\dagger b_{p'}\rangle = \delta_{qp'}n_B(\xi_{p'})$ in Eq. (2.14), where $n_\alpha(\xi_p) = \left(e^{\xi_p/T_\alpha} + 1\right)^{-1}$ is the Fermi distribution function. The sought-for correlation function is

$$\lambda\langle a_p^\dagger b_{p'}\rangle = -i|\lambda|^2(n_A(\xi_p) - n_B(\xi_{p'}))\int_0^t dt'\, e^{i(\xi_p - \xi_{p'})(t - t')}g(t'). \qquad (2.15)$$

It follows form the correlation function (2.15) that $\langle V_{AB}(0)\rangle = 0$ in Eq. (2.12), since there are no correlations between A and B at $t = 0$.

Substituting Eq. (2.15) into Eq. (2.13), we obtain the Fermi golden rule formula for the energy flux

$$\frac{d\langle H_A(t)\rangle}{dt} = -2g(t)\frac{|\lambda|^2}{\varepsilon_{\mathrm{F}}^2}\int d\omega d\omega'\,\omega\,\frac{\sin(\omega-\omega')t}{\omega-\omega'}(n_A(\omega)-n_B(\omega')). \qquad (2.16)$$

Here we introduced the density of states (DoS) for both fermion species $\nu_A(\omega) = \sum_p \delta(\omega-\xi_p)$ and $\nu_B(\omega') = \sum_{p'} \delta(\omega'-\xi_{p'})$ and assume the two-dimensional reservoirs with constant DoS given by the inverse Fermi energy $\nu_\alpha \sim 1/\varepsilon_{\mathrm{F}}$. Then the overall energy shift in A is given by $\Delta E_A = \int_0^{t_0} dt\,\frac{d\langle H_A(t)\rangle}{dt}$. An identical computation of the energy flux can be done for the reservoir B.

Let's consider A and B at zero temperature prior the quench. In equilibrium, there would not be an energy shift in either of the reservoirs. However, turning on the coupling entangles the states in the reservoirs and, therefore, results in presence of entanglement entropy between A and B that can be captured by the particle number fluctuations [76, 77]. So, does the energy of the A-reservoir remain unchanged once A and B are decoupled?

At zero temperature the distribution function $n_\alpha(\omega)$ is a unit-step function $\theta(-\omega)$ for both reservoirs. Substituting the zero temperature distribution functions into the Fermi golden rule formula (2.16) and providing the UV cut-off $\sim \varepsilon_{\mathrm{F}}$ for the frequency integrals, we derive the energy flux

$$\frac{d\langle H_A(t)\rangle}{dt} = 2g(t)|\lambda|^2 \sin(\varepsilon_{\mathrm{F}} t)\frac{\sin^2\left(\varepsilon_{\mathrm{F}} t/2\right)}{\left(\varepsilon_{\mathrm{F}} t/2\right)^2}. \qquad (2.17)$$

Accordingly, the overall energy shift in the reservoir A is

$$\Delta E_A^{\mathrm{Q}} = \frac{2|\lambda|^2}{\varepsilon_{\mathrm{F}}}\int_0^{\varepsilon_{\mathrm{F}} t_0} d\zeta\,\sin\zeta\,\frac{\sin^2\left(\zeta/2\right)}{\left(\zeta/2\right)^2}. \qquad (2.18)$$

As it is shown in Fig. 2.1 (blue solid curve), the energy of the system increases in the absence of temperature or charge imbalance. The effect is suppressed in the continuous limit (small lattice spacing for the free fermions) where the Fermi energy is large. Here we use the superscript Q in Eq. (2.18) to stress that the effect is manifestly quantum since both systems are initially at zero temperature. The system B has the same energy increase.

Now, we move on to finite temperature. To do so, we apply a temperature imbalance between the reservoirs and compute the energy flux. We restrict ourselves to the low temperature regime $\max(T_A, T_B) \ll \varepsilon_{\mathrm{F}}$ and times much less than the inverse temperature. This limitation naturally arises from the perturbative origin of the Fermi golden rule formula (2.16). Indeed, at high temperatures the
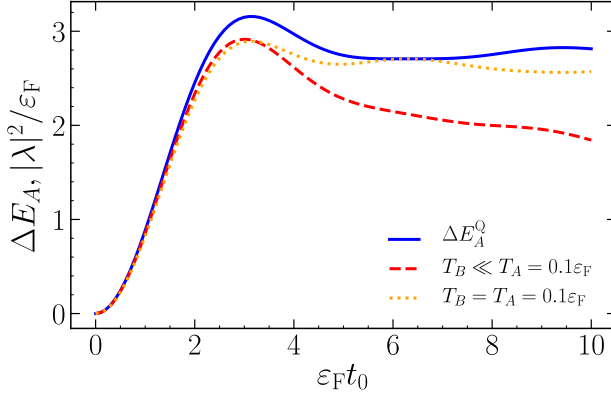
Figure 2.1. Energy increment in the reservoir A due to quench-coupling with the reservoir B as a function of time at low temperature. The energy increment at zero temperature $\Delta E_A^Q \simeq \frac{|\lambda|^2}{\varepsilon_{\mathrm{F}}} \left(\varepsilon_{\mathrm{F}} t_0\right)^2$ for $t_0 \ll 1/\varepsilon_{\mathrm{F}}$ and reaches its maximum value of $3.2\,|\lambda|^2/\varepsilon_{\mathrm{F}}$ at $t_m = \pi/\varepsilon_{\mathrm{F}}$, which is defined by the first zero of the energy flux (2.17).

dynamics in the integral (2.16) is set by $t \sim 1/\max(T_A, T_B) \ll 1/\varepsilon_{\mathrm{F}}$ but the energy flux formula itself is perturbative in $|\lambda|^2/\varepsilon_{\mathrm{F}}^2$. The neglected dynamics of the occupation numbers appears in higher order in $|\lambda|^2/\varepsilon_{\mathrm{F}}^2$. Therefore, once reaching the timescale of $t \sim 1/\max(T_A, T_B)$, the dynamics of the occupation numbers can not be considered slow and, hence, is no longer negligible. Still, consideration of small temperatures allows us to derive the energy dynamics perturbatively at the timescale $t \sim 1/\varepsilon_F \ll 1/\max(T_A, T_B)$. This logic applies to t_0, so that we disregard the thermalization of A and B while they are coupled.

We compute the energy flux (2.16) for $T_A = T \ll \varepsilon_{\mathrm{F}}$ and $T_B \ll T$ using the equilibrium occupation numbers $n_A(\omega) = \left(e^{\omega/T} + 1\right)^{-1}$ and $n_B(\omega) = \theta(-\omega)$. This realises a quantum cooling protocol for the reservoir A. Since A is at low temperature $T \ll \varepsilon_{\mathrm{F}}$, we use the Sommerfeld expansion

$$\int_{-\varepsilon_{\mathrm{F}}}^{\varepsilon_{\mathrm{F}}} d\omega \frac{F(\omega, t)}{e^{\omega/T} + 1} \simeq \int_{-\varepsilon_{\mathrm{F}}}^{0} d\omega F(\omega, t) + \frac{\pi^2 T^2}{6} F'(0, t), \qquad (2.19)$$

where $F'(0, t)$ denotes the frequency derivative of F at $\omega = 0$. Here the function $F(\omega, t) = \omega \int_{-\varepsilon_{\mathrm{F}}}^{\varepsilon_{\mathrm{F}}} d\omega' \frac{\sin\left(\omega - \omega'\right)t}{\omega - \omega'}$ has a well defined derivative $F'(\omega, t)$ in the considered energy interval, so that $F'(0, t) = 2 \int_{0}^{\varepsilon_{\mathrm{F}} t} d\zeta \frac{\sin \zeta}{\zeta}$. Finally, we reinstate the

result in Eq. (2.18) with a small temperature correction:

$$\Delta E_A = \Delta E_A^{\mathrm{Q}} - \frac{2|\lambda|^2}{3\varepsilon_{\mathrm{F}}} \left(\frac{\pi T}{\varepsilon_{\mathrm{F}}}\right)^2 \int_0^{\varepsilon_{\mathrm{F}} t_0} d\zeta \int_0^{\zeta} d\zeta' \, \frac{\sin \zeta'}{\zeta'}, \quad t_0 \ll 1/T. \qquad (2.20)$$

In Fig. 2.1 (the dashed curve) we demonstrate that the overall energy change in the reservoir remains positive. Remarkably, cooling down the system at temperature $T \ll \varepsilon_{\mathrm{F}}$ results in the energy increment of the refrigerated system if the system and the cold bath are coupled for $t_0 \sim 1/\varepsilon_{\mathrm{F}}$.

Finally, we can consider A and B at the same temperature $T_A = T_B = T \ll \varepsilon_{\mathrm{F}}$. We proceed the same way as above and use the Sommerfeld expansion (2.19) for both systems. This produces the energy increment

$$\Delta E_A = \Delta E_A^{\mathrm{Q}} - \frac{8|\lambda|^2}{3\varepsilon_{\mathrm{F}}} \left(\frac{\pi T}{\varepsilon_{\mathrm{F}}}\right)^2 \sin^2\left(\frac{\varepsilon_{\mathrm{F}} t_0}{2}\right), \quad t_0 \ll 1/T. \qquad (2.21)$$

The effect still persists when both systems evolve starting from thermal states, as seen in Fig. 2.1 (dotted curve).

In contrast to the subsystem's energy, the time-dependent correlations between the subsystems initialized at $t = 0$ are well defined by the von Neumann entropy of the corresponding subsystem. The von Neumann entropy of the subpart of a free fermion system is known to be expressed in terms of its occupation numbers $n_\alpha(\xi_p, t)$ [76, 77, 92]. The von Neumann entropy of the reservoir A is

$$S_{\mathrm{vN}}(t) = -\sum_p \Big(n_A(t, \xi_p) \ln n_A(t, \xi_p) + (1 - n_A(t, \xi_p)) \ln\big(1 - n_A(t, \xi_p)\big) \Big). \tag{2.22}$$

Within the accuracy of the Fermi golden rule formula (2.16), the entropy flux can be computed perturbatively in the lowest order in λ:

$$\frac{dS_{\mathrm{vN}}(t)}{dt} = -\sum_p \frac{dn_A(t, \xi_p)}{dt} \ln \frac{n_A(\xi_p)}{1 - n_A(\xi_p)}, \qquad (2.23)$$

where the distribution function inside the logarithm is taken in equilibrium. Using that $\langle H_A(t) \rangle = \sum_p \xi_p n_A(t, \xi_p)$ and $n_A(\xi_p)/(1 - n_A(\xi_p)) = \exp\big(-\xi_p/T_A\big)$, we notice that the entropy and the energy fluxes are related as $T_A dS_{\mathrm{vN}}(t)/dt = d\langle H_A(t) \rangle/dt$. Hence, when the systems are decoupled, we get

$$\Delta E_A = T_A \Delta S_{\mathrm{vN}}, \qquad (2.24)$$

that states that the overall energy change in A (2.20) is set by the amount of correlations the system acquired during the joint evolution of A and B. The

equation (2.24) resembles the lower energy bound in the energy-entropy balance equation (2.7) with zero relative entropy

$$S(\rho_A(t_0)||\rho_A) = 0. \tag{2.25}$$

The relative entropy (2.25) between the evolved and initial state of the reservoir A saturates the lower bound in Klein's inequality [21]. Within the accuracy of our perturbation theory, this means that at $t = t_0$ the evolved state $\rho_A(t_0)$ is indistinguishable from its initial thermal state ρ_A, despite that the reservoirs A and B were evolving together from $t = 0$ to $t = t_0$. The same holds for the reservoir B. Therefore, the correlations between A and B are erased at the moment of decoupling. However, $t = t_0$ is a special moment when, according to Eq. (2.12), the energy is not conserved. Indeed, all the energy acquired by both systems is transferred at the precise moment of decoupling. Using the correlation function (2.15), we derive

$$\frac{d\langle H(t)\rangle}{dt} = -\delta(t - t_0)\langle V_{AB}(t_0)\rangle = \delta(t - t_0)\left(\Delta E_A + \Delta E_B\right). \tag{2.26}$$

In our model the two systems become correlated at $t = 0$ and then are fully decoupled at $t = t_0$. At low temperatures, the amount of energy transferred to the system by the quench at $t = t_0$ is set by the von Neumann entropies of each system accumulated during joint evolution of A and B, which captures the correlations between A and B up to the moment of decoupling. The work produced by the quench $-\Delta E_A - \Delta E_B$ is utilized to erase the correlations between the reservoirs. The information about the erased correlations is stored in the energy increment of each subsystem. As we illustrate in Fig. 2.1, the energy increment of the subsystem is well-described by its quantum part ΔE_A^{Q} for a short quench protocol $t_0 \lesssim 1/\varepsilon_{\mathrm{F}}$ at low temperatures $\max(T_A, T_B) \ll \varepsilon_{\mathrm{F}}$. As such, we refer to $\Delta E_A^{\mathrm{Q}} + \Delta E_B^{\mathrm{Q}}$ as the binding energy of quantum correlations between A and B – the amount of energy required to erase the quantum correlations between the subparts of a quantum composite system.

2.4. Conclusion

In this paper, we discuss non-equilibrium dynamics in quantum composite systems in a thermodynamic framework. We consider two arbitrary quantum systems A and B at finite temperature instantaneously coupled together. We show that the energy of a subpart of a quantum composite system can be related to its entropy properties solely. Specifically, the energy change of the system A is set by the change of its von Neumann entropy and by the relative entropy between the evolved state of A and its initial thermal state.

We consider a quench protocol for the free fermion system, where *A* and *B* are described by non-interacting fermions. Starting with zero temperature limit, we show that the subsystem's energy increases in absence of charge or temperature imbalance. Proceeding to the finite temperature case, we find out that the energy increment is still present for the temperatures much less than the Fermi energy in the system. We demonstrate that the energy is transferred to the system in the moment of decoupling, while the amount of energy is given by change of the von Neumann entropy multiplied by the initial temperature. Here the decoupling quench acts as an external force which produces work to erase the correlations between *A* and *B*. Meanwhile, the von Neumann entropy accumulated during the joint evolution of *A* and *B* is stored in the corresponding energy increment. Hereby, we refer to this effect as an information to energy conversion.

During the final stage of preparing this manuscript, we have noticed a preprint by *Popovic et al.* [86], which shows that there is a heat transfer from the system described by a quantum pure state to the thermal bath at the moment of decoupling. This heat dissipation is argued to originate from an energetic cost for a decoherence process. We note a similar energy transfer in the coupling/decoupling protocol for quantum thermal states, where the system and the bath are described by non-interacting fermions at low temperature. We argue that the amount of energy accumulated by a subpart of a quantum composite system is set by the amount of correlations with the other subpart developed by the moment of decoupling.

The effect of information to energy conversion is quite generic for quantum composite systems and appears as long as the Hamiltonian of the system contains non-commuting parts. The conversion happens when the subpart of the system is separated from the rest of the system as a consequence of the energetic cost of decoupling. The fingerprints of this effect are also present in strongly-correlated systems. In Ref. [89], a quantum system where non-local random interaction is turned on/off by a quench increases its energy drastically after the interaction is off. At the same time, the entropy flux presented in this paper qualitatively explains the anomalous growth of the energy flux in the evaporating Sachdev-Ye-Kitaev quantum dot [15, 13]. This subject will be addressed in details as well as its relation to the recent studies of the evaporating black holes [93, 94, 95] in the upcomming article [96].

Acknowledgments

3 | Quenched cooling and the crossover from quantum to classical thermodynamics

3.1. Introduction

The notion of entropy is more involved in quantum systems than in classical systems as it also includes the information of potential entanglement with another set of dynamical degrees of freedom. This can be another system with which it is (weakly) coupled, the environment, or the measurement apparatus. In classical equilibrium thermodynamics, the change in the entropy is associated with heat flow according to the Second Law while quantum mechanically the entropy can be changed by the quantum correlations in the system that may or may not necessarily involve heat flow. The field of quantum thermodynamics specifically pursues this question how work, heat and entropy are affected by quantum correlations including entanglement; see e.g. [97, 98] for recent reviews. This field is growing rapidly, even though these many-body entanglement effects are still less well understood than entanglement and decoherence in few-qubit systems.

Here we take a quantum thermodynamics point of view on non-equilibrium dynamics in many-body systems with two theoretical models as example: the Sachdev-Ye-Kitaev (SYK) model and a mixed field Ising chain. The Sachdev-Ye-Kitaev model has a computable non-Fermi liquid ground state that is long-range many body entangled [39, 40]. Through the holographic duality between anti-de-Sitter quantum gravity and matrix large N quantum systems, such SYK models at finite temperature are also dual descriptions of black holes in anti-de-Sitter gravity [46]. Using this duality to study the profound question of black hole evaporation through Hawking radiation and its information flow [63, 94, 62, 65, 99], recent studies have considered the quenched cooling of a hot thermal SYK state (the black hole) suddenly being able to "evaporate" into a cooler or even $T = 0$ SYK state (the container for the evaporated radiation) [13, 15, 14].[1] A surprising finding from the perspective of classical thermodynamics has been that

---

[1]Early work on SYK quenches is [57]. For other aspects of SYK dynamics, see this and citations thereof.

these observe an initial energy *increase* [15, 13, 14, 100] in the hot subsystem, confirming results from preceding black hole evaporation studies [101]. It was argued, using Schwinger-Keldysh field theory, that many relativistic continuum field theories will exhibit such an energy increase in the hot system when quench coupling two thermal states [101, 15] even though a fundamental proof or understanding was missing. In particular, a quenched cooling between two two-level systems provides a counterexample [15].[2]

In a recent article, we showed that quantum thermodynamics [97, 98] provides the universal explanation for this counterintuitive rise [102]. In a quenched cooling protocol where a (hot) thermal quantum system with Hamiltonian H_A is brought into instantaneous contact with a (cooler) thermal reservoir at $t = 0$ through $H_{\text{total}} = H_A + H_B + \theta(t)H_{\text{int}}$, the change in the energy of the hot subsystem A equals

$$\Delta E_A(t) = T_A \Delta S_{\text{vN},A}(t) + T_A D(\rho_A(t)||\rho_{T_A}) \ . \tag{3.1}$$

Here $S_{\text{vN}} = -\text{Tr}(\rho_A \ln \rho_A)$ is the von-Neumann entropy of the reduced density matrix of the subsystem A: $\rho_A = \text{Tr}_B \rho$; the energy of the subsystem $E_A(t)$ is the expectation value of its subsystem Hamiltonian $E_A = \text{Tr} H_A \rho(t) = \text{Tr} H_A \rho_A(t)$; and $D(\rho_A(t)||\rho_{T_A}) = \text{Tr} \rho_A(t) \log\left(\rho_A(t)/\rho_{T_A}\right)$ is the relative entropy between the reduced density matrix of system A and the initial thermal density matrix of A at $t = 0$. The change $\Delta E(t) = E(t) - E(0)$ is with respect to the same quantity at $t = 0$. By symmetry an analogous relation holds for subsystem B.

As the relative entropy $D(\rho_A(t)||\rho_{T_A}) \geq 0$ is positive semi-definite, one arrives at an inequality that holds universally for any model Hamiltonian when such a quenched cooling protocol is considered

$$\Delta E_A(t) \geq T_A \Delta S_{\text{vN},A}(t) \ . \tag{3.2}$$

In a quantum system the von-Neumann entropy can have a significant contribution from quantum correlations including entanglement over and above the classical thermal entropy. As the quantum correlations between the system and the reservoir can only increase after a quench, the quantum thermodynamic inequality Eq.(3.2) can therefore force an associated *increase* in energy in system A even if its initial energy density was higher. Moreover, in perturbation theory to leading order the inequality saturates as the contribution of the relative entropy is subleading and one can use the equality as a way to measure the von Neumann entropy in a quenched cooling protocol through the energy difference [102].

A common view on non-equilibrium phenomena is that at the shortest time scales the system is extremely sensitive to microscopic information, details of the quench

---

[2]The thermal state of a two-level system is defined through its density matrix $\rho = \frac{1}{Z}\sum_n |n\rangle e^{-\beta E_n}\langle n|$ with $n = \downarrow, \uparrow$ and Z the appropriate normalization such that $\text{Tr}\rho = 1$.

protocol etc, and it is only the longest-time-scale-relaxation to equilibrium that is universal. Eq.(3.2) surprisingly shows that it need not be so: at the shortest possible non-equilibrium time scale there is still a notion of the first law that entropy is linked to energy, even though the standard first law in the absence of work $dE = TdS$ is relating state functions regarding equilibria.

This positive contribution due to quantum correlations to the von Neumann entropy is present in *any* quantum system, but our classical experience is that the energy in the hot system decreases directly upon contact because heat must flow from hot to cold. What must happen to restore this intuition that the energy in the hot system decreases instantaneously is that the positive quantum correlation- and entanglement- contribution can be overwhelmed by the semi-classical heat and information flow from hot to cold. By studying quenched cooling in SYK models, where entanglement is very strong, and one-dimensional mixed field Ising chains, where entanglement can be made very weak, we exhibit this. Classical experience is restored in a particle-like system at high temperatures where entanglement is weak.

3.2. Energy dynamics in quenched cooling

The setup we study consists of two initially independent quantum subsystems A and B with Hamiltonians H_A and H_B respectively. Initially ($t < 0$), each subsystem is prepared in a thermal state at temperature T_A and T_B, so the full system is in an uncorrelated product state:

$$\rho_0 = \rho_{T_A} \otimes \rho_{T_B}$$
$$\rho_{T_\alpha} = \frac{1}{Z_\alpha} e^{-H_\alpha/T_\alpha}, \quad \alpha = A, B. \tag{3.3}$$

We will study the behaviour of the subsystems when they are brought into instantaneous contact at $t = 0$ through an interaction Hamiltonian H_{int}. The complete setup is a closed system that evolves with the full Hamiltonian:

$$H_{\text{total}} = H_A + H_B + \theta(t) H_{\text{int}} . \tag{3.4}$$

Motivated by current results presented in the introduction, we focus our interest on two different models:

- Finite N Majorana SYK with each subsystem governed by the Hamiltonian

$$H_\alpha = i^{q/2} \sum_{j_1 \dots j_q = 1}^{N_\alpha} J_{j_1 \dots j_q}^\alpha \psi_{j_1}^\alpha \dots \psi_{j_q}^\alpha \qquad \alpha = A, B \tag{3.5}$$

where q is same for both dots and can be either $q = 2$ or $q = 4$, further labeled as SYK$_2$ and SYK$_4$ respectively. The couplings are drawn from a Gaussian distribution with the following parameters:

$$\langle J^\alpha_{j_1\dots j_q}\rangle = 0, \quad \langle J^\alpha_{j_1\dots j_q} J^\alpha_{j_1\dots j_q}\rangle = \frac{(q-1)!J^2}{N_\alpha^{q-1}}. \tag{3.6}$$

Those two SYK dots are coupled through a two Majorana tunneling interaction which couplings are also sampled from a Gaussian distribution:[3]

$$H_{int} = i\sum_{ij}^{N} \lambda_{ij}\psi_i^A\psi_j^B, \tag{3.7}$$

$$\langle\lambda_{ij}\rangle = 0, \quad \langle\lambda_{ij}^2\rangle = \frac{\lambda^2}{N_B}. \tag{3.8}$$

This system is analyzed with exact diagonalization and averaged over $R = 100$ different coupling realizations. To reduce the number of free parameters we take two equal size dots $N_A = N_B \equiv N$.

- The 1D mixed field Ising model, also analyzed using exact diagonalization, with a particle-like contact interaction:

$$H_\alpha = -\sum_i^{N_\alpha} \left(JZ_i^\alpha Z_{i+1}^\alpha + h_x X_i^\alpha + h_z Z_i^\alpha\right), \qquad \alpha = A, B \tag{3.9}$$

$$H_{\text{int}}^{(tunn.)} = -\lambda(X+iY)_{N_A}^A(X-iY)_1^B + h.c. \tag{3.10}$$

Dimensionful parameters are expressed in J, which is usually set to $J = 1$.

Fig. 3.1 shows the classically unexpected rise in energy in system A directly following the cooling quench with $T_A > T_B$ found in [13, 15]. We shall now show that even though E_A initially increases, there is no energy flux from the cold reservoir to the hot system. The energy increase instead follows from the energy contribution of the interaction Hamiltonian solely but it is nevertheless a real modification of energy, as a subsequent decoupling of A and B shows. At the moment of decoupling work must be performed on the combined system-reservoir as we shall show.

The above conclusions follows from the following observations in SYK systems:

1. Directly following the quench, the system-energy $E_A(t)$ and the reservoir-energy $E_B(t)$ *both* grow (Fig.3.2). The fact that there is no net energy flow from cold to hot means the energy must come from somewhere else.

---

[3]We have taken a variance in λ that is asymmetric in N_A and N_B to readily compare with [13, 15]. These authors chose this such that the interaction stays relevant in the large N_A limit.

Figure caption area with plot titled: $\text{SYK}_4 \, ; \, N = 10 \, ; \, T_A = 0.5J, \, T_B = 0.1 \, ; \, \lambda = 0.1J$

Legend: ΔE_A • $\Delta E_m = \Delta E_A(t_m)$
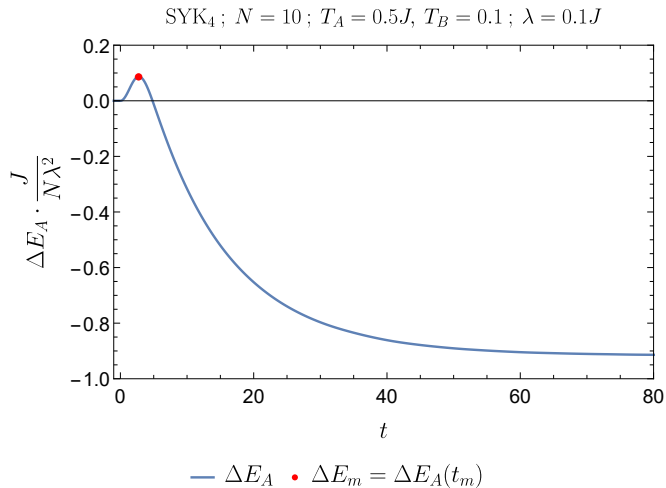
Figure 3.1. Normalized change of the energy of the hotter system A ($\Delta E_A = \text{Tr}\big((\rho_A(t) - \rho_{T_A})H_A\big)$ as a function of time. At short times it increases counter to intuition. Majorana SYK_4 in exact diagonalization averaged over $R = 100$ realizations with parameters of both systems on top of the plot. Red dot marks the bump that is reached at time t_m and has a height E_m relative to the initial energy.

2. The total Hamiltonian $H_{\text{total}} = H_A + H_B + \theta(t)H_{\text{int}}$ contains a third contribution H_{int}. Its contribution to the energy is negative (Fig.3.2).

3. The change in the expectation value in the total Hamiltonian is nevertheless readily computed to vanish.

$$\frac{d}{dt}\langle H_{\text{total}}\rangle = i\langle[H_{\text{total}}, H_{\text{total}}]\rangle + \delta(t)\langle H_{\text{int}}\rangle \tag{3.11}$$

The first term vanishes trivially. When $\langle H_{int}\rangle(0) = 0$ as well, as is the case in all the systems we study, then $\langle H_{total}\rangle$ is constant in time. The "binding"-energy from $E_{\text{bind}} = -E_{\text{int}}(t) = \text{Tr}\big(H_{\text{int}}\rho(t)\big)$ thus completely accounts for the rise in both $E_A(t)$ and $E_B(t)$.

4. More precisely, for $E_A(t)$ to correspond to a *measurable* energy change (in the sense of commuting with the Hamiltonian) one should decouple the system from the reservoir with a second quench at a finite time t_f later, as in the standard two-point measurement protocol in quantum thermodynamics [97, 98, 86]. Then H_A commutes again with the full Hamiltonian for $t > t_f$.[4]

---

[4]Formally, if one does not decouple, the eigenstates of H_{tot} are no longer localized within
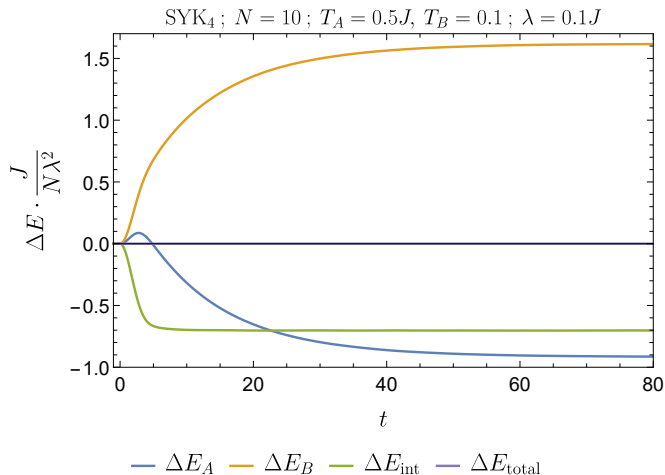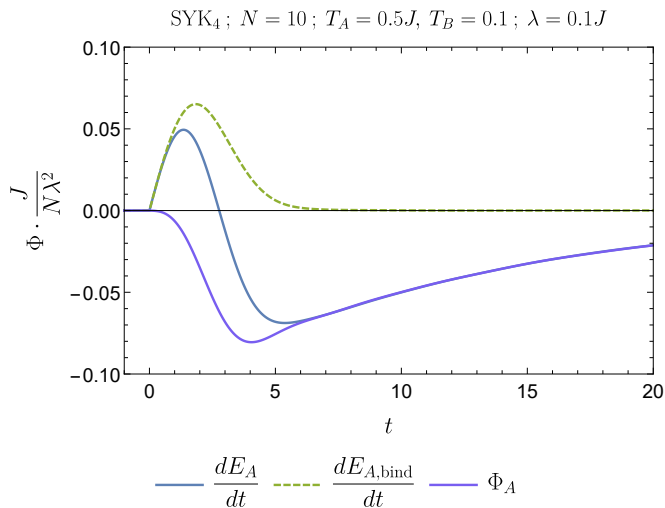
Figure 3.2. Normalized change of energy of the two subsystem A, B, the interaction energy $\Delta E_{\text{int}} = \text{Tr}\big((\rho(t) - \rho_0)H_{\text{int}}\big)$ and the total energy E_{total} as a function of time. Directly following the quench both the system-energy $E_A(t)$ and the reservoir-energy $E_B(t)$ grow, whereas the interaction energy $E_{\text{int}}(t)$ decreases. The sum vanishes as must be as no energy is put into the combined system/reservoir. Majorana SYK in exact diagonalization averaged over $R = 100$ realizations with parameters of both systems on top of the plot.

In other words, as in our previous article [102], one considers the two-quench protocol $H_{\text{total}} = H_A + H_B + (\theta(t) - \theta(t_f))H_{\text{int}}$. Computing the change in total energy, one clearly sees that the energy that must now be supplied equals the binding-energy $E_{\text{bind}} = -E_{\text{int}}(t_f)$.

$$\frac{d}{dt}\langle H_{\text{total}}\rangle = -\delta(t_f)\langle H_{\text{int}}\rangle \ . \tag{3.12}$$

Choosing t_f during the initial time period where both E_A and E_B increase, one concludes that for a two-point measurement protocol of such short duration the total energy in the system has increased. In particular there are initial configurations of T_A, T_B where the final equilibrium temperature after such a short-time two measurement protocol is larger than both T_A and T_B; see Fig.3.3. The decoupling quench must therefore perform work on the system.

A or B, and one cannot really say that the expectation value of H_A is the energy of the sub-system A. The expectation value of H_A nevertheless comes the closest and is therefore what is conveniently called the energy of this subsystem.
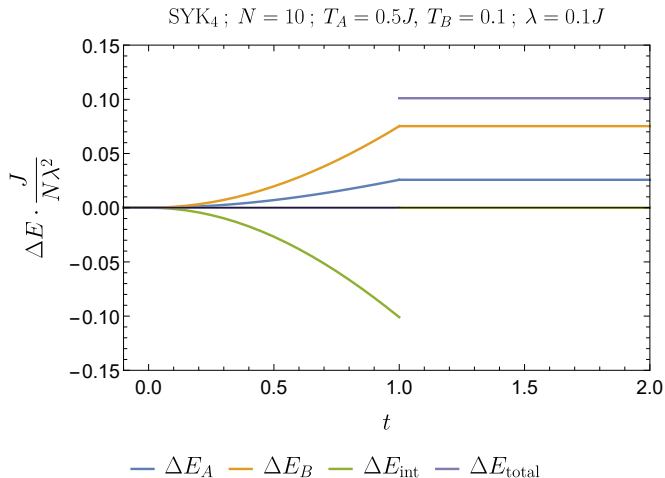
Figure 3.3. Normalized change of energy of the two subsystem A, B, the interaction energy $\Delta E_{\text{int}} = \text{Tr}\big((\rho(t) - \rho_0)H_{\text{int}}\big)$ and the total energy E_{total} as a function of time in a two-quench protocal with the interaction turned of at $t_f = 1$. At t_f the change in total energy shows the energy supplied to the system which exactly equals E_{int}. Majorana SYK in exact diagonalization averaged over $R = 100$ realizations with parameters of both systems are on top of the plot.

5. In general, since the whole system AB is closed, the total change in the energy of each subsystem, A or B, can be due to two components, the contribution from/debit to the "binding"-energy and the thermal exchange between A and B:

$$\Delta E_A = \Delta E_{A,bind} + \Delta E_{B \; to \; A} \tag{3.13a}$$

$$\Delta E_B = \Delta E_{B,bind} - \Delta E_{B \; to \; A}. \tag{3.13b}$$

We can estimate the binding energy for each subsystem A, B with respective initial temperatures $T_A \neq T_B$ separately from the interaction energy of a second quench experiment with an equal temperature setup $E_{\alpha,bind} \approx -\frac{1}{2}E_{\text{int}}(T_A = T_B = T_\alpha)$, i.e. we determine $E_{A,bind}$ from a quench set-up where both system and reservoir have initial temperature T_A, and $E_{B,\text{bind}}$ from a quench set-up where both system and reservoir have initial temperature T_B. Using this estimate in the quenched cooling set-up with different temperatures that are not too different we can numerically compute the

Figure 3.4 title: SYK$_4$; $N = 10$; $T_A = 0.5J$, $T_B = 0.1$; $\lambda = 0.1J$

Legend: $\dfrac{dE_A}{dt}$ $\dfrac{dE_{A,\mathrm{bind}}}{dt}$ Φ_A

Figure 3.4. Time derivatives of the energy E_A of subsystem A; time derivative of an estimate of binding energy contribution $E_{A,\mathrm{bind}}$ from considering an equal temperature quench ($T_A = T_B = 0.5J$), and the resultant thermal flux from cold reservoir B to hot system A. The flux is always negative and always flows from hot to cold. Majorana SYK in exact diagonalization averaged over $R = 100$ realizations with parameters of both systems on top of the plot.

thermal flux from B into A as

$$\Phi_A = \frac{d}{dt}E_{B \ to \ A} = \frac{1}{2}\left(\frac{d}{dt}E_A - \frac{d}{dt}E_B\right) - \frac{1}{2}\left(\frac{d}{dt}E_{A,bind} - \frac{d}{dt}E_{B,bind}\right). \tag{3.14}$$

The flux Φ_A is always negative and at early times it is subdominant to the binding energy Fig. 3.4. This proves that even when E_A increases initially, the energy flux/heat transport is nevertheless always from the hot system A to the cold reservoir B and the supplied energy for the increase comes solely from the binding-energy or the outside when decoupling A and B.

3.2.1. Energy rise driven by quantum correlations

As previewed in the introduction the quantity that controls this rise in energy E_A from the contribution of the "binding"-energy to the combined system-reservoir is the von Neumann entropy of the reduced density matrix of system A: $\rho_A(t) = \mathrm{Tr}_B\, \rho(t)$. To see this, consider the relative entropy between $\rho_A(t)$ and the initial

thermal density matrix

$$D(\rho_A(t)||\rho_{T_A}) = \text{Tr}\big(\rho_A(t)\ln\rho_A(t)\big) - \text{Tr}\big(\rho_A(t)\ln\rho_{T_A}\big) . \qquad (3.15)$$

Substituting that $\rho_{T_A} = \frac{1}{Z_A}e^{-\hat{H}_A/T_A}$ one immediately has

$$T_A D(\rho_A(t)||\rho_{T_A}) + T_A S_{\text{vN},A}(t) = E_A(t) - F_A . \qquad (3.16)$$

where $F_A = -\ln Z_A = E_A(0) - T_A S_A(0)$ is the free energy of the initial thermal state. The time-dependent terms form the definition of the *information free energy*

$$\mathcal{F}(t:T_A) = E_A(t) - T_A S_{\text{vN},A}(t) = F_A + T_A D(\rho_A(t)||\rho_{T_A}). \qquad (3.17)$$

It encodes the energy-available-for-work and its full counting statistics in open quantum systems that decohere due to their interaction with the environment. The loss of information due to decoherence and decorrelation costs work according the Landauer's principle and the information free energy accounts for that [97, 98].

The change in energy of system *A* after the quench directly follows from Eq.(3.16) and immediately brings us to Eq.(3.1).

$$\Delta E_A(t) = E_A(t) - E_A(0) = T_A \Delta S_{\text{vN},A}(t) + T_A D(\rho_A(t)||\rho_{T_A}),$$

and using the semi-positive definiteness of the relative entropy Eq.(3.2)

$$\Delta E_A(t) \geq T_A \Delta S_{\text{vN},A}.$$

Both the equality and the inequality are readily observed in exact diagonalization of Majorana SYK models, see Fig.3.5.

Two important remarks can be made:

1. As the relative entropy is very small at early times the initial rise in energy is completely determined by the rise in the von-Neumann entropy.[5]

2. This rise is even present when the reservoir *B* is at $T_B = 0$, as well as when the system and reservoir are at equal *T* (Fig.3.5). This unambiguously points to the growth of quantum entanglement as the contributing factor to the rise in the von-Neumann entropy; (see also [102]).
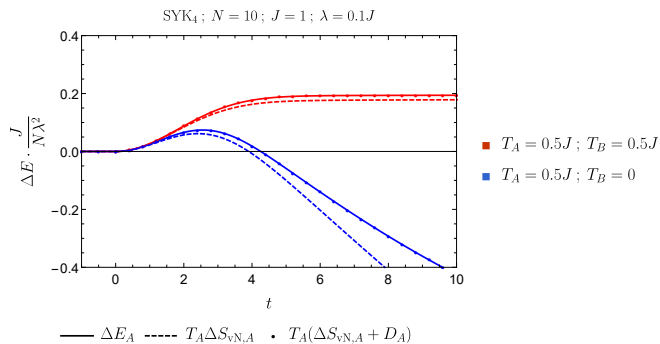
Figure 3.5. The energy E_A is verified to equal the sum of the von Neumann entropy $\Delta S_{\mathrm{vN},A}$ times the initial temperature T_A and the relative entropy $D_A \equiv D(\rho_A(t)\|\rho_{T_A})$. The initial rise in the energy in particular is controlled by the initial rise in the von Neumann entropy. This persists when the reservoir is in the groundstate $T = 0$ and at equal system-and-reservoir temperature $T_A = T_B$ pointing to entanglement as cause of the rise in von-Neumann entropy. Data from Majorana SYK in exact diagonalization averaged over $R = 100$ realizations with parameters on top of the plot.

Given that it is the von Neumann entropy growth that controls the early time dynamics between the two subsystem, it is natural to also consider the evolution of mutual information between the two:[6]

$$I(A:B,t) = S_{\mathrm{vN},A}(t) + S_{\mathrm{vN},B}(t) - S_{\mathrm{vN},A\cup B}(t) \;, \qquad (3.19)$$

where $S_{\mathrm{vN},A\cup B} = -\mathrm{Tr}_{A,B}\,\rho_{A\cup B}\ln\rho_{A\cup B}$ with $\rho_{A\cup B}$ being the density matrix of the full system. It displays two qualitatively distinct regimes: an initial polynomial increase followed by an exponentially decaying approach to equilibrium. Qualitatively, the early time $(t < t_m)$ behaviour of the mutual information re-

---

[5]Strictly speaking fine tuned initial conditions can exist where the von-Neumann entropy decreases, but decreases so little that the small rise in relative entropy nevertheless results in an energy increase in the hotter system.

[6]When the system and the reservoir have equal T, then

$$\Delta E_A(t) + \Delta E_B(t) = T\Delta I(A:B) + D(\rho_A(t)\|\rho_T) + D(\rho_B(t)\|\rho_T)) \;. \qquad (3.18)$$

since $\Delta S_{A\cup B}(t) = \Delta S_{\mathrm{total}}(t) = 0$ due to unitary evolution of the combined system-reservoir combination as a whole. In the early time regime where the relative entropies are very small, the combined energy change in A and B, equal to work needed at the moment of a decoupling quench, is then equal to the mutual information. This was first pointed out in [103] where it was shown that the minimum amount of noise to decorrelate two systems equals the mutual information. By Landauer's principle this is then also the minimal amount of work. Note, however, that the energy increase here is not directly related to decorrelation between A and B.

sembles the results reported in [104, 105] where mutual information was used as a better measure of quantum scrambling, compared to the OTOC. In particular these articles prove that $I(A : B)$ bounds the OTOC from above. This supports our deduction above that the initial energy increase is caused by quantum correlation- and/or entanglement-growth and scrambling. Note that the OTOC of operators between two quenched quantum dots depends on the initial state and interaction between the two dots, hence the early time polynomial increase in our setup. This should not be confused with the exponential growth of OTOC within a single SYK dot, which is driven by strong entanglement. The articles [104, 105] also emphasize the role of decoherence in addition to scrambling. It would be interesting to dissect and analyze their interplay further but we leave this for the future.
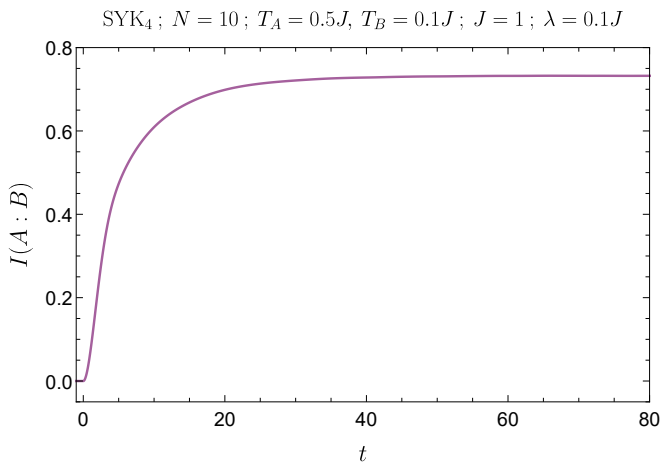
Figure 3.6. Growth of the mutual information between subsystems A and B.

3.3. The transition from quantum to classical cooling

At late times after the quench, the system behaves fully as expected in that the energy of the hotter system exponentially decreases until it equilibrates. Given that the initial rise of energy is controlled by the rise in entanglement driven von-Neumann entropy, there are two clear regimes: this initial rise and the late time relaxation (Fig.3.7). For the specific case of the quenched cooling two SYK dots, one can use the fact that large N SYK is exactly solvable to make analytic estimates for both these regimes as well as the intermediate regime and the long-time hydrodynamic tails which eventually change the relaxation to equilibrium from exponential to power law [15].
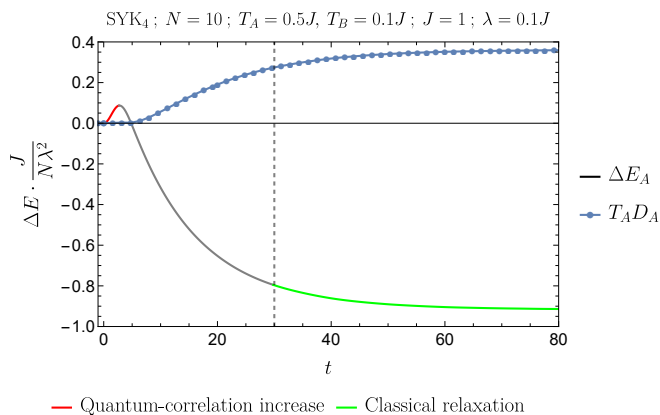
Figure 3.7. The generic contact quench is characterized by an early time quantum scrambling dominated regime (red) that transitions to a regime exhibiting conventional classical relaxation (green). The transitions between these regimes are not sharp, but roughly indicated by the top of the initial energy bump and the saturation of the relative entropy, where the final density matrix has become approximately thermal.

Here we ask a different question. Having argued that the initial rise is generically universally controlled by the rising quantum correlation contribution to the von-Neumann entropy, under what circumstances does the expected classical physics emerge, where heat immediately flows from hot to cold? The quantum correlation- and/or entanglement-growth is always present (except if the full system is purely classical where all the terms in the full Hamiltonian, including the coupling term, commute with each other). This can therefore only happen in circumstances where the "classical" relaxation overwhelms the quantum growth. Or more precisely, knowing that

$$\Delta E_A(t) \geq T_A \Delta S_{\text{vN},A}(t),$$

this transition can only happen if the "classical" thermal contribution to the von-Neumann entropy dominates over the entanglement contribution to the von-Neumann entropy already at the earliest possible time. From the atomic statistical mechanics underpinning of classical thermodynamics we know that this must happen when we have a theory with well defined particles with suppressed quantum correlations. This should be the case at high temperatures (weak coupling) and low densities.

However, when we study the high T ($T_A, T_B \gg J^2$ and $T_A \gg T_B$) regime in quenched cooling two SYK$_4$-dots, this disappearance of the initial rise and a

transition to immediate classical energy flow from hot to cold is not seen to emerge. This is even so when we extrapolate our finite size exact diagonalization result to the thermodynamic limit ($N \to \infty$) (with the assumption that the finite N studies do capture the appropriate large N behavior). Fig. 3.8 shows the height of the energy bump $E_m = E_{max} - E(t = 0)$ per particle (E_m/N) in the Majorana SYK$_4$ model directly before it starts to decrease as a function of the temperature T_A. Any finite N system will always contain quantum signatures and the classical behavior need only emerge in a thermodynamic limit. Numerics directly gives away that E_m has a leading scaling with N. Dividing this overall scaling out, a rough extrapolation to $N = \infty$ nevertheless shows that a positive energy bump remains.[7]

To try to find the crossover to expected classical behavior where the energy rise in the hot system is absent, we change the quenched cooling set-up from two SYK quantum dots to two mixed field Ising half-lines Eq. (4.18) with a tunneling interaction at the end point of each line Eq.(4.19). Both at the free $h_x = 0, h_z = 0$ [106] and at the conformal fixed point $h_x = 1, h_z = 0$ in the continuum (thermodynamic) limit one can use conformal field theory techniques to study this type of quenched cooling [107, 108, 109]. Then one indeed finds that there is no initial energy rise, but the energy starts to flow instantaneously from hot to cold. As is well known by now, in the regime $h = 0$ the late time behavior of the two subsystems, if isolated, is controlled by the large number of conserved charges and an associated generalized hydrodynamical relaxation towards a generalized Gibbs ensemble [110, 111]. The presence of the coupling term λ makes the full system not integrable.

Indeed for the case $h_x = 0$ ($h_z \neq 0$) there is for any system size an immediate energy decrease in the hot subsystem, as shown in Fig. 3.9 (top). This case is classical with only a small quantum tunneling between the two subsystems. For generic values of h_x and h_z, on the other hand, there is an initial rise in energy in accordance with the universal relation Eq.(3.2). The height of the energy bump (E_m) is now independent of N, due to the more local point-like interaction compared to the SYK non-local all-to-all tunneling. This suggests that the bump energy per particle (E_m/N) will vanish in the thermodynamic limit to match our classical intuition. However, instead of such a thermodynamic vanishing, we should expect that also a finite-size system exists where semi-classical hot-to-cold energy dynamics overwhelms the information-driven gain at short times. Indeed for a fixed temperature, we can estimate where the bump disappears, by extrapolating the E_m/N to large N. Now we see the foretold disappearance of the bump at a fixed finite temperature at a finite value of N, restoring our classical

---

[7]This turns out to also be true for SYK$_2$ models. Though within the random ensemble of SYK$_2$ couplings, there are empirically always realizations for which the energy E_A does decrease instantaneously.
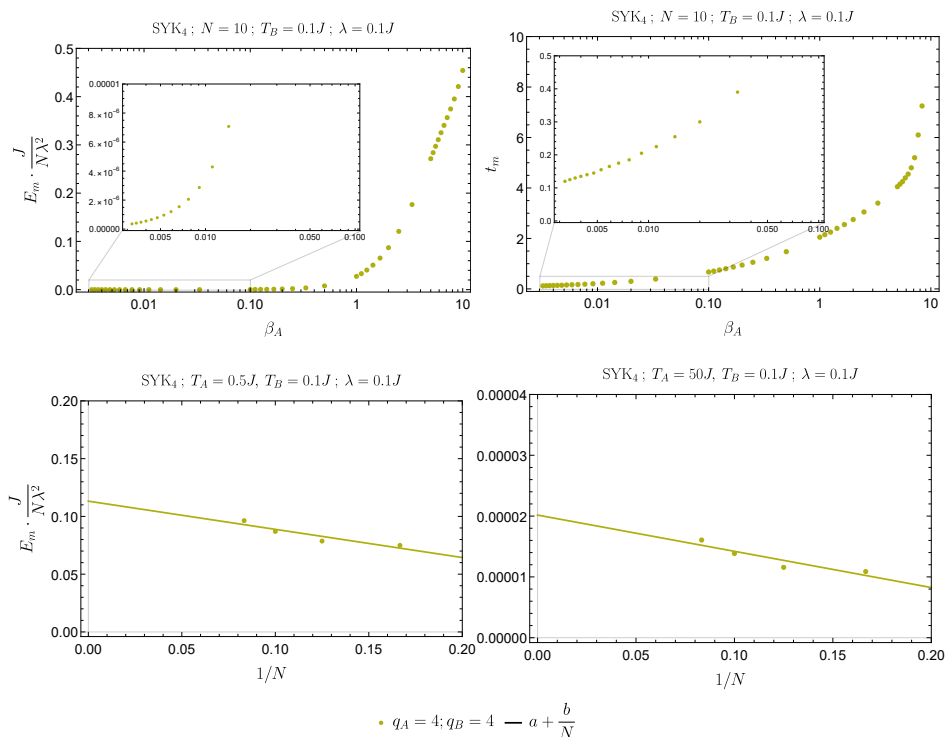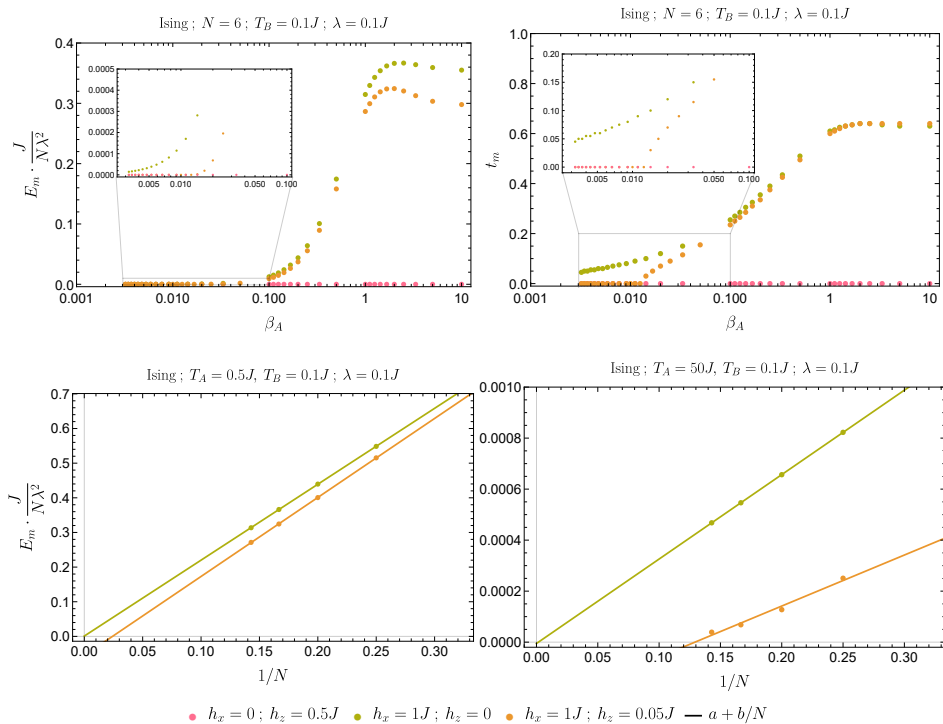
Figure 3.8. Quenched cooling of two SYK$_4$ dots. **Top:** Height E_m of the energy bump (left) and time t_m of the bump (right) for various initial temperatures $T_A = 1/\beta_A$. **Bottom:** Height E_m of the energy bump roughly extrapolated to larger N for two different initial temperatures β_A. The height stays finite in this thermodynamic limit, indicated by $a > 0$. Combining the top and the bottom, the initial rise in the hotter system energy E_A seems to persist for any finite T_A and infinite N.

intuition (Fig.3.9). An explicit finite N example is given in Fig.3.10. This finite N example shows that it is not simply the fact that the interaction is local and thus non-extensive in the thermodynamic limit, that causes it to vanish for higher temperatures.

The most interesting case is the conformal point of the Ising model (Fig. 3.9) (see also [112]). At exactly $h_x = 1, h_z = 0$ the bump only disappears by extrapolation to the continuum limit, similar to the SYK$_4$ results. This is still consistent with the earlier results on quenched cooling in conformal systems [107, 108, 109]. The absence of a bump found there relies on conformal symmetry which is only a true

Figure 3.9. Quenched cooling in two Ising half lines. **Top:** Height E_m of the energy bump (left) and time t_m of the bump (right) in for various parameter choices. **Bottom:** Height E_m of the energy bump extrapolated to larger N for various initial temperatures $T_A = 1/\beta_A$. For each initial temperature there is a finite extrapolated value of N for which the bump disappears ($a \leq 0$) and the system will cool instantaneously upon contact. The higher the initial temperature, the lower is this value of N.

symmetry in the continuum limit. At the same time for any finite size quantum system at low T, there appears to always be a small but non-zero counterintuitive initial rise. The bump is a correlation driven effect, as a simple ballistic collision model based on the Boltzmann equation will never have an initial energy rise in the hot system [106].[8] The correlation can still be either quantum or classical statistical. In the latter case, this classical statistical two-particle correlation

---

[8]Perhaps the easiest way to see this is to realize that the quenched cooling protocol is the quantum version of the Riemann problem in hydrodynamics. In hydrodynamics one assumes local equilibrium and thus an absence of correlations between different spatial points at distances larger than the local mean free path.
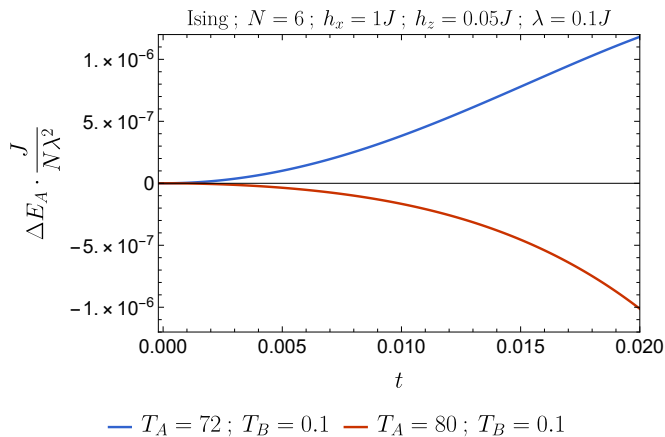
Figure 3.10. Quenched cooling in two Ising half lines. For $T < T_c \simeq 77.845J$ one still observes the initial rise in the hotter system A, but for $T > T_c$ one transitions to a regime where classical intuition is restored and the system cools instantaneously upon contact.

(the two-particle distribution function) vanishes in the thermodynamic limit in accordance with the assumption of molecular chaos.

In summary, classical thermodynamics — or rather hydrodynamics as we are studying time-dependent processes — emerges in the quasi-particle (high temperature low density) limit with a non-extensive interaction between system and reservoir and after taking the thermodynamic limit. The converse is that in quantum systems the initial rise in energy in the hot system that undergoes quenched cooling is robust and generic, though not required, and universally explained by Eq.(3.1).

3.4. Conclusion

In this manuscript, we have analyzed the origins of the observed counter-intuitive early time energy increase in hotter systems quench-coupled to a cooler reservoir in quantum simulations. Our numerical study of Majorana SYK$_4$, using exact diagonalization demonstrates that the early time energy behaviour is proportional to the increase of the von Neumann entropy and is not related to a thermal flux from the cold to the hot system, demonstrating the quantum nature of this phenomenon. The energy increase is counterbalanced by the negative interaction potential (expectation value of the tunneling term in the Hamiltonian). In the setup here, the coupling quench does not supply energy into the system and the

total energy is conserved. The same potential sets the amount of work needed to decouple the systems at given later time.

This peculiar phenomenon is well explained by the quantum non-equilibrium extension of the first law of thermodynamics Eq.(3.1) where the relative entropy $D(\rho(t)||\rho_T)$ plays a crucial role. Starting from a thermal state $D(\rho(t=0)||\rho_T) = 0$ and using the positive semi-definiteness $D(\rho(t)||\rho_T) \geq 0$ the von Neumann entropy, scaled by the initial temperature, then sets a lower bound on the energy in each subsystem (3.2). This links the observed energy increase even in the hotter subsystem to an increase of the von Neumann entropy. Moreover, at sufficiently early times the change of the relative entropy is negligible compared to the energy which has two interesting consequences. Firstly, the early time evolution of the energy is almost directly proportional to the von Neumann entropy as we emphasized in our earlier paper [102]; this provides a way to measure (dynamical) entanglement between two subsystems.[9] Secondly, it proves that the initial thermal state isn't instantaneously destroyed, hence the initial energy rise is not related to a temperature increase.

The universality of this bound gives rise to an even more puzzling question: Why is such an energy increase not commonly encountered in our daily life? The reason lies in the quantum nature of this phenomenon. We show that at high temperatures in weakly interacting quasi-particle systems the height of the bump is suppressed and the time it crests gets very short. In the thermodynamic limit it vanishes altogether, making it essentially unnoticeable at everyday macroscopic scales. As our results for SYK and the conformal point of the mixed field Ising model show, the more quantum mechanical the system is the closer one must push to the continuum quasiparticle limit for this bump to disappear and classical intuition to be restored. By extrapolation of our numerical simulation this is only ever possible to achieve in the strict thermodynamic limit.

This energy increase of the hotter system defies our intuition and understanding of classical thermodynamics but, as demonstrated here, it is well in accord with the laws of quantum thermodynamics.

There are three notable considerations that follow: There has been an substantial amount of research in the past few years on the out-of-time-ordered correlation function as a probe of classical and quantum chaos resulting in information exchange, scrambling and entropy growth (see e.g. [113]). The standard wisdom is that this information flow is separate and faster than energy flow, because the latter is constrained by a conservation equation, as recalled for instance in [114].

---

[9]As the relative entropy is a measure of how distinguishable two states are, extremely small relative entropy means that at early times the subsystem is nearly indistinguishable from its initial thermal state implying that the energy increase is not related to a temperature rise, contrary to what was suggested in other papers [13, 15].

The result here and particular the inequality Eq.(3.2) shows that this information flow, even though it is faster, must always drag some energy with it.

Secondly, one of the motivations to study SYK quenched cooling has been the equivalence with black hole evaporation through the holographic AdS/CFT correspondence. Because the evaporation of the black hole must expose the information behind the horizon, the quench can be modeled in the black hole context by a negative energy shock wave [44, 101], which shrinks the horizon upon contact. The result here shows that at very early times (before the shock hits the horizon in global time), there should be an interesting connection between the Ryu-Takayanagi entanglement surface encoding the von-Neumann entropy and the dynamics of the energy wavefront that holographically encodes Eq.(3.2).

Finally, as already emphasized in [102], the inequality Eq.(3.2) saturates in perturbation theory and can therefore be used in quenched cooling of weakly coupled systems to probe the von-Neumann entropy. Moreover, this is a universal result in the short time scale regime which is normally considered too sensitive to peculiar details of the experimental set-up and the system to be of interest. It invites an experimental measurement of this universal way the von-Neumann entropy determines the energy response.

Acknowledgements

3.A. Numerical Disorder Averaging

Disorder averaging of observables $O(t)$ in an SYK system was computed by numerically evaluating their evolution R-times $(O^i(t), \quad i \in \{1, 2, \cdots R\})$, for R SYK Hamiltonians drawn from the same distribution, and then computing the average at each time point:

$$O(t) = \frac{1}{R} \sum_i^R O^i(t) \tag{3.20}$$

Below, we present descriptive plots of the energy Fig.3.11 (top row) and entropy (bottom row) of system A where one can see 30 different realizations (gray) of the respective observable and the disorder averaged analog (blue) obtained from by disorder averaging over $R = 100$ realizations.
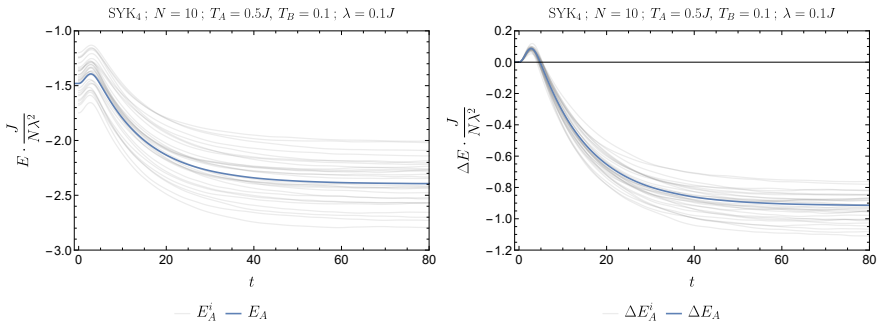
Figure 3.11. Different realizations of the energy (gray) and the disordered averaged energy (blue) obtained from averaging over $R = 100$ realizations. The left plot is the energy of system A, and the right plot is the same energy with the initial value subtracted $\Delta E_A(t) = E_A(t) - E_A(t = 0)$.

Additionally, one can compute the confidence interval of an averaged observable $O(t)$ (3.20), depicted as colored bands in Figure 3.13, with the following relation:

$$O(t) \pm z \frac{\sigma_{O(t)}}{\sqrt{R}} \tag{3.21}$$

where z is the normal distribution score (e.g. $z = 3$ results in a 3σ, or equivalently 99.7%, confidence interval) and $\sigma_{O(t)}$ is the standard deviation of the observable:

$$\sigma_{O(t)} = \sqrt{\frac{1}{R-1} \sum_i^R \left(O^i(t) - O(t)\right)^2}. \tag{3.22}$$

Next, Fig. 3.12 depicts the same averaging procedure but for the entropy.
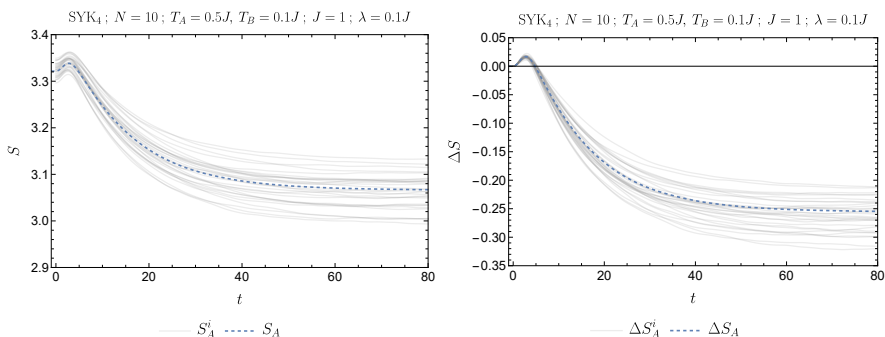
Figure 3.12. Different realizations of the entropy (gray) and the disordered averaged entropy (blue) obtained from averaging over $R = 100$ realizations. The left plot is the entropy of system A, and the right plot is the same entropy with the initial value subtracted $\Delta S_A(t) = S_A(t) - S_A(t = 0)$.

3.B. Reduced Number of Inter-dot Interacting Majoranas

In the initial phase of the project, we were not aware if and why the bump would always appear when the quench is between two SYKs at different temperatures. The analytical proof, presented here in Chapter 4, that this is always the case came much later. In the meantime, we had analyzed if excessive temperature gradients between the two subsystems (e.g. $T_A = 1000$ and $T_B = 0.1$), or reducing the number of Majoranas that participate in the inter-dot interaction ($P < N$), might lead to a disappearance of the bump in the hotter system, however, the initial energy rise was always present. While it now seems trivial, thanks to (4.15), here we present some legacy results in Figure 3.13 that reinforced our motivation to look for the analytical explanation of this phenomenon.

Even though we tested much higher temperatures the outcome was always the same hence, for clarity in the plot, we show results from a setup where the initial temperatures of the two SYKs are $T_A = 250$ and $T_B = 0.1$. They are quench coupled at $t = 0$ with the same protocol that's been described before, the only difference here is that the number of Majoranas (P) that participate in the interaction Hamiltonian can be varied:

$$H_{int} = i \sum_{ij}^{P} \lambda_{ij} \psi_i^A \psi_j^B, \tag{3.23}$$

As is obvious from Figure 3.13 the energy of the hotter system initially increases

even at very high temperature gradients. Additionally, although the increase is slower when only a few Majoranas couple the two dots ($P < N$), qualitatively the energy bump appears even in the extreme case of a single coupling between the SYKs.
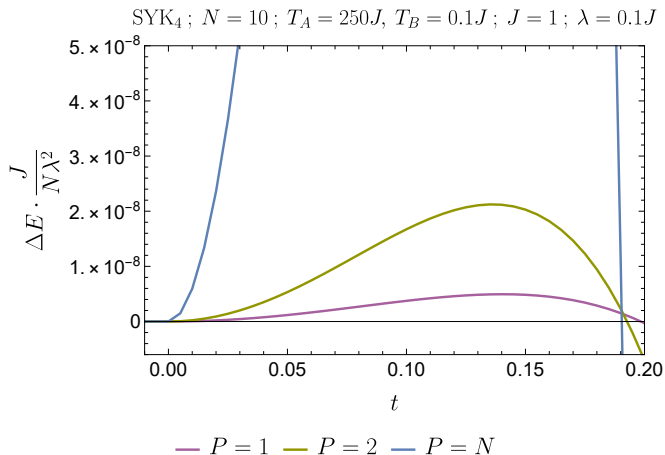
Figure 3.13. Early time energy evolution of an SYK system ($T_A = 250$), when it is quenched coupled to another colder SYK ($T_B = 0.1$) with the interaction Hamiltonian (3.23). Three different scenarios are presented, when only one ($P = 1$), two ($P = 2$), and all $P = N$ Majoranas from each dot participate in the interaction between the two SYKs.

3.C. SYK Hamiltonians and Late Time Thermalisation

When the quench between two SYK systems is analyzed, for each realization, the two Hamiltonians (H_A and H_B) are drawn separately, even when they have the same parameters $q_A = q_B = q$, $J_A = J_B = J$ and $N_A = N_B = N$. This way, even though the two systems have identical dynamics after disorder averaging they still differ, not only on a single realization but also when the disorder averaging is performed on a finite number of realizations R. This difference is especially prominent in the post-quench thermalization of two SYK systems at late, but finite, times when finite system sizes are considered, as is the case with the exact diagonalization numerical studies in this thesis. For example, looking into the disorder averaged late time energies of two SYKs ($q = 4$, $J = 1$, and $N = 12$) that are quench coupled from temperatures $T_A = 0.5$ and $T_B = 0.01$, one expects

they thermalize at the same value. However, looking into their time evolution Figure 3.14 (blue and yellow lines) seems like they saturate at different energies, although within one standard deviation of each other. It is worth noting that the higher temperature of system A doesn't precondition its saturation at higher energy, since that varies with each realization and there certainly are realizations where the initially colder system B saturates above the energy of A, see gray lines in Figure 3.14.
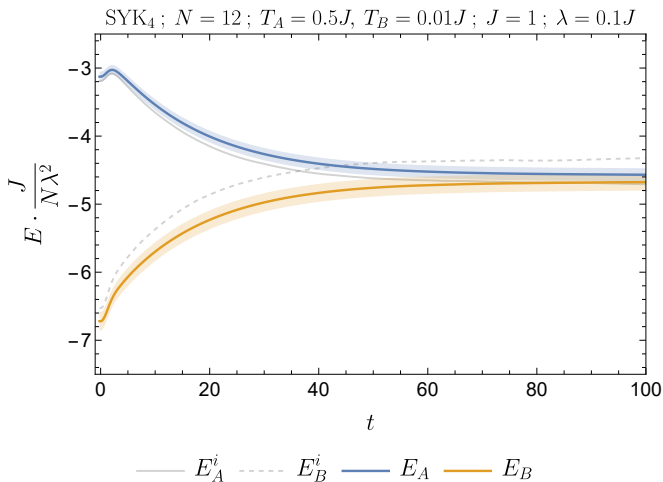
Figure 3.14. Energy and 99.7% confidence interval bands (3.21) of the disorder averaged energies of system A (blue) and B (yellow), computed with $R = 60$ realizations. At late times, when the system thermalizes, the two energies do not exactly match but get close to each other within their 3σ confidence interval. Additionally, the energies of the systems, full and dashed gray lines respectively, are presented for a single realization which was particularly chosen to demonstrate that for some combination of couplings the initially colder system B can thermalize at a higher energy than the hotter system A.

We tested our hypothesis, that the difference in the averaged energies of systems A and B is coming from the limited number of realizations R, as well as the finite system size N, and results are presented in Figure 3.15. There we study the dependence of the energy difference $(E_A(t = 100) - E_B(t = 100))$ at time $t = 100$ as a function of the number of realizations R that the average is computed with 3.20. Additionally, we analyze the dependence on the size of the SYK dot by repeating the same exercise for SYKs with different numbers of Majoranas N. As can be clearly seen from Figure 3.15 the two energies are coming closer and closer as one considers more and more realizations. Additionally, the difference

drastically decreases when the number of Majoranas, in each of the dots, increases from 8 to 10 and then to 12. This confirms that when $R \to \infty$ and $N \to \infty$, at late times, the two energies will be indistinguishable, in line with the large N results. Note that, since analyzing systems with $N = 12$ is computationally expensive, we have evaluated the energy difference only for up to $R = 60$ realizations. However, even this is enough to see that the system size plays a crucial role in the late time thermalization.
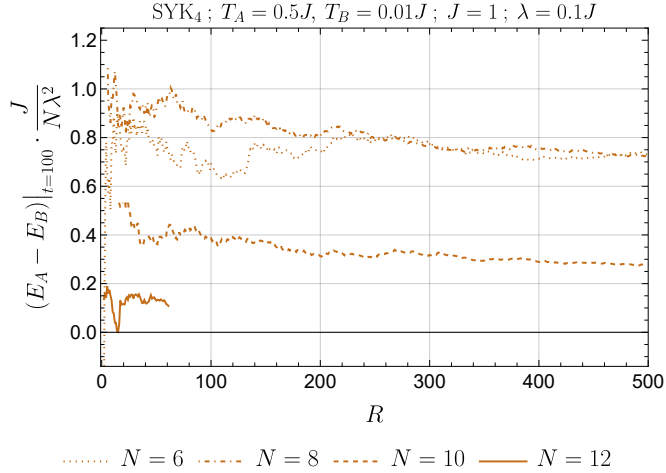
Figure 3.15. Dependence of the difference between the averaged energies of the two systems at $t = 100$ as a function of the number of realizations used in the disorder averaging procedure. To test the dependence on the system size we analyzed the same quantity for SYK dots with $N = 6, 8, 10$ and12 Majoranas in each. Limited by the CPU time when evaluating systems with $N = 12$ Majoranas we have computed the energies for only 60 realizations.

4 | Early post-quench perturbative expansion

4.1. Early time expansion

We study the early time evolution of two, initially independent, subsystems (A and B) after coupling them with an instantaneous quench at $t = 0$:

$$\hat{H}(t) = \hat{H}_A \otimes \mathbb{1}_{d_B} + \mathbb{1}_{d_A} \otimes \hat{H}_B + \theta(t)\hat{H}_{int} \tag{4.1a}$$

$$\hat{H}_{int} = \sum_{IK} \lambda_{IK} \, \hat{\Psi}_I \otimes \hat{\Gamma}_K \tag{4.1b}$$

Before the quench ($t < 0$), each subsystem is governed by the Hamiltonians $\hat{H}_A$ and $\hat{H}_B$ respectively, and the identity matrix action on the complementary Hilbert space encodes their independence. The subscript on the identity operators indicates the dimensionality of the respective Hilbert space: $d_A = \dim\mathcal{H}_A$ and $d_B = \dim\mathcal{H}_B$. Initially, we consider a generic interaction Hamiltonian $\hat{H}_{int}$ (4.1b), given in a tensor-product basis of the individual Hilbert spaces $\hat{\Psi}_I \in \mathcal{H}_A$ and $\hat{\Gamma}_K \in \mathcal{H}_B$ and later we will demonstrate our results on two specific models, SYK and Mixed Field Ising.

Before the quench, the whole system is prepared in a tensor product state of the two individual subsystems:

$$\rho_0 = \rho_A \otimes \rho_B, \tag{4.2}$$

and the post-quench time evolution is given by the unitary transformation with the full interacting Hamiltonian which can be expanded as a time series with operator-valued coefficients $\hat{R}_n$:

$$\rho(t) = e^{-iHt}\rho_0 e^{iHt} = \left(1 - iHt - \frac{1}{2}H^2 t^2 \dots\right)\rho_0\left(1 + iHt - \frac{1}{2}H^2 t^2 \dots\right) =$$

$$= \sum_{n=0}^{\infty} \frac{t^n}{n!}\hat{R}_n$$
$$\tag{4.3a}$$

$$R_0 = \rho_0 \quad ; \quad \hat{R}_{n+1} = i[\hat{R}_n, \hat{H}] \tag{4.3b}$$

By explicitly computing the first few terms in the expansion (4.3a), a recursive relation appears that determines all of the $\hat{R}_n$ operators (4.3b). However, in this letter, we are interested in the evolution of the reduced density matrices which, similarly to ρ, can be expressed as a time series by simply tracing out the complementary subsystem from $\hat{R}_n$. So, to obtain the reduced density matrix $\rho_A(t)$ of subsystem A one traces out the subsystem B, and tracing out subsystem A yields $\rho_B(t)$.

$$\rho_A(t) = \text{Tr}_B(\rho(t)) = \sum_{n=0} \frac{t^n}{n!} \hat{A}_n \quad ; \quad \hat{A}_n = \text{Tr}_B(\hat{R}_n) \tag{4.4a}$$

$$\rho_B(t) = \text{Tr}_A(\rho(t)) = \sum_{n=0} \frac{t^n}{n!} \hat{B}_n \quad ; \quad \hat{B}_n = \text{Tr}_A(\hat{R}_n) \tag{4.4b}$$

Once the reduced density matrices are obtained, we can compute the time evolution of any observable in each individual subsystem, for example the behavior of the energy $E_A(t)$ is:

$$E_A(t) = \text{Tr}_A(\rho_A(t)\hat{H}_A) = \sum_{n=0}^{N} \frac{t^n}{n!} \text{Tr}_A(\hat{A}_n \hat{H}_A) = \sum_n \frac{e_n}{n!} t^n. \tag{4.5}$$

Despite the compactness of the expansion, evaluating the operators $\hat{R}_n$ and subsequently $\hat{A}_n$ or $\hat{B}_n$ is rather tedious for $n > 2$, so we will restrict our study to only the second-order expansion of the energy of the subsystem A:

$$E_A(t) = \text{Tr}_A(\rho_A(t)\hat{H}_A) = e_0 + e_1 t + \frac{e_2}{2} t^2 + \mathcal{O}(t^3) \tag{4.6}$$

The particular initial states we are interested in — thermal or energy eigenstates — commute with their respective Hamiltonians (e.g. $[\rho_A(0), H_A] = 0$) leading to many vanishing terms in the coefficients $\hat{A}_n$ (4.7), when compared to the coefficients from a general state (4.28). We will drop the time $t = 0$ argument $\rho_A(0)$ from here on, and implicitly will mean the density matrix at $t = 0$ when no argument is given $\rho_A \equiv \rho_A(0)$.

$$\hat{A}_0 = \rho_A; \tag{4.7a}$$

$$\hat{A}_1 = i \sum_{IK} \lambda_{IK} [\rho_A, \hat{\Psi}_I] \, \text{Tr}_B(\rho_B \, \hat{\Gamma}_K); \tag{4.7b}$$

$$\hat{A}_2 = i^2 \left\{ \sum_{IK} \lambda_{IK} [[\rho_A, \hat{\Psi}_I], \hat{H}_A] \, \text{Tr}_B(\rho_B \, \hat{\Gamma}_K) + \right.$$

$$+ \sum_{IK} \sum_{K'I'} \lambda_{IK} \lambda_{I'K'} \left([\rho_A \hat{\Psi}_I, \hat{\Psi}_{I'}] \, \text{Tr}_B(\rho_B \, \hat{\Gamma}_K \, \hat{\Gamma}_{K'}) - \right. \tag{4.7c}$$

$$\left. \left. - [\hat{\Psi}_I \, \rho_A, \hat{\Psi}_{I'}] \, \text{Tr}_B(\rho_B \, \hat{\Gamma}_{K'} \, \hat{\Gamma}_K) \right) \right\};$$

Additionally, when studying the time evolution of observables that commute with the Hamiltonian the coefficients in their expansion simplify even further. This condition is trivially satisfied for the energy of the subsystem $E_A(t)$ and using the relation (4.40) we can compute the first three coefficients:

$$e_0 = \text{Tr}_A(\rho_A \hat{H}_A) \equiv E_A(0) \tag{4.8a}$$

$$\begin{aligned}
e_1 =& i \sum_{IK} \lambda_{IK} \, \text{Tr}_A\left([\rho_A, \hat{\Psi}_I] \hat{H}_A\right) \text{Tr}_B(\rho_B \, \hat{\Gamma}_K) = \\
=& i \sum_{IK} \lambda_{IK} \, \text{Tr}_A\left([\hat{H}_A, \rho_A] \hat{\Psi}_I\right) \text{Tr}_B(\rho_B \, \hat{\Gamma}_K) = 0;
\end{aligned} \tag{4.8b}$$

$$\begin{aligned}
e_2 =& i^2 \Bigg\{ \sum_{IK} \lambda_{IK} \, \text{Tr}_A\left([[\rho_A, \hat{\Psi}_I], \hat{H}_A] \hat{H}_A\right) \text{Tr}_B(\rho_B \, \hat{\Gamma}_K) + \\
&+ \sum_{IK} \sum_{I'K'} \lambda_{IK} \lambda_{I'K'} \Bigg(\text{Tr}_A\left([\rho_A \, \hat{\Psi}_I, \hat{\Psi}_{I'}] \hat{H}_A\right) \text{Tr}_B(\rho_B \, \hat{\Gamma}_K \, \hat{\Gamma}_{K'}) - \\
&- \text{Tr}_A\left([\hat{\Psi}_I \, \rho_A, \hat{\Psi}_{I'}] \hat{H}_A\right) \text{Tr}_B(\rho_B \, \hat{\Gamma}_{K'} \, \hat{\Gamma}_K) \Bigg) \Bigg\} = \\
=& i^2 \Bigg\{ \sum_{IK} \sum_{I'K'} \lambda_{IK} \lambda_{I'K'} \Bigg(\text{Tr}_A\left(\rho_A \, \hat{\Psi}_I [\hat{\Psi}_{I'}, \hat{H}_A]\right) \text{Tr}_B(\rho_B \, \hat{\Gamma}_K \, \hat{\Gamma}_{K'}) \\
&- \text{Tr}_A\left(\rho_A [\hat{\Psi}_{I'}, \hat{H}_A] \hat{\Psi}_I\right) \text{Tr}_B(\rho_B \, \hat{\Gamma}_{K'} \, \hat{\Gamma}_K) \Bigg) \Bigg\}.
\end{aligned} \tag{4.8c}$$

Naturally, the time-independent contribution e_0 is equal to the pre-quench energy and the first term is zero due to the aforementioned vanishing commutators. Therefore, we need to determine only the e_2 term, which is presented in the next section for two specific models.

4.2. Examples

In this section, we derive the early time evolution of the energy $E_A(t)$, to the second order in time, for two models the SYK_4 and Mixed Field Ising model (MFI). The analytical expressions help us understand why the energy bump in the SYK_4 happens for any temperature T_A, and provide an insight into the emergence of the critical temperature $T_c(h_x, h_z)$ in the MFI that marks the disappearance of the energy bump for $T_A > T_c$.

4.2.1. SYK

First, we consider two, initially decoupled SYK dots of size N_A and N_B governed by the following Hamiltonians:

$$\hat{H}_A = -\sum_{j=1}^{N_A} J^A_{j_1,j_2,j_3,j_4} \hat{\psi}_{j_1} \hat{\psi}_{j_2} \dots \hat{\psi}_{j_4} \quad ; \quad \hat{H}_B = -\sum_{l=1}^{N_B} J^B_{l_1,l_2\dots l_4} \hat{\chi}_{l_1} \hat{\chi}_{l_2} \hat{\chi}_{l_3} \hat{\chi}_{l_4} \quad (4.9)$$

$$\langle J^\alpha_{j_1,j_2,j_3,j_4} J^\alpha_{j_1,j_2,j_3,j_4} \rangle_J = \frac{J_\alpha^2}{N^3}, \quad \alpha \in \{A,B\} \quad (4.10)$$

We prepare the system in a tensor product state (4.2) then, at $t = 0$, we quench couple both SYKs with a two-point interaction Hamiltonian with random interactions:

$$\hat{H}_{int} = i \sum_{ij} \lambda_{ij} \hat{\psi}_i \hat{\gamma}_c \otimes \hat{\chi}_j \quad (4.11a)$$

$$\langle \lambda_{ij} \lambda_{i'j'} \rangle_\lambda = \frac{\lambda^2}{N_B} \delta_{ii'} \delta_{jj'} \quad (4.11b)$$

Here, $\hat{\gamma}_c$ is proportional to the product of all Majorana fields in A and, as explained in Appendix 4.B, it is necessary for proper anti-commutation relations between the two subsystems. Substituting this interaction Hamiltonian in (4.8) we get the second order coefficient of $E_A(t)$:

$$e_2 = i^4 \sum_{ii'}^{N_A} \sum_{jj'}^{N_B} \lambda_{ij} \lambda_{i'j'} \bigg(\text{Tr}_A \left(\rho_A \hat{\psi}_i \hat{\gamma}_c [\hat{\psi}_{i'} \hat{\gamma}_c, \hat{H}_A] \right) \text{Tr}_B (\rho_B \hat{\chi}_j \hat{\chi}_{j'}) - $$
$$- \text{Tr}_A \left(\rho_A [\hat{\psi}_{i'} \hat{\gamma}_c, \hat{H}_A] \hat{\psi}_i \hat{\gamma}_c \right) \text{Tr}_B (\rho_B \hat{\chi}_{j'} \hat{\chi}_j) \bigg). \quad (4.12)$$

For SYK-like interactions, the coefficients e_n simplify even further upon disorder-averaging which, due to the independence between the inter-dot and intra-dots couplings, can either be averaged simultaneously or one after the other. Here, we

take the latter route and initially average e_2 over the inter-dot coupling λ_{ij}:

$$
\begin{aligned}
\langle e_2 \rangle_\lambda =& \frac{\lambda^2}{N_B} \sum_i^{N_A} \bigg(\mathrm{Tr}_A \left(\rho_A \hat{\psi}_i \hat{\gamma}_c [\hat{\psi}_i \hat{\gamma}_c, \hat{H}_A] \right) - \\
& - \mathrm{Tr}_A \left(\rho_A [\hat{\psi}_i \hat{\gamma}_c, \hat{H}_A] \hat{\psi}_i \hat{\gamma}_c \right) \bigg) \sum_j^{N_B} \mathrm{Tr}_B (\rho_B \hat{\chi}_j \hat{\chi}_j) \\
=& \frac{\lambda^2}{N_B} \sum_i^{N_A} \bigg(\mathrm{Tr}_A \left(\rho_A \hat{\psi}_i \hat{\gamma}_c [\hat{\psi}_i \hat{\gamma}_c, \hat{H}_A] \right) - \mathrm{Tr}_A \left(\rho_A [\hat{\psi}_i \hat{\gamma}_c, \hat{H}_A] \hat{\psi}_i \hat{\gamma}_c \right) \bigg) \frac{N_B}{2} \\
=& \frac{\lambda^2}{2} \sum_i^{N_A} \mathrm{Tr}_A \left(\rho_A \left[\hat{\psi}_i \hat{\gamma}_c, [\hat{\psi}_i \hat{\gamma}_c, \hat{H}_A] \right] \right) = -\frac{\lambda^2}{2} 2 \cdot 4 \, \mathrm{Tr}_A \left(\rho_A \hat{H}_A \right) \\
=& - 4\lambda^2 E_A(0).
\end{aligned}
\tag{4.13}
$$

In the second row we used the Majorana identity $\hat{\chi}_j^2 = 1/2$. The double commutator on the last line is evaluated in Appendix 4.C.2 with result (4.50) for $q = 4$. Lastly, by disorder-averaging over the intra-dot couplings $\langle \cdot \rangle_J$:

$$
\begin{aligned}
\langle e_0 \rangle =& \langle E_A(0) \rangle_J \tag{4.14a} \\
\langle e_1 \rangle =& 0; \tag{4.14b} \\
\langle e_2 \rangle =& - 4\lambda^2 \langle E_A(0) \rangle_J, \tag{4.14c}
\end{aligned}
$$

we notice that the first two non-zero coefficients depend only on the initial energy of the analyzed subsystem and the interaction constant λ. Using these coefficients in (4.6), we obtain the averaged energy of the subsystem A up to the second order in time:

$$
\langle \Delta E(t) \rangle = \frac{\langle e_2 \rangle}{2} t^2 = -2\lambda^2 \langle E_A(0) \rangle_J t^2.
\tag{4.15}
$$

In Fig. 4.1, we compare this expression with the energy obtained from a numerical time evolution of two equally-sized SYKs ($N_A = N_B$) with $J_A = J_B \equiv J$ when the quench happens from two independent thermal states at temperatures $T_A = 0.5J$ and $T_B = 0.1J$. We observe that (4.15) qualitatively matches the early time behavior of $\langle E_A(t) \rangle_J$. In order to quantify how well the analytical expression explains the behavior of the numerical results, we fit the data from the early-time interval to a quadratic model (4.16) and study the ratio between the two coefficients a_2/e_2.

$$
f(t) = a_0 + \frac{a_2}{2} t^2
\tag{4.16}
$$
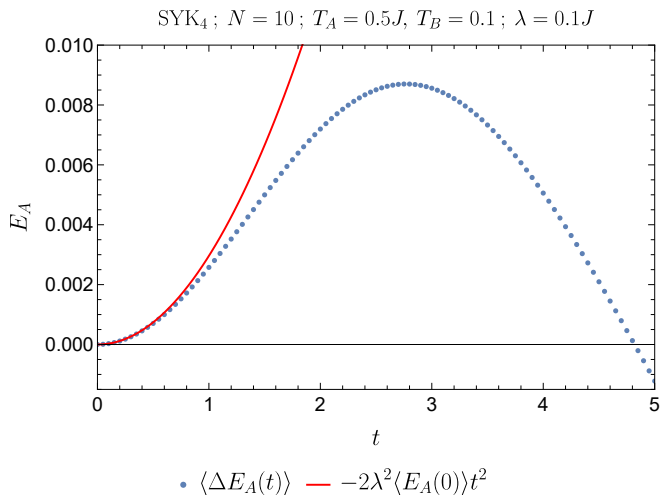
Figure 4.1. Early time evolution of $\langle \Delta E_A(t) \rangle$ computed numerically (blue dots) and analytically from (4.15) (red line). Numerical results are obtained from a quench of two equally sized ($N_A = N_B = 10$) SYK$_4$ dots.

Fig. 4.2 shows that this ratio is close to 1 for a few different temperatures T_A, proving the validity of the analytical expression (4.15) and the perturbative approach in general. The error bars on this Fig. 4.2 are computed with the error propagation relation using 99.7% confidence estimators for the errors σ_{a_2} and σ_{E_A} (3.21).

$$\sigma_{a_2/e_2} = \left| \frac{a_2}{e_2} \right| \sqrt{\left(\frac{\sigma_{a_2}}{a_2} \right)^2 + \left(\frac{\sigma_{E_A}}{\langle E_A(0) \rangle_J} \right)^2} \tag{4.17}$$

It is important to emphasize that for SYK dots with random interaction of the form (4.11a) the time evolution of $E_A(t)$, up to the second order, depends on the temperature T_A only implicitly through $E_A(0)$, and is completely impartial to any parameter of the subsystem B. The same holds, the other way around, for $E_B(t)$. From the exposition above, we see that the initial energy rise happens when $\langle E_A(0) \rangle_J < 0$, regardless of the initial temperature T_B. Recalling that $\langle E_A(0) \rangle_J < 0$ holds always for the SYK$_4$ [55] explains why the energy increases initially for any temperature T_A.

$\mathrm{SYK}_4 \,;\; N = 10 \,;\; T_B = 0.1 \,;\; \lambda = 0.1J \,;\; NR = 30000$
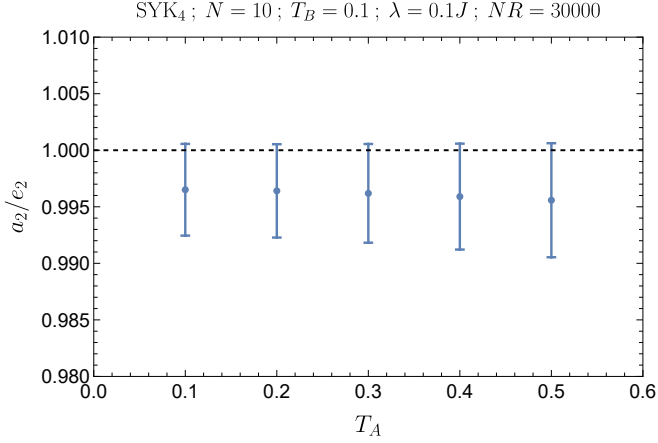
Figure 4.2. The ratio of the second order coefficients obtained from a fit of the numerical results a_2 and the analytical perturbative expansion e_2 with error bars given by the error propagation relation (4.17).

4.2.2. Mixed Field Ising

Next, we consider a system composed of two Mixed Field Ising models:

$$H_\alpha = -\sum_i^{N_\alpha} \left(JZ_i^\alpha Z_{i+1}^\alpha + gX_i^\alpha + hZ_i^\alpha \right), \qquad \alpha = A, B \tag{4.18}$$

coupled at $t = 0$, by the same quench procedure as before, with an interaction Hamiltonian that connects the last site of A to the first site of B:

$$H_{\mathrm{int}} = -\lambda_{+-}\hat{\sigma}_{N_A}^+ \otimes \hat{\sigma}_{1_B}^- - \lambda_{-+}\hat{\sigma}_{N_A}^- \otimes \hat{\sigma}_{1_B}^+ = -\sum_{ab\in\{+,-\}} \lambda_{a,b}\hat{\sigma}_{N_A}^a \otimes \hat{\sigma}_{1_B}^b,$$
$$\lambda_{-+}^* = \lambda_{+-} \equiv \lambda, \qquad \lambda_{++} = \lambda_{--} = 0. \tag{4.19}$$

Here, $\sigma^\pm = X \pm iY$ are the ladder operators and we express H_{int} in this particular form so it is readily usable in the general relations (4.8). Then we proceed the same as before, preparing the system in a tensor product of two decoupled subsystems, with density matrices that satisfy $[\rho_\alpha, \hat{H}_\alpha] = 0$, and directly substituting those parameters in (4.8) to obtain the early time evolution of the MFI subsystem A. As explained in Sec. 4.1, the time-independent contribution is equal to the pre-quench energy $e_0 = E_A(0)$, the first-order term vanishes $e_1 = 0$ and e_2 is evaluated

69

below:

$$e_2 = i^2 \sum_{aa'} \sum_{bb'} \lambda_{ab} \lambda_{a'b'} \bigg(\text{Tr}_A \left(\rho_A \hat{\sigma}_{N_A}^a [\hat{\sigma}_{N_A}^{a'}, \hat{H}_A] \right) \text{Tr}_B(\rho_B \hat{\sigma}_{1_B}^b \hat{\sigma}_{1_B}^{b'}) - $$
$$- \text{Tr}_A \left(\rho_A [\hat{\sigma}_{N_A}^{a'}, \hat{H}_A] \hat{\sigma}_{N_A}^a \right) \text{Tr}_B(\rho_B \hat{\sigma}_{1_B}^{b'} \hat{\sigma}_{1_B}^b) \bigg). \tag{4.20}$$

First we expand the double sum:

$$e_2 = i^2 \bigg\{ \lambda_{+-}\lambda_{+-} \bigg(\text{Tr}_A \left(\rho_A \hat{\sigma}_{N_A}^+ [\hat{\sigma}_{N_A}^+, \hat{H}_A] \right) \text{Tr}_B(\rho_B \hat{\sigma}_{1_B}^- \hat{\sigma}_{1_B}^-) - $$
$$- \text{Tr}_A \left(\rho_A [\hat{\sigma}_{N_A}^+, \hat{H}_A] \hat{\sigma}_{N_A}^+ \right) \text{Tr}_B(\rho_B \hat{\sigma}_{1_B}^- \hat{\sigma}_{1_B}^-) \bigg) + $$
$$+ \lambda_{+-}\lambda_{-+} \bigg(\text{Tr}_A \left(\rho_A \hat{\sigma}_{N_A}^+ [\hat{\sigma}_{N_A}^-, \hat{H}_A] \right) \text{Tr}_B(\rho_B \hat{\sigma}_{1_B}^- \hat{\sigma}_{1_B}^+) - $$
$$- \text{Tr}_A \left(\rho_A [\hat{\sigma}_{N_A}^-, \hat{H}_A] \hat{\sigma}_{N_A}^+ \right) \text{Tr}_B(\rho_B \hat{\sigma}_{1_B}^+ \hat{\sigma}_{1_B}^-) \bigg) + $$
$$+ \lambda_{-+}\lambda_{+-} \bigg(\text{Tr}_A \left(\rho_A \hat{\sigma}_{N_A}^- [\hat{\sigma}_{N_A}^+, \hat{H}_A] \right) \text{Tr}_B(\rho_B \hat{\sigma}_{1_B}^+ \hat{\sigma}_{1_B}^-) - $$
$$- \text{Tr}_A \left(\rho_A [\hat{\sigma}_{N_A}^+, \hat{H}_A] \hat{\sigma}_{N_A}^- \right) \text{Tr}_B(\rho_B \hat{\sigma}_{1_B}^- \hat{\sigma}_{1_B}^+) \bigg) + $$
$$+ \lambda_{-+}\lambda_{-+} \bigg(\text{Tr}_A \left(\rho_A \hat{\sigma}_{N_A}^- [\hat{\sigma}_{N_A}^-, \hat{H}_A] \right) \text{Tr}_B(\rho_B \hat{\sigma}_{1_B}^+ \hat{\sigma}_{1_B}^+) - $$
$$- \text{Tr}_A \left(\rho_A [\hat{\sigma}_{N_A}^-, \hat{H}_A] \hat{\sigma}_{N_A}^- \right) \text{Tr}_B(\rho_B \hat{\sigma}_{1_B}^+ \hat{\sigma}_{1_B}^+) \bigg) \bigg\}, \tag{4.21}$$

and notice that the terms on the first and last lines of (4.21) vanish due to identity $\hat{\sigma}^\pm \hat{\sigma}^\pm = 0$ (4.54). Taking this into account and regrouping the other four terms the expression for e_2 simplifies to:

$$e_2 = i^2 |\lambda|^2 \bigg\{ \left(\text{Tr}_A \left(\rho_A \hat{\sigma}_{N_A}^- [\hat{\sigma}_{N_A}^+, \hat{H}_A] \right) - \text{Tr}_A \left(\rho_A [\hat{\sigma}_{N_A}^-, \hat{H}_A] \hat{\sigma}_{N_A}^+ \right) \right) \text{Tr}_B(\rho_B \hat{\sigma}_{1_B}^+ \hat{\sigma}_{1_B}^-) + $$
$$+ \left(\text{Tr}_A \left(\rho_A \hat{\sigma}_{N_A}^+ [\hat{\sigma}_{N_A}^-, \hat{H}_A] \right) - \text{Tr}_A \left(\rho_A [\hat{\sigma}_{N_A}^+, \hat{H}_A] \hat{\sigma}_{N_A}^- \right) \right) \text{Tr}_B(\rho_B \hat{\sigma}_{1_B}^- \hat{\sigma}_{1_B}^+) \bigg\} \tag{4.22}$$

Additionally, using (4.57), (4.58) and the relation between the ladder operators and Pauli matrices $\hat{\sigma}^\pm \hat{\sigma}^\mp = 2(1 - \hat{Z})$ we can express this coefficient in terms of

one-point and two-point functions of the spin operators:

$$
\begin{aligned}
e_2 =& 2i^2|\lambda|^2 \Bigg\{ \left(\mathrm{Tr}_A \left(\rho_A \left[\hat{\sigma}^-_{N_A}, [\hat{\sigma}^+_{N_A}, \hat{H}_A] \right] \right) + \mathrm{Tr}_A \left(\rho_A \left[\hat{\sigma}^+_{N_A}, [\hat{\sigma}^-_{N_A}, \hat{H}_A] \right] \right) \right) + \\
& + \left(\mathrm{Tr}_A \left(\rho_A \left\{ \hat{\sigma}^-_{N_A}, [\hat{\sigma}^+_{N_A}, \hat{H}_A] \right\} \right) - \mathrm{Tr}_A \left(\rho_A \left\{ \hat{\sigma}^+_{N_A}, [\hat{\sigma}^-_{N_A}, \hat{H}_A] \right\} \right) \right) \mathrm{Tr}_B(\rho_B \hat{Z}_{1_B}) \Bigg\} \\
=& 2i^2|\lambda|^2 \Bigg(\left(-16J\langle \hat{Z}_{N-1}\hat{Z}_N \rangle_A - 8h^x_N \langle \hat{X}_N \rangle_A - 16h^z_N \langle \hat{Z}_N \rangle_A \right) + \\
& + \left(16J\langle \hat{Z}_{N-1} \rangle_A + 16h^z_N \right) \langle \hat{Z}_{1_B} \rangle_B \Bigg) \\
=& -32i^2|\lambda|^2 \Bigg(J \left(\langle \hat{Z}_{N-1}\hat{Z}_N \rangle_A - \langle \hat{Z}_{N-1} \rangle_A \langle \hat{Z}_{1_B} \rangle_B \right) + \\
& + \frac{1}{2}h^x_N \langle \hat{X}_N \rangle_A + h^z_N \left(\langle \hat{Z}_N \rangle_A - \langle \hat{Z}_{1_B} \rangle_B \right) \Bigg).
\end{aligned}
\tag{4.23}
$$

With this, we have solved the early time behavior of $E_A(t)$ up to the second order in time, however, there are no analytical relations for the temperature dependence of the one-point and two-point functions at arbitrary field strengths (h_x, h_z). Therefore, in order to evaluate e_2, we numerically compute the thermal expectation values in the last line of (4.23).

In Chapter 3, using numerical time evolution of the whole system, we discovered that when A is coupled to an equivalent MFI at temperature $T_B = 0.1$ there is no energy increase in the classical case $h_x = 0$, and on the other extreme, the increase appears for any temperature T_A when the system is at the critical point $h_x = 1, h_z = 0$. Interestingly, moving slightly away from $h_x = 1, h_z = 0$ a finite critical temperature T_c emerges above which the early time energy increase disappears, but below which it is present. The height of the numerically obtained energy bump E_m for those three examples is depicted in Figure 4.3 (left), and the critical temperature for the particular case $h_x = 1$ and $h_z = 0.05$ is $T_c \simeq 77.845J$.

The newly derived analytical relation for the energy (4.6) predicts the existence of an initial energy increase when $e_2 > 0$ in the case under consideration when $e_1 = 0$. Now, using the expansion for e_2 in (4.23), we compute and show in Fig. 4.3 (right) the e_2 value as a function of T_A for the three particular cases elaborated above. These results confirm our previous findings on the existence of the energy increase. For any T_A, $e_2 < 0$ in the classical case, $e_2 > 0$ at the quantum critical
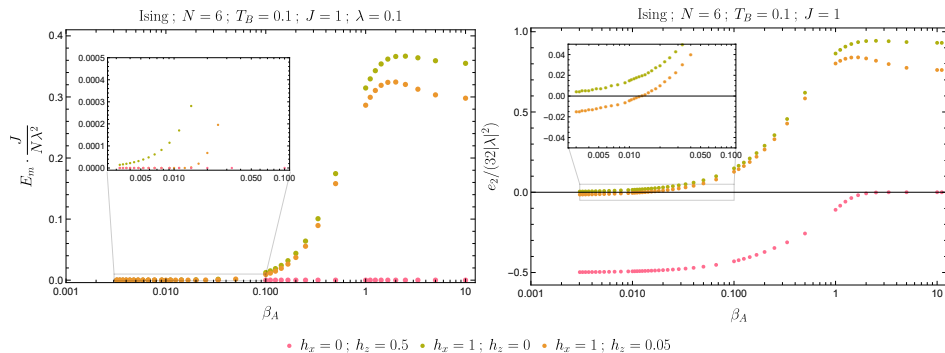
Figure 4.3. Existence of the early time energy bump in the classical ($h_x = 0, h_z = 1$), quantum critical ($h_x = 1, h_z = 0$) and arbitrary case with ($h_x = 1, h_z = 0.05$). On the left, the height of the energy bump E_m is presented with $E_m = 0$ indicating its absence. The right panel presents the e_2 coefficient (4.23), for the same three models. The energy bump disappears when $e_2 < 0$.

point and when the system is tuned slightly away from it the coefficient changes from a positive sign when $T_A < 77.5$ to negative for $T_A > 77.5$.

To show that this match between the numerical results and the analytical expression is not limited to these three special cases we apply the same reasoning to three other models with results presented in Fig. 4.4. As before, the left panel displays the height of the energy bump E_m, which goes to zero when the bump disappears. On the right panel, which plots the second coefficient e_2, one notices that it turns negative exactly at the same temperature for which $E_m \rightarrow 0$.

This match in the critical temperature demonstrates the equivalence and validity of our two approaches and allows us to use the early time expansion to understand the early time behavior and in particular the quantum energy ruse in the hot system A. Note that for the MFI we can write the second coefficient (4.23) as a difference of two separate contributions, e_2^A that depends only on the subsystem under consideration A and e_2^{AB} which depends on both A and B, therefore being sensitive on the temperature T_B:

$$e_2 = 32|\lambda|^2 \left(e_2^A - e_2^{AB} \right), \tag{4.24a}$$

$$e_2^A = J\langle \hat{Z}_{N-1}\hat{Z}_N \rangle_A + \frac{h_N^x}{2}\langle \hat{X}_N \rangle_A + h_N^z\langle \hat{Z}_N \rangle_A; \tag{4.24b}$$

$$e_2^{AB} = \left(J\langle \hat{Z}_{N-1} \rangle_A + h_N^z \right) \langle \hat{Z}_{1_B} \rangle_B. \tag{4.24c}$$

Here we see that, similar to the SYK model, the result for e_2^A depends only on the
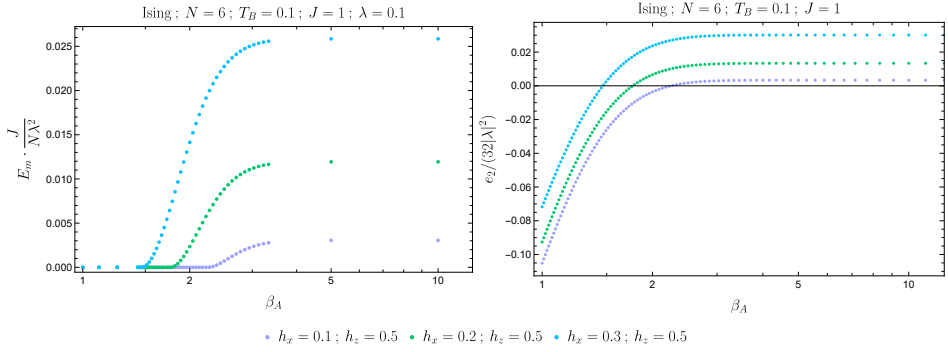
Figure 4.4. Disappearance of the energy bump, for three different models, computed by a time evolution of the full model (left) and from the exact thermodynamic evaluation of the e_2 coefficient (right).

properties of the subsystem under consideration A. However, unlike before, the additional term e_2^{AB} depends also on the subsystem B, therefore being sensitive to the temperature T_B. Since both of these terms are positive, the energy bump disappears ($e_2 < 0$) in the temperature regime where $e_2^A < e_2^{AB}$, as shown on Fig. 4.5.
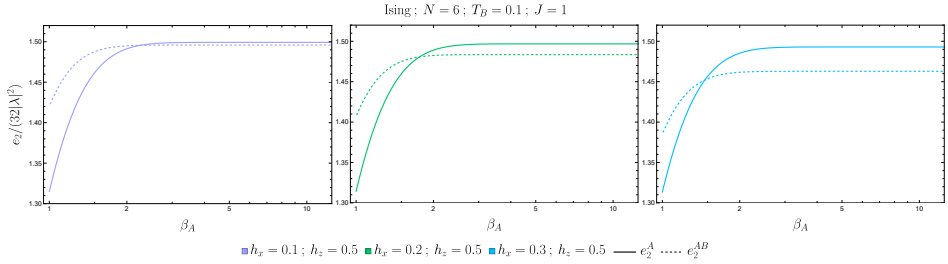
Figure 4.5. Those plots present the e_2^A (full line) and the e_2^{AB} (dashed line) terms of the e_2 coefficient (4.24), for the same models as on Fig. 4.4.

4.3. Conclusion

In this Chapter we presented how to expand the post-quench time evolution of the density matrix into a time series and how to obtain from there the time evolution of the subsystem-reduced density matrices perturbatively in the time t since the quench. We have derived a general expression for the first three coefficients of the expansion and used it to analyze the early time behavior of the subsystems

energies for two distinct models. Namely, in order to compare results we studied the same models as Chapter 3: SYK as a representative of a strongly interacting highly entangled, and chaotic model and the Mixed Field Ising in its classical, fully quantum quantum critical, and mixed quantum-classical regimes.

We have shown that this analytical approach not only reproduces the results from our study on a numerical time evolution but it provides an explanation for the omnipresence of the bump in the SYK and its disappearance above a critical temperature in the MFI models. The peculiar nature of the Majorana SYK conspires in such a way that the first three coefficients of the energy expansion are completely independent of the other subsystem resulting in an energy increase even when the analyzed subsystem is at a higher temperature than the other one. On the other hand, the second term e_2 of the MFI expansion depends on both subsystems leading to the appearance of the critical temperature T_c.

Continuing this analytic approach to derive the third and fourth coefficients of the energy expansion might give access to the time at which the maximum in the bump appears. This would be useful in understanding how the system transitions from this early-time quantum behavior to the late-time evaporation. Additionally, one expects a universal behavior of the energy coefficients in the SYK setup and it would be interesting to see what other thermodynamic quantities appear in those higher-order terms. We leave this for future work.

4.A. General State Expansion

Series expansion of the density matrix — Here we represent the time-dependent density matrix, after an instantaneous quench (4.1b), as a time series, similar to the main text, under the assumption of a separable initial state $\rho_0 = \rho_A \otimes \rho_B$ composed of arbitrary subsystem states ρ_α:

$$\rho(t) = e^{-iHt}\rho_0 e^{iHt} = \left(1 - iHt - \frac{1}{2}H^2t^2 \dots\right)\rho_0\left(1 + iHt - \frac{1}{2}H^2t^2 \dots\right) =$$

$$= \sum_{n=0}\frac{t^n}{n!}R_n \tag{4.25a}$$

$$R_0 = \rho_0 \quad ; \quad R_{n+1} = i[R_n, H] \tag{4.25b}$$

Where R_n are operator-valued coefficients and the first four are given below:

$$\hat{R}_0 = \rho_0 \tag{4.26a}$$

$$\hat{R}_1 = i[\hat{R}_0, H] = i\left([\rho_1, H_1] \otimes \rho_2 + \rho_1 \otimes [\rho_2, H_2] + [\rho_0, H_{int}]\right) \tag{4.26b}$$

$$\hat{R}_2 = i[\hat{R}_1, H] = i\left([\hat{R}_1, H_1 \otimes \mathbb{1}_{d_2}] + [\hat{R}_1, \mathbb{1}_{d_1} \otimes H_2] + [R_1, H_{int}]\right) \tag{4.26c}$$

$$\hat{R}_3 = i[R_2, H] = i\left([\hat{R}_2, H_1 \otimes \mathbb{1}_{d_2}] + [\hat{R}_2, \mathbb{1}_{d_1} \otimes H_2] + [R_2, H_{int}]\right) \tag{4.26d}$$

Expanding the commutators we obtain:

$$\hat{R}_0 = \rho_0 \tag{4.27a}$$

$$\hat{R}_1 = i[\hat{R}_0, \hat{H}] = i[\rho_A, \hat{H}_A] \otimes \rho_B + i\rho_A \otimes [\rho_B, \hat{H}_B] +$$
$$+ i\sum_{IK}\lambda_{IK}[\rho_A \otimes \rho_B, \hat{\Psi}_I \otimes \hat{\Gamma}_K] \tag{4.27b}$$

$$\hat{R}_2 = i[\hat{R}_1, \hat{H}] = i[\hat{R}_1, \hat{H}_A \otimes \mathbb{1}_{d_B}] + i[\hat{R}_1, \mathbb{1}_{d_A} \otimes \hat{H}_B] + i\sum_{IK}\lambda_{IK}[\hat{R}_1, \hat{\Psi}_I \otimes \hat{\Gamma}_K]$$

$$= i^2\Bigg\{\left[[\rho_A, \hat{H}_A], \hat{H}_A\right] \otimes \rho_B + \rho_A \otimes \left[[\rho_B, \hat{H}_B], \hat{H}_B\right] + 2[\rho_A, \hat{H}_A] \otimes [\rho_B, \hat{H}_B] +$$

$$+ \sum_{IK}\lambda_{IK}\Bigg(\left[[\rho_A \otimes \rho_B, \hat{\Psi}_I \otimes \hat{\Gamma}_K], \hat{H}_A\right] + \left[[\rho_A \otimes \rho_B, \hat{\Psi}_I \otimes \hat{\Gamma}_K], \hat{H}_B\right] +$$

$$+ \left[[\rho_A, \hat{H}_A] \otimes \rho_B, \hat{\Psi}_I \otimes \hat{\Gamma}_K\right] + \left[\rho_A \otimes [\rho_B, \hat{H}_B], \hat{\Psi}_I \otimes \hat{\Gamma}_K\right]\Bigg)$$

$$+ \sum_{IK}\sum_{I'K'}\lambda_{IK}\lambda_{I'K'}\left[[\rho_A \otimes \rho_B, \hat{\Psi}_I \otimes \hat{\Gamma}_K], \hat{\Psi}_{I'} \otimes \hat{\Gamma}_{K'}\right]\Bigg\} \tag{4.27c}$$

$$\hat{R}_3 = i[\hat{R}_2, \hat{H}] = i[\hat{R}_2, \hat{H}_A \otimes \mathbb{1}_{d_B}] + i[\hat{R}_2, \mathbb{1}_{d_A} \otimes \hat{H}_B] + i \sum_{IK} \lambda_{IK}[\hat{R}_2, \hat{\Psi}_I \otimes \hat{\Gamma}_K] \ .$$

(4.27d)

Next, we present the operator-valued coefficients $\hat{A}_n$ (4.28) which define the time evolution of the reduced density matrix $\rho_A(t)$ (4.4a). Note that many terms vanish due to (4.39a).

$$\hat{A}_0 = \mathrm{Tr}_B(\hat{R}_0) = \mathrm{Tr}_B(\rho_0) = \rho_A; \tag{4.28a}$$

$$\hat{A}_1 = \mathrm{Tr}_B(\hat{R}_1) = i\left\{ [\rho_A, \hat{H}_A] + \sum_{IK} \lambda_{IK}[\rho_A, \hat{\Psi}_I] \, \mathrm{Tr}_B(\rho_B \, \hat{\Gamma}_K) \right\}; \tag{4.28b}$$

$$\hat{A}_2 = \mathrm{Tr}_B(\hat{R}_2) = i^2 \left\{ \Big[[\rho_A, \hat{H}_A], \hat{H}_A\Big] + \right.$$

$$+ \sum_{IK} \lambda_{IK} \left(\Big(\Big[[\rho_A, \hat{\Psi}_I], \hat{H}_A\Big] + \Big[[\rho_A, \hat{H}_A], \hat{\Psi}_I\Big] \Big) \mathrm{Tr}_B(\rho_B \, \hat{\Gamma}_K) + \right.$$

$$+ [\rho_A, \hat{\Psi}_I] \, \mathrm{Tr}_B([\rho_B, \hat{H}_B], \hat{\Gamma}_K) \Big)$$

$$+ \sum_{IK} \sum_{K'I'} \lambda_{IK} \lambda_{I'K'} \Big([\rho_A \hat{\Psi}_I, \hat{\Psi}_{I'}] \, \mathrm{Tr}_B(\rho_B \, \hat{\Gamma}_K \, \hat{\Gamma}_{K'}) - $$

$$\left. - [\hat{\Psi}_I \rho_A, \hat{\Psi}_{I'}] \, \mathrm{Tr}_B(\rho_B \, \hat{\Gamma}_{K'} \, \hat{\Gamma}_K) \Big) \right\}. \tag{4.28c}$$

4.B. Proper anti-commuting interactions between coupled SYK dots

There are different ways to study two N-Majorana SYK dots. For example, one can take $2N$ Majoranas and model the subsystems through the interactions. However, we want to have manifestly separate subsystems so we will generate two Hilbert spaces using the techniques from [115]. First dot has $N_1 = 2K_1$ Majoranas denoted with ψ_i and the second has $N_2 = 2K_2$ Majoranas denoted with χ_j, living in their respective Hilbert spaces, $\mathcal{H}_1$ and $\mathcal{H}_2$:

$$N_1 = 2K_1 : \quad \tilde{\psi}_i \in \mathcal{H}_1, \quad \dim \mathcal{H}_1 = 2^{K_1}; \quad \{\tilde{\psi}_i, \tilde{\psi}_j\} = \delta_{i,j}\mathbb{1} \quad \tilde{\psi}_i^2 = \frac{1}{2}\mathbb{1}$$

$$[\tilde{\psi}_i, \tilde{\psi}_j] = 2\tilde{\psi}_i\tilde{\psi}_j - \delta_{ij} = -2\tilde{\psi}_j\tilde{\psi}_i + \delta_{ij} \tag{4.29a}$$

$$[\tilde{\psi}_i, \tilde{\psi}_j\gamma_c] = \{\tilde{\psi}_i, \tilde{\psi}_j\}\gamma_c = \delta_{ij}\gamma_c \quad ; \quad (\psi_i\gamma_c)^2 = -\psi_i^2\gamma_c^2 = -\frac{1}{2}$$

$$N_2 = 2K_2 : \quad \tilde{\chi}_i \in \mathcal{H}_2, \quad \dim \mathcal{H}_2 = 2^{K_2}; \quad \{\tilde{\chi}_i, \tilde{\chi}_j\} = \delta_{i,j}\mathbb{1} \quad \tilde{\chi}_i^2 = \frac{1}{2}\mathbb{1} \tag{4.29b}$$

$$h_1 = -\sum_{j=1}^{N_1} J_{j_1 j_2 j_3 j_4}^{(1)} \tilde{\psi}_{j_1} \tilde{\psi}_{j_2} \tilde{\psi}_{j_3} \tilde{\psi}_{j_4} \quad ; \quad h_2 = -\sum_{l=1}^{N_2} J_{l_1 l_2 l_3 l_4}^{(2)} \tilde{\chi}_{l_1} \tilde{\chi}_{l_2} \tilde{\chi}_{l_3} \tilde{\chi}_{l_4} \quad (4.30)$$

The whole Hilbert space consists of the two dots $\mathcal{H}$ has $N = 2K = N_1 + N_2$ Majoranas in total:

$$N = N_1 + N_2 : \quad \psi_i, \chi_j \in \mathcal{H}, \quad \dim \mathcal{H} = 2^K$$
$$\{\psi_i, \psi_j\} = \delta_{i,j}\mathbb{1}, \quad \{\chi_i, \chi_j\} = \delta_{i,j}\mathbb{1}, \quad \{\psi_i, \chi_j\} = 0 \quad (4.31)$$

In order to generate those Majoranas we need to recall that Majorana operators are closely related to the Clifford algebra of dimension $n = 2k$:

$$\{\gamma_i, \gamma_j\} = 2\delta_{ij}\mathbb{1} \quad \Rightarrow \quad \gamma_i^2 = \mathbb{1} \quad (4.32)$$

$$\gamma_c = (-i)^k \gamma_1 \gamma_2 \dots \gamma_n, \quad \gamma_c^\dagger = \gamma_c; \quad \gamma_c^2 = \mathbb{1} \quad ; \quad \{\gamma_i, \gamma_c\} = 0 \quad (4.33)$$

4.B.1. Numerical implementation of Majoranas

Now we would like to generate the two dots from Clifford algebra $\{\Gamma_i\}$. We will consider the simple case when $N_1 = N_2$ so $N = 2N_1 = 4K_1$, which would be easy to extend to a system of asymmetric dots. The Clifford algebra $\{\Gamma_i\}$ can be written in terms of subsystem algebra $\{\gamma_i\}$:

$$\gamma_i \in \mathcal{H}_1, \quad \dim \mathcal{H}_1 = 2^{K_1} \quad (4.34a)$$
$$\Gamma_i = \gamma_i \otimes \mathbb{1}, \quad i \in \{1, 2, \dots N_1\} \quad (4.34b)$$
$$\Gamma_{N_1+j} = \gamma_c \otimes \gamma_j, \quad j \in \{1, 2, \dots N_2\} \quad (4.34c)$$

The Majorana operators are obtained by renormalizing $\{\Gamma_i\}$:

$$\Gamma_1, \Gamma_2 \dots \Gamma_N \quad (4.35a)$$

$$\psi_i = \frac{1}{\sqrt{2}}\Gamma_i = \frac{1}{\sqrt{2}}\gamma_i \otimes \mathbb{1} \equiv \tilde{\psi}_i \otimes \mathbb{1}, \quad i \in \{1, 2, \dots N_1\} \quad (4.35b)$$

$$\chi_j = \frac{1}{\sqrt{2}}\Gamma_{N_1+j} = \frac{1}{\sqrt{2}}\gamma_c \otimes \gamma_j \equiv \gamma_c \otimes \tilde{\chi}_j, \quad j \in \{1, 2, \dots N_2\}. \quad (4.35c)$$

The noteworthy part is the appearance of the matrix γ_c that ensures anticommutation between the Majoranas in the two dots:

$$\{\psi_i, \psi_j\} = \frac{1}{2}\{\gamma_i, \gamma_j\} \otimes \mathbb{1} = \delta_{ij}\mathbb{1} \otimes \mathbb{1} \quad (4.36a)$$

$$\{\chi_i, \chi_j\} = \frac{1}{2}\gamma_c^2 \otimes \{\gamma_i, \gamma_j\} \equiv \frac{1}{2}\mathbb{1} \otimes \{\gamma_i, \gamma_j\} = \delta_{ij}\mathbb{1} \otimes \mathbb{1} \quad (4.36b)$$

$$\{\psi_i, \chi_j\} = \frac{1}{2}\{\gamma_i, \gamma_c\} \otimes \gamma_j = 0 \quad (4.36c)$$

In this basis, before the quench, the two Hamiltonians are manifestly decoupled :

$$H_1 = -\sum_{i_1,\dots i_4} J_{i_1\dots i_4}\psi_{i_1}\psi_{i_2}\psi_{i_3}\psi_{i_4}$$
$$= -\sum_{i_1,\dots i_4} J_{i_1\dots i_4}\tilde\psi_{i_1}\tilde\psi_{i_2}\tilde\psi_{i_3}\tilde\psi_{i_4} \otimes \mathbb{1}^4 = h_1 \otimes \mathbb{1} \tag{4.37a}$$

$$H_2 = -\sum_{l_1,\dots l_4} J_{l_1\dots l_4}\chi_{l_1}\chi_{l_2}\chi_{l_3}\chi_{l_4}$$
$$= -\gamma_c^4 \otimes \sum_{l_1,\dots l_4} J_{l_1\dots l_4}\tilde\chi_{l_1}\tilde\chi_{i_2}\tilde\chi_{i_3}\tilde\chi_{i_4} \otimes \mathbb{1}^4 = \mathbb{1} \otimes h_2 \tag{4.37b}$$

$$H_{int} = i\sum_{xy}\lambda_{xy}\psi_x\chi_y = \sum_{xy}\lambda_{xy}\tilde\psi_x\gamma_c \otimes \tilde\chi_y \tag{4.37c}$$

4.C. Operators relations

In this appendix we gather some useful relations needed for coefficients derivation in the early time expansion.

4.C.1. General relations

$$[AB,C] = [A,C]B + A[B,C] \tag{4.38a}$$
$$\{AB,C\} = A[B,C] + \{A,C\}B \tag{4.38b}$$
$$[\rho_1 \otimes \rho_2, \hat O_X \otimes \hat O_Y] = \rho_1\hat O_X \otimes \rho_2\hat O_Y - \hat O_X\rho_1 \otimes \hat O_Y\rho_2 \tag{4.38c}$$

$$\mathrm{Tr}\left([\hat A,\hat B]\right) = \mathrm{Tr}\left(\hat A\hat B\right) - \mathrm{Tr}\left(\hat B\hat A\right) = 0 \tag{4.39a}$$
$$\mathrm{Tr}_2\left([\hat\alpha \otimes \hat\beta, \hat O_X \otimes \hat O_Y]\right) = \hat\alpha\hat O_X \otimes \mathrm{Tr}\left(\hat\beta\hat O_Y\right) - \hat O_X\hat\alpha \otimes \mathrm{Tr}\left(\hat O_Y\hat\beta\right) =$$
$$= [\hat\alpha,\hat O_X]\,\mathrm{Tr}\left(\hat\beta\hat O_Y\right) \tag{4.39b}$$

$$\mathrm{Tr}\left([A,B]C\right) = \mathrm{Tr}\left(ABC - BAC\right) = \mathrm{Tr}\left(ABC - ACB\right) =$$
$$= \mathrm{Tr}\{A[B,C]\} = \mathrm{Tr}\{[C,A]B\} \tag{4.40a}$$
$$\mathrm{Tr}\left([[[[R,A_1],A_2],\cdots],A_{n-1}]A_n\right) = \mathrm{Tr}\left(R,[A_1,[A2,[\cdots,[A_{n-1},A_n]]]]\right) \tag{4.40b}$$

4.C.2. Majoranas

General Majoranas —

Here, we consider a system with N Majoranas, forming a $d = \dim(\mathcal{H}) = 2^{N/2}$ dimensional Hilbert space $\mathcal{H}$, and we use the same normalization for the Majoranas as in the numerical code.

$$\{\psi_i, \psi_j\} = \delta_{ij} \quad ; \quad \{\psi_c, \psi_j\} = 0 \quad ; \quad \psi_i^2 = \frac{1}{2}\mathbb{1}_d \quad ; \quad \gamma_c^2 = 1 \quad ; \quad (\psi_i\gamma_c)^2 = -\frac{1}{2}$$
(4.41a)

$$[\psi_i, \psi_j] = 2\psi_i\psi_j - \delta_{ij} = -2\psi_j\psi_i + \delta_{ij} \quad ; \quad [\psi_i\gamma_c, \psi_j] = -\{\psi_i, \psi_j\}\gamma_c = -\delta_{ij}\gamma_c$$
(4.41b)

Next, we present some common commutators of Majorana strings, but first, we introduce a notation for such strings that will help us write more compact expressions, especially for large q SYKs.

$$\Psi_I^{(q)} = \psi_{i_1}\psi_{i_2}\ldots\psi_{i_q}$$
(4.42a)

$$\Psi_{I_\sigma}^{(q-1)} = \psi_{i_1}\ldots\psi_{i_{\sigma-1}}\psi_{i_{\sigma+1}}\ldots\psi_{i_q}$$
(4.42b)

The easiest is to start with four Majoranas Strings ($q = 4$):

$$\begin{aligned}
[\psi_\alpha, \Psi_I^{(4)}] &= [\psi_\alpha, \psi_{i_1}\psi_{i_2}\psi_{i_3}\psi_{i_4}] \\
&= (\delta_{i_1\alpha}\psi_{i_2}\psi_{i_3}\psi_{i_4} - \delta_{i_2\alpha}\psi_{i_1}\psi_{i_3}\psi_{i_4} + \delta_{i_3\alpha}\psi_{i_1}\psi_{i_2}\psi_{i_4} - \delta_{i_4\alpha}\psi_{i_1}\psi_{i_2}\psi_{i_3}) \\
&= \sum_{\sigma=1}^{4} \delta_{\alpha i_\sigma}(-1)^{\sigma+1}\Psi_{I_\sigma}^{(3)}
\end{aligned}$$
(4.43a)

$$\begin{aligned}
[\psi_\alpha\gamma_c, \Psi_I^{(4)}] &= [\psi_\alpha\gamma_c, \psi_{i_1}\psi_{i_2}\psi_{i_3}\psi_{i_4}] \\
&= -(\delta_{i_1\alpha}\gamma_c\psi_{i_2}\psi_{i_3}\psi_{i_4} + \delta_{i_2\alpha}\psi_{i_1}\gamma_c\psi_{i_3}\psi_{i_4} + \delta_{i_3\alpha}\psi_{i_1}\psi_{i_2}\gamma_c\psi_{i_4} + \delta_{i_4\alpha}\psi_{i_1}\psi_{i_2}\psi_{i_3}\gamma_c) \\
&= -\gamma_c\sum_{\sigma=1}^{4} \delta_{\alpha i_\sigma}(-1)^{\sigma+1}\Psi_{I_\sigma}^{(3)}
\end{aligned}$$
(4.43b)

Then, those results can be generalized for an arbitrarily sized string with ($q = 2p$):

$$[\psi_\alpha, \Psi_I^{(q)}] = \sum_{\sigma=1}^{q} \delta_{\alpha i_\sigma}(-1)^{\sigma+1}\Psi_{I_\sigma}^{(q-1)}$$
(4.44a)

$$[\psi_\alpha\gamma_c, \Psi_I^{(q)}] = -\gamma_c\sum_{\sigma=1}^{q} \delta_{\alpha i_\sigma}(-1)^{\sigma+1}\Psi_{I_\sigma}^{(q-1)}$$
(4.44b)

SYK like interaction —

Relations obtained in the previous paragraph can be used for commutators of an SYK Hamiltonian with a string of Majoranas. Initially we're interested in a $(q = 4)$ SYK Hamiltonians (4.9) :

$$
\begin{aligned}
[\psi_\alpha, H^{(4)}] =& i^2 \sum_{i_1\cdots i_4=1}^{N} J_{i_1 i_2 i_3 i_4}[\psi_\alpha, \psi_{i_1}\psi_{i_2}\psi_{i_3}\psi_{i_4}] \\
=& -4i^2 \sum_{i_1 i_2 i_3=1}^{N} J_{i_1 i_2 i_3 \alpha}\psi_{i_1}\psi_{i_2}\psi_{i_3},
\end{aligned}
\tag{4.45a}
$$

$$
\begin{aligned}
[\psi_\alpha \gamma_c, H^{(4)}] =& i^2 \sum_{i_1\cdots i_4=1}^{N} J_{i_1 i_2 i_3 i_4}[\psi_\alpha \gamma_c, \psi_{i_1}\psi_{i_2}\psi_{i_3}\psi_{i_4}] \\
=& 4i^2 \sum_{i_1 i_2 i_3=1}^{N} J_{i_1 i_2 i_3 \alpha}\gamma_c\psi_{i_1}\psi_{i_2}\psi_{i_3}.
\end{aligned}
\tag{4.45b}
$$

Same as before, those commutators can be easily generalized to $(q = 2p)$ SYK Hamiltonians:

$$
[\psi_\alpha, H^{(q)}] = i^{q/2} \sum_{I=1}^{N} J_I[\psi_\alpha, \Psi_I^{(q)}] = -qi^{q/2} \sum_{i_1\cdots i_{q-1}=1}^{N} J_{i_1\cdots i_{q-1}\alpha}\Psi_{I_q}^{(q-1)}, \tag{4.46a}
$$

$$
[\psi_\alpha \gamma_c, H^{(q)}] = i^{q/2} \sum_{I=1}^{N} J_I[\psi_\alpha \gamma_c, \Psi_I^{(q)}] = qi^{q/2} \sum_{i_1\cdots i_{q-1}=1}^{N} J_{i_1\cdots i_{q-1}\alpha}\gamma_c\Psi_{I_q}^{(q-1)}.
\tag{4.46b}
$$

When analyzing the time evolution of operators similar expressions to (4.46) appear with an additional sum over the Majorana field (ψ_α):

$$
\begin{aligned}
\sum_{\alpha=1}^{N} \psi_\alpha[\psi_\alpha, H^{(q)}] =& -qi^{q/2} \sum_{i_1\cdots i_{q-1}=1}^{N} \sum_{\alpha=1}^{N} J_{i_1\cdots i_{q-1}\alpha}\psi_\alpha \Psi_{I_q}^{(q-1)} \\
=& qi^{q/2} \sum_{i_1\cdots i_{q-1}=1}^{N} \sum_{\alpha=1}^{N} J_{i_1\cdots i_{q-1}\alpha}\Psi_{I_q}^{(q-1)}\psi_\alpha = qH^{(q)}
\end{aligned}
\tag{4.47a}
$$

$$
\begin{aligned}
\sum_{\alpha=1}^{N} \psi_\alpha \gamma_c[\psi_\alpha \gamma_c, H^{(q)}] =& qi^{q/2} \sum_{i_1\cdots i_{q-1}=1}^{N} \sum_{\alpha=1}^{N} J_{i_1\cdots i_{q-1}\alpha}\psi_\alpha \gamma_c^2 \Psi_{I_q}^{(q-1)} \\
=& -qi^{q/2} \sum_{i_1\cdots i_{q-1}=1}^{N} \sum_{\alpha=1}^{N} J_{i_1\cdots i_{q-1}\alpha}\Psi_{I_q}^{(q-1)}\psi_\alpha = -qH^{(q)},
\end{aligned}
\tag{4.47b}
$$

$$\sum_{\alpha=1}^{N}[\psi_\alpha, H^{(q)}]\psi_\alpha = -qH^{(q)}, \tag{4.48a}$$

$$\sum_{\alpha=1}^{N}[\psi_\alpha\gamma_c, H^{(q)}]\psi_\alpha\gamma_c = qH^{(q)}, \tag{4.48b}$$

where we have used $(\gamma_c^2 = 1)$ and the fact that the interaction constant $(J_{i_1\cdots i_{q-1}\alpha})$ vanishes in the case of at least two identical indices, hence permuting (ψ_α) past the other Majoranas results only in an additional minus sign since $((-1)^{q-1} = (-1)^{2p-1} = -1)$.

Other related expressions are:

$$\sum_{\alpha=1}^{N}[\psi_\alpha, [\psi_\alpha, H^{(q)}]] = 2qH^{(q)}, \tag{4.49a}$$

$$\sum_{\alpha=1}^{N}[\psi_\alpha\gamma_c[\psi_\alpha\gamma_c, H^{(q)}]] = -2qH^{(q)}. \tag{4.49b}$$

$$\begin{aligned}
\sum_{\alpha=1}^{N}&[\psi_\alpha\gamma_c, [H^{(q)}, [\psi_\alpha\gamma_c, H^{(q)}]]] = \\
&= \sum_{\alpha=1}^{N} \big(2\psi_\alpha\gamma_c H^{(q)}\psi_\alpha\gamma_c H^{(q)} - 2H^{(q)}\psi_\alpha\gamma_c H^{(q)}\psi_\alpha\gamma_c - (\psi_\alpha\gamma_c)^2(H^{(q)})^2 + \\
&\quad + (\psi_\alpha\gamma_c)(H^{(q)})^2(\psi_\alpha\gamma_c) - (\psi_\alpha\gamma_c)(H^{(q)})^2(\psi_\alpha\gamma_c) + (H^{(q)})^2(\psi_\alpha\gamma_c)^2 \big) \\
&= 2\sum_{\alpha=1}^{N} \big(\psi_\alpha\gamma_c H^{(q)}\psi_\alpha\gamma_c H^{(q)} - H^{(q)}\psi_\alpha\gamma_c H^{(q)}\psi_\alpha\gamma_c \big) \\
&= 2\sum_{\alpha=1}^{N}[\psi_\alpha\gamma_c, H^{(q)}\psi_\alpha\gamma_c H^{(q)}] \\
&= 2\sum_{\alpha=1}^{N} \big([\psi_\alpha\gamma_c, H^{(q)}]\psi_\alpha\gamma_c H^{(q)} + H^{(q)}\psi_\alpha\gamma_c[\psi_\alpha\gamma_c, H^{(q)}] \big) = 0
\end{aligned} \tag{4.50}$$

4.C.3. Pauli

General Pauli matrices - Single site —

Note that the following (anti)commutation relations are for same site operators. Operators on different sites act on different spin states, so they commute.

$$X \equiv \sigma^x = \begin{pmatrix} 0 & 1 \\ 1 & 0 \end{pmatrix} \quad ; \quad Y \equiv \sigma^y = \begin{pmatrix} 0 & -i \\ i & 0 \end{pmatrix} \quad ; \quad Z \equiv \sigma^z = \begin{pmatrix} 1 & 0 \\ 0 & -1 \end{pmatrix} \quad (4.51)$$

$$\sigma^{\alpha\dagger} = \sigma^\alpha \quad ; \quad \sigma^{\alpha 2} = \mathbb{1}_d \quad ; \quad \alpha, \beta, \gamma \in \{x, y, z\} \tag{4.52a}$$

$$\{\sigma^\alpha, \sigma^\beta\} = 2\delta_{\alpha\beta}\mathbb{1}_d \quad ; \quad [\sigma^\alpha, \sigma^\beta] = 2i\epsilon_{\alpha\beta\gamma}\sigma^\gamma \tag{4.52b}$$

From the Pauli matrices ladder operators can be formed

$$\sigma^+ \equiv X + iY = \begin{pmatrix} 0 & 2 \\ 0 & 0 \end{pmatrix} \quad ; \quad \sigma^- \equiv X - iY = \begin{pmatrix} 0 & 0 \\ 2 & 0 \end{pmatrix} \tag{4.53}$$

$$\sigma^{\pm\dagger} = \sigma^\mp \quad ; \quad \sigma^\pm\sigma^\pm = 0 \quad ; \quad \sigma^\pm\sigma^\mp = 2\left(1 \pm Z\right)$$

$$[\sigma^\pm, X] = \pm 2Z \quad ; \quad [\sigma^\pm, Y] = \mp 2iZ \quad ; \quad [\sigma^\pm, Z] = \mp 2\sigma^\pm \quad ; \quad [\sigma^+, \sigma^-] = 4Z$$

$$\{\sigma^\pm, X\} = 2\mathbb{1} \quad ; \quad \{\sigma^\pm, Y\} = \pm i\mathbb{1} \quad ; \quad \{\sigma^\pm, Z\} = 0 \quad ; \quad \{\sigma^+, \sigma^-\} = 4\mathbb{1}$$

Mixed Field Ising with position-dependent fields (h_i^x, h_i^z) —

Here we present commutator/anti-commutator relations for the most generic Mixed Field Ising with position-dependent couplings (4.55). Setting the couplings to the same constant at each site one recovers the standard MFI.

$$H_{MFI1} = -J \sum_{i=1}^{N-1+p_f} \hat{Z}_i \hat{Z}_{i+1} - \sum_{i=1}^{N} h_i^x \hat{X}_i - \sum_{i=1}^{N} h_i^z \hat{Z}_i \tag{4.55}$$

$$[\hat{\sigma}_N^-, \hat{H}_{MFI1}] = -2J\left(\hat{Z}_{N-1}\hat{\sigma}_N^- + p_f\hat{\sigma}_N^-\hat{Z}_1\right) + 2h_N^x\hat{Z}_N - 2h_N^z\hat{\sigma}_N^- \tag{4.56a}$$

$$[\hat{\sigma}_N^+, \hat{H}_{MFI1}] = -2J\left(-Z_{N-1}\hat{\sigma}_N^+ - p_f\hat{\sigma}_N^+Z_1\right) - 2h_N^xZ_N + 2h_N^z\hat{\sigma}_N^+ \tag{4.56b}$$

$$[\hat{\sigma}_N^+, [\hat{\sigma}_N^-, \hat{H}_{MFI1}]] = -8J\left(\hat{Z}_{N-1}\hat{Z}_N + p_f\hat{Z}_N\hat{Z}_1\right) - 4h_N^x\hat{\sigma}_N^+ - 8h_N^z\hat{Z}_N \tag{4.57a}$$

$$[\hat{\sigma}_N^-, [\hat{\sigma}_N^+, \hat{H}_{MFI1}]] = -8J\left(\hat{Z}_{N-1}\hat{Z}_N + p_f\hat{Z}_N\hat{Z}_1\right) - 4h_N^x\hat{\sigma}_N^- - 8h_N^z\hat{Z}_N \quad (4.57b)$$

$$[\hat{\sigma}_N^-, [\hat{\sigma}_N^+, \hat{H}_{MFI1}]] + [\hat{\sigma}_N^+, [\hat{\sigma}_N^-, \hat{H}_{MFI1}]] =$$
$$= -16J\left(\hat{Z}_{N-1}\hat{Z}_N + p_f\hat{Z}_N\hat{Z}_1\right) - 8h_N^x\hat{X}_N - 16h_N^z\hat{Z}_N \tag{4.57c}$$

$$\{\hat{\sigma}_N^+, [\hat{\sigma}_N^-, \hat{H}_{MFI1}]\} = -8J\left(\hat{Z}_{N-1} + p_f\hat{Z}_1\right) - 8h_N^z \tag{4.58a}$$

$$\{\hat{\sigma}_N^-, [\hat{\sigma}_N^+, \hat{H}_{MFI1}]\} = 8J\left(\hat{Z}_{N-1} + p_f\hat{Z}_1\right) + 8h_N^z \tag{4.58b}$$

$$\{\hat{\sigma}_N^-, [\hat{\sigma}_N^+, \hat{H}_{MFI1}]\} - \{\hat{\sigma}_N^+, [\hat{\sigma}_N^-, \hat{H}_{MFI1}]\} = 16J\left(\hat{Z}_{N-1} + p_f\hat{Z}_1\right) + 16h_N^z$$
$$\tag{4.58c}$$

5 | Quantum tunneling in a fermionic Sachdev-Ye-Kitaev model

5.1. Introduction

Non-equilibrium dynamics of the celebrated Sachdev-Ye-Kitaev (SYK) model [40, 39] – dual to a black hole in a two-dimensional anti-de Sitter space – instantaneously coupled to a larger cold media has been recently scrutinized [15, 13] intending to mimic black hole evaporation [116, 117, 118, 94, 64] in a compact quantum mechanical setup. Alongside, several platforms have been proposed for experimental realization of the SYK model: as a low-energy effective description of a topological insulator/superconductor interface with an irregular opening [119], Majorana wires coupled through a disordered quantum dot [120], ultracold atoms trapped in optical lattices [121, 122], graphene flake with a random boundary [123], and digital quantum simulation [124, 125, 126]. In this context, opening up the system to an outer environment arises naturally as the "black-hole chip" [119] is necessarily in contact with a substrate and probes.

Once the system is opened due to quench-coupling, it starts to equilibrate with the external reservoir. Of particular interest is how the initial shock and the subsequent equilibration affects the initial SYK state and transport observables. The SYK model describes strongly interacting fermions in $(0 + 1)$-dimensions. As such, it can be considered as a quantum dot that is usually characterized via tunneling current. In this manuscript, we consider the complex SYK model [46, 47] abruptly coupled to a zero temperature bath. We input the initial electrochemical potential in the SYK subsystem to enable quantum charge tunneling apart from the temperature drop between the SYK dot and the reservoir [15, 13]. Unlike equilibrium transport in the SYK quantum dot coupled to metallic leads [127, 128, 129, 130, 131], we are focused on the time evolution of both spectral properties and the tunneling current.

It was indicated earlier that right after the quench the SYK subsystem surprisingly heats up despite coupling to the colder bath [15, 13] and cools down later

equilibrating with the reservoir's temperature. In the holographic picture this initial heating is aligned with the increase of the subsystem energy that accompanies the information carried by the quench-induced shock-wave falling into the black hole [94]. We recover this result in the absence of a potential difference and confirm that the applied quench protocol cools down the SYK dot preserving an exotic SYK non-Fermi liquid phase after the relaxation. Proceeding to transport, we analyze the tunneling current evolution at low temperatures. We observe numerically that the current half-life – the time required for current to relax back to half its maximum value – grows linearly with the initial temperature of the SYK quantum dot. In contrast, replacing the SYK subsystem with a disordered Fermi liquid leads to a quadratic temperature increment of the current's half-life. This enables one to distinguish the SYK non-Fermi liquid from a more common disordered phase by means of the quench-tunneling protocol.

5.2. The model

We begin our analysis with the SYK model in thermal equilibrium (chemical potential μ, temperature T) coupled to a reservoir at zero chemical potential and zero temperature via tunneling term at time $t = 0$. The Hamiltonian reads

$$H = H_{SYK} + H_{res} + \theta(t)H_{tun}, \tag{5.1}$$

$$H_{SYK} = \frac{1}{(2N)^{3/2}} \sum_{i,j,k,l=1}^{N} J_{ij;kl} c_i^\dagger c_j^\dagger c_k c_l - \mu \sum_{i=1}^{N} c_i^\dagger c_i, \tag{5.2}$$

$$H_{res} = \frac{1}{\sqrt{M}} \sum_{\alpha,\beta=1}^{M} \xi_{\alpha\beta} \psi_\alpha^\dagger \psi_\beta + h.c., \tag{5.3}$$

$$H_{tun} = \frac{1}{(NM)^{1/4}} \sum_{i=1}^{N} \sum_{\alpha=1}^{M} \lambda_{i\alpha} c_i^\dagger \psi_\alpha + h.c., \tag{5.4}$$

where $J_{ij;kl} = J_{kl;ij}^* = -J_{ji;kl} = -J_{ij;lk}$, $\xi_{\alpha\beta}$, and $\lambda_{i\alpha}$ are Gaussian random variables with finite variances $\overline{|J_{ij;kl}|^2} = J^2$, $\overline{|\xi_{\alpha\beta}|^2} = \xi^2$, $\overline{|\lambda_{i\alpha}|^2} = \lambda^2$ and zero means. Below we assume the reservoir much larger than the SYK subsystem, which imposes $M \gg N$ for the modes numbers. The charging energy [129, 131, 132, 133] is supposed to be negligible comparing to the SYK band-width J.

The conventional way to address non-equilibrium dynamics of a quantum many-body system is solving Kadanoff-Baym (KB) equations for the two-point functions

$G^{\gtrless}(t,t') = -iN^{-1} \sum_{i=1}^{N} \langle c_i(t_{\mp}) \bar{c}_i(t'_{\pm}) \rangle$, where $\pm$ denotes the top/bottom branches of the Keldysh time contour [134]. Inasmuch as Schwinger-Keldysh formalism has been widely applied to the SYK model in both thermalization [57, 135, 13, 15, 136, 137] and transport [138, 127, 128] context, we leave the detailed derivation for Appendix 5.A and proceed straight to the Kadanoff-Baym equations that hold in the large N, M limit:

$$(i\partial_t + \mu) \, G^{\gtrless}(t,t') = \int_{-\infty}^{+\infty} du \Big(\Sigma_R(t,u) G^{\gtrless}(u,t') \\ + \Sigma^{\gtrless}(t,u) G_A(u,t') \Big),$$

(5.5)

$$(-i\partial_{t'} + \mu) \, G^{\gtrless}(t,t') = \int_{-\infty}^{+\infty} du \Big(G_R(t,u) \Sigma^{\gtrless}(u,t') \\ + G^{\gtrless}(t,u) \Sigma_A(u,t') \Big),$$

(5.6)

The self-energy

$$\Sigma^{\gtrless}(t,t') = J^2 G^{\gtrless}(t,t')^2 G^{\lessgtr}(t',t) \\ + \sqrt{p}\, \lambda^2 \theta(t)\theta(t') Q^{\gtrless}(t,t')$$

(5.7)

includes the contribution of the cool-bath as a time dependent background

$$Q^{\gtrless}(t,t') = -\frac{\mathbf{H}_1\big(2\xi(t-t')\big) \pm iJ_1\big(2\xi(t-t')\big)}{2\xi(t-t')}$$

(5.8)

expressed through Struve $\mathbf{H}_1$ and Bessel J_1 functions [139]; see Appendix 5.A. Here we introduce the ratio $p = M/N$ and limit ourselves to the large reservoir case $p \gg 1$. Below we assume $\xi = J$ for brevity.

The initial state of the system is settled by the thermal state of the bare SYK model (5.2) in absence of coupling to the reservoir. At the moment of quench the SYK subsystem (5.2) begins to deviate from the initial thermal state until it finally thermalizes at late times. Characterizing thermalization dynamics requires notion of the retarded, advanced, and Keldysh Green's functions

$$G_R(t,t') = \theta(t-t') \Big(G^{>}(t,t') - G^{<}(t,t') \Big),$$

(5.9)

$$G_A(t,t') = -\theta(t'-t) \Big(G^{>}(t,t') - G^{<}(t,t') \Big),$$

(5.10)

$$G_K(t,t') = G^{>}(t,t') + G^{<}(t,t')$$

(5.11)

expressed above in terms of the "greater" and "lesser" components. The same rules (5.9–5.11) apply to the self-energy (5.7).

The Green's functions are found numerically from the KB equations (5.5,5.6) with the self-energies (5.7,5.8). At first, we calculate the equilibrium Green's functions of the bare SYK model using an iterative approach [140, 141]. We apply an extra constraint manifesting the fluctuation-dissipation relation at initial temperature and chemical potential [1]. The equilibrium Green's functions set the initial condition for the Kadanoff-Baym equations and evolve as follows: the integrals in the KB equations are computed with the trapezoidal rule and the remaining differential equations are solved by the predictor-corrector scheme. The corrector adjusts self-consistently at every iteration [57, 135]. For the spectral properties we use the two-dimensional time grid with a step $\delta t = 0.02$ and $n \sim 10^4$ points in each direction, while for the transport calculations the numerical grid is more refined $\delta t = 0.005$ but has a smaller size $n \sim 10^3$.

5.3. Relaxation after the quench

In a while after the quench the system relaxes and approaches a thermal state. To demonstrate that, we rotate the time frame t, t' in the numerically computed Green's functions towards $\tau = t - t'$, $\mathcal{T} = (t + t')/2$ and make a Fourier transform along τ. Indeed, the system returns to a nearly-thermal state if the extended fluctuation dissipation relation

$$\frac{iG_K(\omega, \mathcal{T})}{A(\omega, \mathcal{T})} = \tanh \frac{\omega - \widetilde{\mu}(\mathcal{T})}{2\widetilde{T}(\mathcal{T})} \tag{5.12}$$

is fulfilled at frequencies in the vicinity of $\widetilde{\mu}$, where $A(\omega, \mathcal{T}) = -2\mathrm{Im}G_R(\omega, \mathcal{T})$ is the SYK spectral function. In contrast to the equilibrium case, the extended fluctuation dissipation relation (5.12) is manifestly time dependent via the "centre of mass" coordinate $\mathcal{T}$ which enters the effective temperature $\widetilde{T}$ and chemical potential $\widetilde{\mu}$. Overall, the ratio (5.12) determines the effective distribution function of the SYK fermions in a quasi-equilibrium state, since $\tanh \frac{\omega - \widetilde{\mu}}{2\widetilde{T}} = 1 - 2n_\mathrm{F}(\omega - \widetilde{\mu}, T)$, where n_F is the Fermi distribution function.

The effective temperature can be extracted from the fluctuation dissipation relation (5.12) by an inverse slope of the Green's functions ratio

$$\widetilde{T}(\mathcal{T}) = \left(\frac{\partial}{\partial \omega} \frac{2iG_K(\omega, \mathcal{T})}{A(\omega, \mathcal{T})} \bigg|_{\omega = \widetilde{\mu}} \right)^{-1} \tag{5.13}$$

---

[1] In thermal equilibrium the fluctuation dissipation relation states [134]: $G_K(\omega) = 2i\,\mathrm{Im}G_R(\omega) \tanh \frac{\omega - \mu}{2T}$
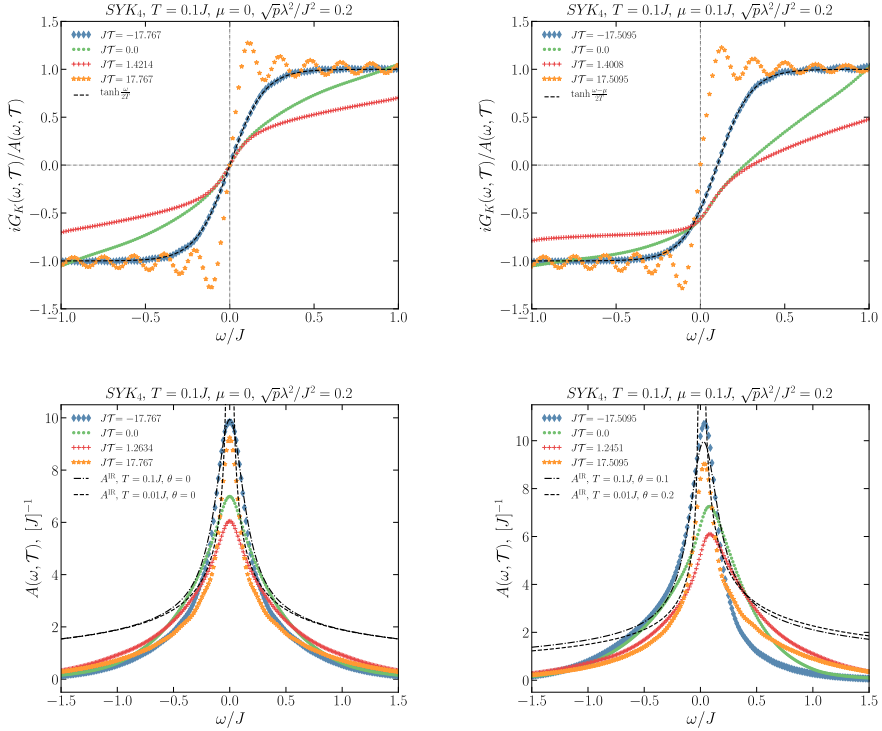
Figure 5.1. [**Top**] **Deviation of the SYK subsystem from the initial thermal state:** ratio between the Keldysh Green's function and the spectral function of the SYK model at charge neutrality (*Left panel*) and at finite chemical potential (*Right panel*). The equilibrium distribution functions at the initial temperature are profiled with the dashed lines. The oscillations noticeable in the orange curves have a numerical origin, viz. the quality of the computation depends on the size and refinement of the time grid. The time grid is designated in the t, t' space, while Fourier transform is done along diagonal $\tau = t - t'$. Ergo, the τ-lattices differ by length for separate slices of $\mathcal{T}$. Extension and refinement of the time grid suppress the oscillations. [**Bottom**] **Spectral function of the SYK model** as a function of frequency at charge neutrality (*Left panel*) and at finite chemical potential (*Right panel*). The dashed/dash-dot lines show the equilibrium SYK spectral function in the infrared regime for different parameters.

at $\omega = \widetilde{\mu}$. Following the top panel of Fig. 5.1, which shows the ratio (5.12), one notices the effective temperature increase around $\mathcal{T} = 0$, in spite of coupling to a colder reservoir. The initial effective temperature increment is followed by the subsequent temperature decay to the reservoir's temperature $T = 0$. This behavior was revealed earlier for the SYK model with Majorana zero-modes [15,
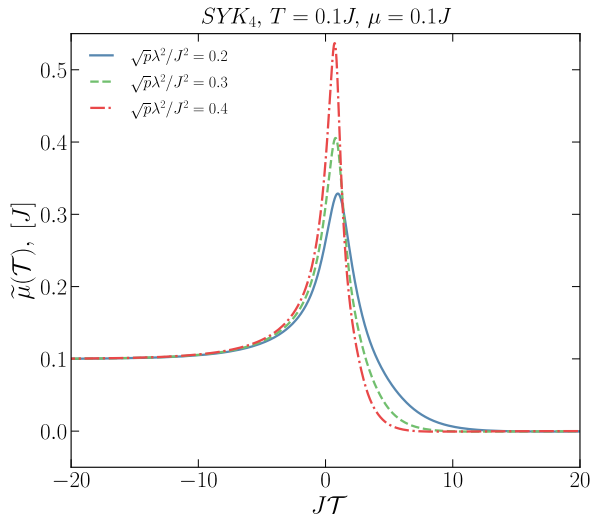
Figure 5.2. **Effective chemical potential in the SYK quantum dot** coupled to a large reservoir with $T_{res} = 0$ and $\mu_{res} = 0$.

13], however, as we show in a follow-up work [72, 102], this doesn't result in an increase of the actual temperature of the system unless there is a second decoupling quench. At late times $J\mathcal{T} \simeq 17.8$, the system clearly relaxes after the quench since the ratio (5.12) corresponds to the Fermi distribution at low temperature.

In comparison to the previous studies [13, 15], the new ingredient here is a charge imbalance between the SYK quantum dot and the cool-bath. Thereby, we track the electrochemical potential in the SYK subsystem which changes substantially once the quench is on. The effective chemical potential $\widetilde{\mu}(\mathcal{T})$ is set by the frequency where the ratio (5.12) turns to zero, as shown in Fig. 5.1 (*top right*). We plot the SYK chemical potential in Fig. 5.2, where $\widetilde{\mu}$ originates from the initial value $\mu = 0.1J$ in the SYK quantum dot for $\mathcal{T} \to -\infty$ and adjusts to the reservoir's $\mu_{res} = 0$ at late times $\mathcal{T} \to +\infty$. As noted in Fig. 5.2, the chemical potential responds to the quench with a non-monotonic behavior as a function of time $\mathcal{T}$, akin to the effective temperature. Note that the "centre of mass" time coordinate $\mathcal{T}$ and the actual time are not equivalent unless in a long-time limit. This explains why the chemical potential can already rise at small negative $\mathcal{T}$.

Since the tunneling between the SYK quantum dot and the reservoir turns on not adiabatically, of importance is whether the SYK non-Fermi liquid phase survives
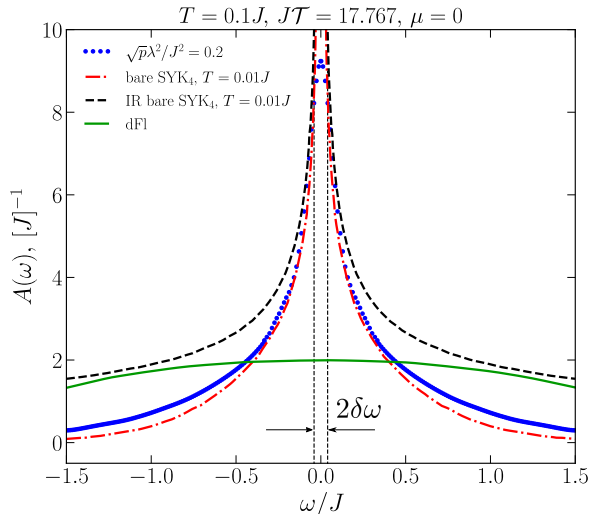
Figure 5.3. **Spectral of the SYK quantum dot** after the quench as a function of frequency. The blue dots show the result of the saddle-point numerics done for the evolution of the SYK subsystem with the initial temperature $T = 0.1J$ connected to a zero temperature reservoir with a coupling strength $\sqrt{p}\lambda^2/J^2 = 0.2$. The red dash-dot curve is the equilibrium saddle-point numerics for the bare SYK model at low temperatures, the black dashed line is the infrared (IR) solution of the bare SYK model (5.14), and the green line is the spectral function of the disordered Fermi liquid (dFl). The energy scale $\delta\omega = p\lambda^4/J^3$ indicates the region where the SYK nFl crosses over to a Fermi liquid.

the quench. We compare the SYK spectral function $A(\omega, \mathcal{T})$ a while after the quench to the equilibrium spectral function of the bare SYK model $A^{\mathrm{IR}}(\omega) = -2\mathrm{Im}G_R^{\mathrm{IR}}(\omega)$ in the infrared regime $J/N \ll \omega, T \ll J$, where

$$G_R^{\mathrm{IR}}(\omega) = -i\frac{C(\theta)e^{-i\theta}}{\sqrt{2\pi JT}}\frac{\Gamma\left(\frac{1}{4} - i\frac{\omega}{2\pi T} + i\mathcal{E}\right)}{\Gamma\left(\frac{3}{4} - i\frac{\omega}{2\pi T} + i\mathcal{E}\right)}, \tag{5.14}$$

$$e^{2\pi\mathcal{E}} = \frac{\sin\left(\frac{\pi}{4} + \theta\right)}{\sin\left(\frac{\pi}{4} - \theta\right)}, \quad C(\theta) = \left(\frac{\pi}{\cos 2\theta}\right)^{1/4}. \tag{5.15}$$

The low-frequency asymptotic (5.14), known as the conformal Green's function of the SYK model, does not explicitly depend on chemical potential. Instead, it depends on the independent parameter – the spectral asymmetry angle [46, 47]. The asymmetry angle θ [142] is nonzero away from charge neutrality ($\mu \neq 0$) and

related to the charge per site on the SYK quantum dot

$$\langle \mathcal{Q} \rangle = \frac{1}{N} \sum_{i=1}^{N} \langle c_i^\dagger c_i \rangle - \frac{1}{2} = -\frac{\theta}{\pi} - \frac{\sin 2\theta}{4}, \tag{5.16}$$

where $\langle \mathcal{Q} \rangle \in (-1/2, 1/2)$ and $\theta \in (-\pi/4, \pi/4)$ [46, 47].

As mentioned earlier, the system relaxes to the low-temperature Fermi distribution at $J\mathcal{T} \simeq 17.8$ (see Fig. 5.1 (*top left*)). In Fig. 5.3 we plot the spectral function of the SYK quantum dot in this regime. The spectral function after the quench is well aligned with the bare SYK spectral function at low temperatures. The SYK nFl state is known to break down in the presence of a Fermi liquid [143, 144]. Here we can estimate the timescale of the crossover to a Fermi liquid from the self-energy (5.7) comparing the SYK nFl and the reservoir's contributions. Indeed, substitution of the Green's functions $G(t) \propto 1/\sqrt{Jt}$ and $Q(t) \propto 1/(Jt)$ to the self-energy (5.7) shows that the crossover to a Fermi liquid happens for $t_{FL} \gtrsim 1/\delta\omega$, where $\delta\omega = p\lambda^4/J^3$. This implies that after relaxation from the quench the SYK nFl behavior can be read out from the spectral function for

$$\delta\omega \lesssim \omega \ll J. \tag{5.17}$$

The lower bound in inequality (5.17) can be suppressed as $\sqrt{p}\lambda^2/J \ll J$ in the weak tunneling limit. This observation agrees with the long timescale of the SYK nFl/Fermi liquid crossover found earlier in equilibrium studies [138, 145, 143, 129].

In Figs. 5.1 (*top right*), 5.2 we demonstrate that the system at finite initial μ tends to zero chemical potential in the long time limit. This is aligned with the discharging of the SYK quantum dot coupled to the large reservoir, which is kept at charge neutrality. At the level of the equilibrium SYK Green's function (5.14), this naively implies $\theta \approx 0$. However, the spectral function in Fig. 5.1 (*bottom right*) at long times is close enough to the conformal one with non-zero asymmetry angle θ. We plot the conformal spectral function with $\theta = 0.2$ as a reference. The origin of this mismatch may be that the asymmetry parameter θ is usually related to $\partial\mu/\partial T$ but not to the equilibrium value of the chemical potential [46]. In its turn, the temperature-independent part of the chemical potential in the SYK model is not a monotonic function of the asymmetry parameter [146]. Additionally, the SYK subsystem after the quench suffers the particle leak, that may require to account not only for a self-energy shift by the real-valued μ [46], but also an extra imaginary contribution to the self-energy. This issue could lead to the renormalization of θ in the final state, which is beyond the scope of this paper.

5.4. Tunneling current

Having discussed the SYK subsystem inner properties we proceed to transport. Specifically, we focus on the tunneling current:

$$\dot{\mathcal{Q}} = i[H, \mathcal{Q}] = -\frac{i}{N}\frac{\theta(t)}{(NM)^{1/4}}\sum_{i=1}^{N}\sum_{\alpha=1}^{M}\lambda_{i\alpha}c_i^{\dagger}\psi_{\alpha} + h.c. \tag{5.18}$$

The current's expectation value in the SYK quantum dot/cool-bath system is found from the generating functional $\ln Z[\chi]$ [127]

$$\mathcal{I} = \frac{1}{t_{\mathrm{m}}}\int_0^{t_{\mathrm{m}}}dt\langle\dot{\mathcal{Q}}(t)\rangle = \frac{1}{t_{\mathrm{m}}}\frac{\partial}{\partial(i\chi)}\ln Z[\chi]\Big|_{\chi=0}, \tag{5.19}$$

$$Z[\chi] = \left\langle \mathrm{T}_C e^{-i\int_C dt H(\chi)}\right\rangle = \int \mathcal{D}[\bar{c}, c]\mathcal{D}[\bar{\psi}, \psi]e^{iS[\chi]}, \tag{5.20}$$

where T_C is the time ordering along the Keldysh contour, t_{m} is the measurement time, and $S[\chi]$ is the effective action of the model with a counting field χ [147, 148]. The counting field χ transforms the tunneling Hamiltonian

$$H(\chi) = H_{SYK} + H_{res} + \theta(t)H_{tun}(\chi), \tag{5.21}$$

$$H_{tun}(\chi) = \frac{1}{(NM)^{1/4}}\sum_{i=1}^{N}\sum_{\alpha=1}^{M}\lambda_{i\alpha}e^{\frac{i\chi(t)}{2N}}c_i^{\dagger}\psi_{\alpha} + h.c., \tag{5.22}$$

so that

$$\chi(t) = \begin{cases} \chi & \text{for} \quad 0 < t < t_{\mathrm{m}} \\ 0 & \text{otherwise} \end{cases}, \tag{5.23}$$

The factor of two in the coupling phase in the tunneling term (5.22) accounts for the doubling due to the forward and backward branches of the Keldysh time contour.

One notices that the Hamiltonian transformation (5.22) is equivalent to a simple rotation of the coupling constants $\lambda_{i\alpha} \to \lambda_{i\alpha}e^{\frac{i\chi(t)}{2N}}$ in the original theory (5.1). Thus, the Kadanoff-Baym equations (5.5,5.6) describe the valid saddle-point for the partition function (5.20) up to the redefinition of the coupling constants λ_i. Indeed, the current can be deduced from the tunneling part of the effective action

$$S_{tun}(\chi) = i\sqrt{NM}\lambda^2 \sum_{ss'=\pm}\int_0^{+\infty}dt dt' ss' e^{\frac{i(s\chi(t)-s'\chi(t'))}{2N}}$$
$$\times G_{ss'}(t, t')Q_{s's}(t', t). \tag{5.24}$$
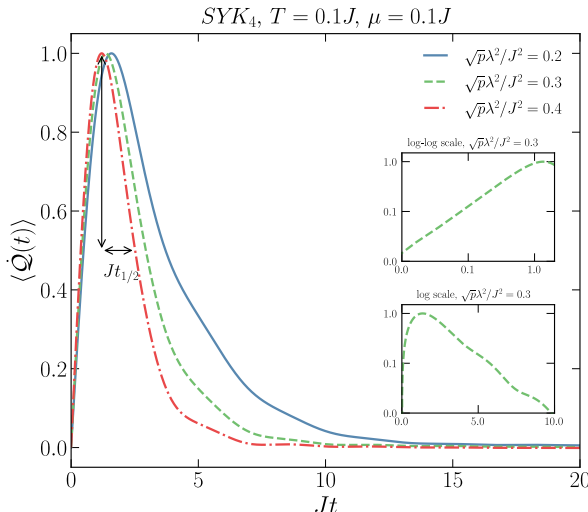
Figure 5.4. **Tunneling current** as a function of time normalized on its maximum value. The insets show time dependence of the current in log-log and log scales for $\sqrt{p}\lambda^2/J^2 = 0.3$. The log-log plot reveals the initial power law increase of the tunneling current, while the log plot is consistent with the exponential decay. We illustrate the current's half-life $t_{1/2}$ for $\sqrt{p}\lambda^2/J^2 = 0.4$.

Here the Green's functions $G_{ss'}$ and $Q_{ss'}$ describe the saddle-point of the SYK-bath system and are found from the equations (5.5-5.8), where $s = \pm$ denotes the forward and backward branch of the Keldysh contour. Accordingly, the counting field χ is defined on the Keldysh contour as $\chi_s(t) = s\chi(t)$. Leaving the detailed derivation of the full effective action of the SYK-bath coupled system for the Appendix 5.A, we proceed to the tunneling current

Applying the prescription (5.19), we derive the expectation value of current as a function of the measurement time t_{m}:

$$
\begin{aligned}
\mathcal{I} = &-\frac{\sqrt{p}\lambda^2}{2t_{\mathrm{m}}} \sum_{ss'} \int_0^{t_{\mathrm{m}}} dt \int_0^{+\infty} dt' \Big(G_{ss'}(t,t')s'Q_{s's}(t',t) \\
&- Q_{s's}(t,t')s\, G_{ss'}(t',t) \Big) \\
= &-\frac{\sqrt{p}\lambda^2}{2t_{\mathrm{m}}} \int_0^{t_{\mathrm{m}}} dt \int_0^{+\infty} dt' \operatorname{tr}\Big(\sigma^x \hat{G}(t,t')\hat{Q}(t',t) \\
&- \sigma^x \hat{Q}(t,t')\hat{G}(t',t) \Big),
\end{aligned}
\tag{5.25}
$$
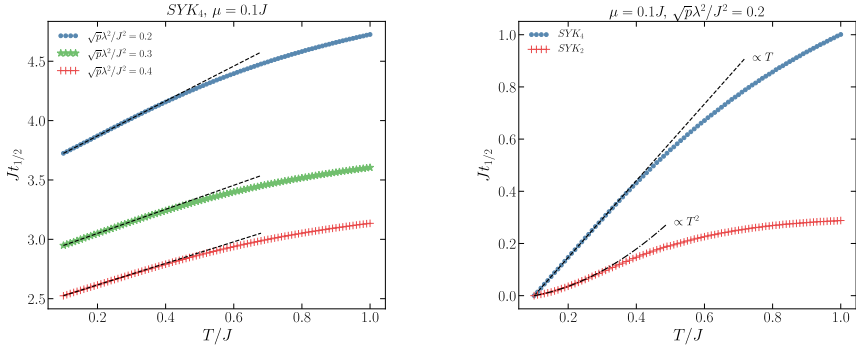
Figure 5.5. **Half-life of the tunneling current** as a function of the initial temperature. In the *left panel*, we compare the half-lives for the SYK model connected to a cool-bath for different coupling strengths. Meanwhile in the *right panel*, we show the difference between **SYK₄** (SYK non-Fermi liquid initial state) and **SYK₂** (disordered Fermi liquid initial state) behavior as a tested subsystem; the curves are shifted to the same origin for better visual comparison. The initial temperature changes from $T = 0.1J$ to $T = J$ with a step $\delta T = 0.01J$. The dashed/dashdot lines stand for the linear/quadratic fits made for the temperature interval $T \in [0.1J, 0.2J]$.

where

$$\hat{G} = \begin{pmatrix} G_R & G_K \\ 0 & G_A \end{pmatrix}, \quad \hat{Q} = \begin{pmatrix} Q_R & Q_K \\ 0 & Q_A \end{pmatrix} \tag{5.26}$$

are the Green's functions of the SYK quantum dot and the cool-bath set by the equations (5.5-5.8) and transformed to the R, A, K basis according to the rules (5.9-5.11) [2]. From here, the dynamics of the tunneling current is given by

$$\langle \dot{\mathcal{Q}}(t) \rangle = -\frac{\sqrt{p}\lambda^2}{2}\theta(t)\int_0^t dt' \mathcal{J}(t,t'), \tag{5.27}$$

$$\mathcal{J}(t,t') = G_R(t,t')Q_K(t',t) - Q_K(t,t')G_A(t',t)$$
$$- Q_R(t,t')G_K(t',t) + G_K(t,t')Q_A(t',t). \tag{5.28}$$

Time dependence of the tunneling current is shown in Fig. 5.4. The current grows initially as a power law, reaches the maximum value, and decays exponentially

---

[2]In equilibrium the fluctuation dissipation relation holds $G_K(\omega) = -2\pi i(1 - 2n_{SYK}(\omega))\nu_{SYK}(\omega)$, $Q_K(\omega) = -2\pi i(1 - 2n_{res}(\omega))\nu_{res}(\omega)$, where n_{SYK} and n_{res} are the Fermi distribution functions and $\nu_{SYK} = -\frac{1}{\pi}\mathrm{Im}G_R$ and $\nu_{res} = -\frac{1}{\pi}\mathrm{Im}Q_R$ are the densities of states. Substituting those to Eq. (5.25), one gets a familiar Fermi golden rule formula for the tunneling current [134]:
$\mathcal{I} = 2\pi\sqrt{p}\lambda^2 \int d\omega\, \nu_{SYK}(\omega)\nu_{res}(\omega)(n_{SYK}(\omega) - n_{res}(\omega))$.

to zero consistently with the discharging process of the SYK quantum dot. With intention to mark the lifetime of the effect we extract the half-life – the time in which the current is decreased in half of its maximum value. Varying the initial temperature T of the SYK quantum dot, we show the current's half-life for several coupling strengths in Fig. 5.5 (*left*). The stronger the coupling, the shorter the half-life of the tunneling current. Oppositely, the half-life increases with the initial temperature rise. For the temperatures $T \lesssim 0.4J$ the tunneling current half-life grows linearly in T.

To check if the T-linear current's half-life is specific for the SYK state, we substitute the SYK model with the one-body random Hamiltonian (5.3), often referred to as the SYK_2 model, the same that describes the reservoir. This model has a typical Fermi liquid Green's function $G_R(t) \propto 1/t$ in the long time limit $Jt \gg 1$, which makes it legitimate to build the SYK nFl/Fermi liquid comparison. Matching the tunneling current half-life for the SYK vs SYK_2 model in Fig. 5.5 (*right*), we ascertain that their temperature dependencies are drastically different. The current's half-life in the system of the SYK_2 quantum dot coupled to the cold bath increases as T^2 at low temperatures, which discerns it from the SYK model cooling protocol displaying the linearin temperature increase.

The duration of the tunneling event in our system is defined by the tunneling contact resistance, similarly to an exponentially relaxing capacitor discharge. As such, our results resemble the prominent resistivity predictions for strange metals $\rho_{SM} \sim T$ [149, 138, 145] and Fermi liquid $\rho_{FL} \sim T^2$.

5.5. Conclusion

The Sachdev-Ye-Kitaev model quench-coupled with a cold bath has been a subject of close attention aiming to simulate evaporation of a black hole [15, 13]. At the same time, both connecting the system to the environment and its further characterization are inherent for realization proposals of the SYK model in condensed matter systems [119, 123, 120, 121, 122]. In this manuscript, we consider a quantum dot described by the complex SYK model at finite temperature instantaneously coupled to a zero temperature reservoir. Analyzing the dynamical spectral function of the SYK quantum dot at charge neutrality, we show that the considered quench protocol preserves the SYK non-Fermi liquid state for the energies $\delta\omega \ll \omega \ll J$. Here the lower bound $\delta\omega$ is suppressed in the weak tunneling limit. Further, we put an initial electrochemical potential in the quantum dot and compute the tunneling current dynamics due to the discharging of the dot. The tunneling current half-life shows distinct temperature dependencies for different systems that are being cooled down. In case of the SYK quantum dot, the half-life increases linearly in the initial temperature T, while for the Fermi liquid the increase is $\propto T^2$. Therefore, this temperature dependence of the tunneling

current half-life provides a distinguishing feature for the disordered quantum dot exhibiting the SYK nFl phase against more common Fermi liquid behavior.

Acknowledgements

5.A. Derivation of the Kadanoff-Baym equations from the SYK saddle-point

Here we derive the Kadanoff-Baym equations for the SYK quantum dot coupled to a cool-bath by a quench.

5.A.1. Saddle-point equations

We perform the disorder average of with the Hamiltonian (5.1), pursuing [138, 128]. The effective action can be written in terms of bilocal fields $G_{s's}(t',t) = iN^{-1}\sum_i \bar{c}_{is}(t)c_{is}(t')$, $Q_{s's}(t',t) = iM^{-1}\sum_\alpha \bar{\psi}_{\alpha s}(t)\psi_{\alpha s}(t')$ and $\Sigma_{ss'}(t,t')$, $\Pi_{ss'}(t,t')$ as the corresponding Lagrange multipliers

$$
\begin{aligned}
S = &- iN\mathrm{trln}\Big[\sigma^z_{ss'}\delta(t-t')\,(i\partial_t + \mu) - \Sigma_{ss'}(t,t')\Big] - \\
&- iN\sum_{ss'}\int dtdt'\left(\Sigma_{ss'}(t,t')G_{s's}(t',t) - \frac{ss'J^2}{4}G_{ss'}(t,t')^2 G_{s's}(t',t)^2\right) - \\
&- iM\mathrm{trln}\Big[\sigma^z_{ss'}\delta(t-t')\,i\partial_t - \Pi_{ss'}(t,t')\Big] - \\
&- iM\sum_{ss'}\int dtdt'\left(\Pi_{ss'}(t,t')Q_{s's}(t',t) - \frac{ss'\xi^2}{2}Q_{ss'}(t,t')Q_{s's}(t',t)\right) + \\
&+ i\sqrt{NM}\sum_{ss'}\int dtdt'\, ss'\lambda^2\theta(t)\theta(t')G_{ss'}(t,t')Q_{s's}(t',t).
\end{aligned}
\tag{5.29}
$$

where $s = \pm$ denotes forward and backward branches of the Keldysh time contour [134]. In the large N, M limit, the saddle-point equations are

$$
\Sigma_{ss'}(t,t') = J^2 G_{ss'}(t,t')^2 G_{s's}(t',t) + \sqrt{p}\,\lambda^2\theta(t)\theta(t')Q_{ss'}(t,t'),
\tag{5.30}
$$

$$
\Pi_{ss'}(t,t') = \xi^2 Q_{ss'}(t,t') + \frac{\lambda^2}{\sqrt{p}}\,\theta(t)\theta(t')G_{ss'}(t,t'),
\tag{5.31}
$$

$$
\sum_r \int_{-\infty}^{+\infty} du\Big(\sigma^z_{sr}\delta(t-u)\,(i\partial_t + \mu) - sr\,\Sigma_{sr}(t,u)\Big)G_{rs'}(u,t') = \delta_{ss'}\delta(t-t'),
\tag{5.32}
$$

$$
\sum_r \int_{-\infty}^{+\infty} du\Big(\sigma^z_{sr}\delta(t-u)i\partial_t - sr\,\Pi_{sr}(t,u)\Big)Q_{rs'}(u,t') = \delta_{ss'}\delta(t-t'),
\tag{5.33}
$$

where $p = M/N$ is the mode ratio.

Following Ref. [57], we derive the self-consistent Kadanoff-Baym equations considering $s, s' = \pm, \mp$ components of Eqs. (5.32, 5.33):

$$(i\partial_t + \mu)\, G^{\gtrless}(t, t') = \int_{-\infty}^{+\infty} du \Big(\Sigma_R(t, u) G^{\gtrless}(u, t') + \Sigma^{\gtrless}(t, u) G_A(u, t') \Big), \quad (5.34)$$

$$(-i\partial_{t'} + \mu)\, G^{\gtrless}(t, t') = \int_{-\infty}^{+\infty} du \Big(G_R(t, u) \Sigma^{\gtrless}(u, t') + G^{\gtrless}(t, u) \Sigma_A(u, t') \Big), \quad (5.35)$$

$$i\partial_t Q^{\gtrless}(t, t') = \int_{-\infty}^{+\infty} du \Big(\Pi_R(t, u) Q^{\gtrless}(u, t') + \Pi^{\gtrless}(t, u) Q_A(u, t') \Big), \quad (5.36)$$

$$-i\partial_{t'} Q^{\gtrless}(t, t') = \int_{-\infty}^{+\infty} du \Big(Q_R(t, u) \Pi^{\gtrless}(u, t') + Q^{\gtrless}(t, u) \Pi_A(u, t') \Big), \quad (5.37)$$

where the self-energies are

$$\Sigma^{\gtrless}(t, t') = J^2 G^{\gtrless}(t, t')^2 G^{\lessgtr}(t', t) + \sqrt{p}\, \lambda^2 \theta(t) \theta(t') Q^{\gtrless}(t, t'), \quad (5.38)$$

$$\Pi^{\gtrless}(t, t') = \xi^2 Q^{\gtrless}(t, t') + \frac{\lambda^2}{\sqrt{p}}\, \theta(t) \theta(t') G^{\gtrless}(t, t'). \quad (5.39)$$

5.A.2. Reservoir as an external potential

Since we assume the reservoir to be large enough $p \gg 1$, it can be considered as a closed dynamic background to the SYK subsystem

$$\int_{-\infty}^{+\infty} du \Big(\delta(t - u) i\partial_t - \xi^2 \hat{Q}(t, u) \Big) \hat{Q}(u, t') = \delta(t - t') \quad (5.40)$$

describing a decoupled random free fermion in equilibrium. Here we perform a rotation towards retarded, advanced, and Keldysh basis

$$\hat{Q} = \begin{pmatrix} Q_R & Q_K \\ 0 & Q_A \end{pmatrix} = L\sigma^z \begin{pmatrix} Q_{++} & Q_{+-} \\ Q_{-+} & Q_{--} \end{pmatrix} L^\dagger, \quad L = \frac{1}{\sqrt{2}} \begin{pmatrix} 1 & -1 \\ 1 & 1 \end{pmatrix}.$$

The retarded Green's function is found from

$$\Big(\omega - \xi^2 Q_R(\omega) \Big) Q_R(\omega) = 1 \quad \Rightarrow \quad Q_R(\omega) = \frac{\omega}{2\xi^2} - \frac{i}{\xi}\sqrt{1 - \frac{\omega^2}{4\xi^2}} =$$

$$= \frac{2}{\omega + 2i\xi\sqrt{1 - \big(\omega/2\xi\big)^2}},$$

where the spectral function obeys the semicircle law $\rho(\omega) = -2\operatorname{Im}Q_R(\omega) = \frac{2}{\xi}\operatorname{Re}\sqrt{1 - \frac{\omega^2}{4\xi^2}}$. Let's derive the time representation of Q_R:

$$Q_R(t,t') = Q_A(t',t)^* = \int_{-\infty}^{+\infty} \frac{d\omega}{2\pi} e^{-i\omega(t-t')} Q_R(\omega) =$$
$$= -\lim_{\delta\to 0^+} \int_{-\infty}^{+\infty} \frac{d\omega}{2\pi} e^{-i\omega(t-t')} e^{\delta(t-t')} \frac{1}{2\xi^2} \sqrt{(\omega+i\delta)^2 - 4\xi^2}.$$
$$(5.41)$$

Here the branch cut is in the lower half plane, so we close the contour correspondingly for $t - t' > 0$. Since there are no poles in the lower half plane, we shrink the contour to the anticlockwise traverse around the branch cut. Note that an additional phase is acquired when crossing the branch cut $\sqrt{\omega^2 - 4\xi^2} \to e^{\frac{1}{2}\ln(\omega^2 + 4\xi^2) + i\pi} = e^{i\pi}\sqrt{\omega^2 - 4\xi^2}$. Therefore, we get

$$Q_R(t,t') = -\theta(t-t')\frac{1 - e^{i\pi}}{4\pi\xi^2} \int_{-2\xi}^{2\xi} d\omega\, e^{-i\omega(t-t')}\sqrt{\omega^2 - 4\xi^2} =$$
$$= -i\theta(t-t')\frac{J_1\big(2\xi(t-t')\big)}{\xi(t-t')},$$
$$(5.42)$$

where J_1 is the first Bessel function of the first kind. The Keldysh component at zero temperature is

$$Q_K(t,t') = \int_{-\infty}^{+\infty} \frac{d\omega}{2\pi} e^{-i\omega(t-t')} Q_K(\omega) = \int_{-\infty}^{+\infty} \frac{d\omega}{2\pi} e^{-i\omega(t-t')} 2i\operatorname{sgn}(\omega)\operatorname{Im}Q_R(\omega)$$
$$= -\frac{i}{2\pi\xi^2} \int_{-2\xi}^{2\xi} d\omega\, e^{-i\omega(t-t')} \operatorname{sgn}(\omega)\sqrt{4\xi^2 - \omega^2} = -\frac{\mathbf{H}_1\big(2\xi(t-t')\big)}{\xi(t-t')},$$
$$(5.43)$$

where $\mathbf{H}_1$ is the first Struve function.

5.A.3. Dynamics of the SYK subsystem

In the large p limit, the dynamics of the SYK subsystem is described by Eqs. (5.34,5.35,5.38), where the reservoir Green's function $Q(t - t')$ enters the SYK self-energy (5.38) as the external potential derived in Section 5.A.2. Thereby, the Kadanoff-Baym equations simplify to

$$(i\partial_t + \mu)\, G^{\gtrless}(t,t') = \int_{-\infty}^{+\infty} du\Big(\Sigma_R(t,u)G^{\gtrless}(u,t') + \Sigma^{\gtrless}(t,u)G_A(u,t')\Big), \quad (5.44)$$

$$(-i\partial_{t'} + \mu)\, G^{\gtrless}(t,t') = \int_{-\infty}^{+\infty} du\Big(G_R(t,u)\Sigma^{\gtrless}(u,t') + G^{\gtrless}(t,u)\Sigma_A(u,t')\Big), \quad (5.45)$$

with the self-energy (5.30)

$$\Sigma^{\gtrless}(t,t') = J^2 G^{\gtrless}(t,t')^2 G^{\lessgtr}(t',t) + \sqrt{p}\,\lambda^2 \theta(t)\theta(t')Q^{\gtrless}(t,t'), \tag{5.46}$$

$$Q^{\gtrless}(t,t') = -\frac{1}{2\xi(t-t')}\Big(\mathbf{H}_1\big(2\xi(t-t')\big) \pm iJ_1\big(2\xi(t-t')\big)\Big). \tag{5.47}$$

Here we introduced [134] $G^>(t,t') \equiv G_{-+}(t,t')$, $G^<(t,t') \equiv G_{+-}(t,t')$, $\Sigma^>(t,t') \equiv \Sigma_{-+}(t,t')$, $\Sigma^<(t,t') \equiv \Sigma_{+-}(t,t')$ and account for

$$G_{++}(t,t') = \theta(t-t')G^>(t,t') + \theta(t'-t)G^<(t,t'), \tag{5.48}$$

$$G_{--}(t,t') = \theta(t'-t)G^>(t,t') + \theta(t-t')G^<(t,t'), \tag{5.49}$$

$$\Sigma_{++}(t,t') = \theta(t-t')\Sigma^>(t,t') + \theta(t'-t)\Sigma^<(t,t'), \tag{5.50}$$

$$\Sigma_{--}(t,t') = \theta(t'-t)\Sigma^>(t,t') + \theta(t-t')\Sigma^<(t,t'). \tag{5.51}$$

The retarded, advanced, and Keldysh components are expressed in terms of $>$ and $<$ as

$$G_R(t,t') = \theta(t-t')\Big(G^>(t,t') - G^<(t,t')\Big), \tag{5.52}$$

$$G_A(t,t') = -\theta(t'-t)\Big(G^>(t,t') - G^<(t,t')\Big), \tag{5.53}$$

$$G_K(t,t') = G^>(t,t') + G^<(t,t'), \tag{5.54}$$

$$\Sigma_R(t,t') = \theta(t-t')\Big(\Sigma^>(t,t') - \Sigma^<(t,t')\Big), \tag{5.55}$$

$$\Sigma_A(t,t') = -\theta(t'-t)\Big(\Sigma^>(t,t') - \Sigma^<(t,t')\Big), \tag{5.56}$$

$$\Sigma_K(t,t') = \Sigma^>(t,t') + \Sigma^<(t,t'). \tag{5.57}$$

Bibliography

[1] Marcos Rigol, Vanja Dunjko, and Maxim Olshanii. "Thermalization and its mechanism for generic isolated quantum systems". In: *Nature* 452.7189 (Apr. 2008), pp. 854–858. DOI: 10.1038/nature06838.

[2] J. M. Deutsch. "Quantum statistical mechanics in a closed system". In: *Phys. Rev. A* 43 (4 Feb. 1991), pp. 2046–2049. DOI: 10.1103/PhysRevA.43.2046.

[3] Mark Srednicki. "Chaos and quantum thermalization". In: *Phys. Rev. E* 50 (2 Aug. 1994), pp. 888–901. DOI: 10.1103/PhysRevE.50.888.

[4] Luca D'Alessio et al. "From quantum chaos and eigenstate thermalization to statistical mechanics and thermodynamics". In: *Advances in Physics* 65.3 (May 2016), pp. 239–362. DOI: 10.1080/00018732.2016.1198134.

[5] Andrew Hallam, James Morley, and Andrew G. Green. "The Lyapunov Spectrum of Quantum Thermalisation". In: *Nature Communications* 10.1 (2019), p. 2708. ISSN: 2041-1723. DOI: 10.1038/s41467-019-10336-4. arXiv: 1806.05204 [cond-mat, physics:quant-ph].

[6] Stefan Trotzky et al. "Probing the Relaxation towards Equilibrium in an Isolated Strongly Correlated 1D Bose Gas". In: *Nature Physics* 8.4 (2012), pp. 325–330. ISSN: 1745-2473, 1745-2481. DOI: 10.1038/nphys2232. arXiv: 1101.2659 [cond-mat, physics:quant-ph].

[7] Tim Langen et al. "Local Emergence of Thermal Correlations in an Isolated Quantum Many-Body System". In: *Nature Physics* 9.10 (2013), pp. 640–643. ISSN: 1745-2473, 1745-2481. DOI: 10.1038/nphys2739. arXiv: 1305.3708 [cond-mat, physics:quant-ph].

[8] Govinda Clos et al. "Time-Resolved Observation of Thermalization in an Isolated Quantum System". In: *Physical Review Letters* 117.17 (2016), p. 170401. ISSN: 0031-9007, 1079-7114. DOI: 10.1103/PhysRevLett.117.170401. arXiv: 1509.07712 [quant-ph].

[9] Adam M. Kaufman et al. "Quantum Thermalization through Entanglement in an Isolated Many-Body System". In: *Science* 353.6301 (2016), pp. 794–800. ISSN: 0036-8075, 1095-9203. DOI: 10.1126/science.aaf6725. arXiv: 1603.04409 [cond-mat, physics:physics, physics:quant-ph].

[10] C. Neill et al. "Ergodic Dynamics and Thermalization in an Isolated Quantum System". In: *Nature Physics* 12.11 (2016), pp. 1037–1041. ISSN: 1745-2473, 1745-2481. DOI: 10.1038/nphys3830. arXiv: 1601.00600 [quant-ph].

[11] Yijun Tang et al. "Thermalization near Integrability in a Dipolar Quantum Newton's Cradle". In: *Physical Review X* 8.2 (2018), p. 021030. ISSN: 2160-3308. DOI: 10.1103/PhysRevX.8.021030. arXiv: 1707.07031 [cond-mat, physics:physics, physics:quant-ph].

[12] "7th Les Houches School in Computational Physics: Dynamics of Complex Quantum Systems, from Theory to Computation". In: (2021).

[13] Pengfei Zhang. "Evaporation dynamics of the Sachdev-Ye-Kitaev model". In: *Phys. Rev. B* 100 (24 Dec. 2019), p. 245104. DOI: 10.1103/PhysRevB.100.245104.

[14] Juan Maldacena and Alexey Milekhin. *SYK wormhole formation in real time.* 2020. arXiv: 1912.03276 [hep-th].

[15] Ahmed Almheiri, Alexey Milekhin, and Brian Swingle. "Universal Constraints on Energy Flow and SYK Thermalization". In: (2019). arXiv: 1912.04912 [hep-th].

[16] Daniel L. Jafferis et al. "Relative entropy equals bulk relative entropy". In: *Journal of High Energy Physics* 2016.6 (June 2016). DOI: 10.1007/jhep06(2016)004.

[17] B. Keimer et al. "From quantum matter to high-temperature superconductivity in copper oxides". In: *Nature* 518.7538 (Feb. 2015), pp. 179–186. ISSN: 1476-4687. DOI: 10.1038/nature14165.

[18] N. F. Balm et al. "T-linear resistivity, optical conductivity, and Planckian transport for a holographic local quantum critical metal in a periodic potential". In: *Physical Review B* 108.12 (Sept. 2023). DOI: 10.1103/physrevb.108.125145.

[19] Aavishkar A. Patel, Michael J. Lawler, and Eun-Ah Kim. "Coherent Superconductivity with a Large Gap Ratio from Incoherent Metals". In: *Physical Review Letters* 121.18 (Oct. 2018). DOI: 10.1103/physrevlett.121.187001.

[20] Peter Cha et al. "Linear resistivity and Sachdev-Ye-Kitaev (SYK) spin liquid behavior in a quantum critical metal with spin-1/2 fermions". In: *Proceedings of the National Academy of Sciences* 117.31 (July 2020), pp. 18341–18346. DOI: 10.1073/pnas.2003179117.

[21] Michael A. Nielsen and Isaac L. Chuang. *Quantum Computation and Quantum Information.* Cambridge University Press, 2009. DOI: 10.1017/cbo9780511976667.

[22] Sebastian Deffner and Steve Campbell. *Quantum Thermodynamics.* Morgan & Claypool Publishers, 2019. ISBN: 978-1-64327-658-8. DOI: 10.1088/2053-2571/ab21c6.

[23] Ken Funo, Yu Watanabe, and Masahito Ueda. "Thermodynamic work gain from entanglement". In: *Phys. Rev. A* 88 (5 2013), p. 052319. DOI: 10.1103/PhysRevA.88.052319.

[24] Anatoly I. Larkin and Yu. N. Ovchinnikov. "Quasiclassical Method in the Theory of Superconductivity". In: *Journal of Experimental and Theoretical Physics* (1969).

[25] Juan Maldacena, Stephen H. Shenker, and Douglas Stanford. "A bound on chaos". In: *Journal of High Energy Physics* 2016.8 (Aug. 2016). ISSN: 1029-8479. DOI: 10.1007/jhep08(2016)106.

[26] Aurelio Romero-Bermúdez, Koenraad Schalm, and Vincenzo Scopelliti. "Regularization dependence of the OTOC. Which Lyapunov spectrum is the physical one?" In: *Journal of High Energy Physics* 2019.7 (July 2019). DOI: 10.1007/jhep07(2019)107.

[27] M.L. Mehta and M. Gaudin. "On the density of Eigenvalues of a random matrix". In: *Nuclear Physics* 18 (1960), pp. 420–427. ISSN: 0029-5582. DOI: https://doi.org/10.1016/0029-5582(60)90414-4.

[28] Thomas Guhr, Axel Müller–Groeling, and Hans A. Weidenmüller. "Random-matrix theories in quantum physics: common concepts". In: *Physics Reports* 299.4-6 (June 1998), pp. 189–425. DOI: 10.1016/s0370-1573(97)00088-4.

[29] Freeman J. Dyson. "Statistical Theory of the Energy Levels of Complex Systems. I". In: *Journal of Mathematical Physics* 3.1 (Dec. 2004), pp. 140–156. ISSN: 0022-2488. DOI: 10.1063/1.1703773. eprint: https://pubs.aip.org/aip/jmp/article-pdf/3/1/140/8157927/140_1_online.pdf.

[30] Freeman J. Dyson. "Statistical Theory of the Energy Levels of Complex Systems. II". In: *Journal of Mathematical Physics* 3.1 (Dec. 2004), pp. 157–165. ISSN: 0022-2488. DOI: 10.1063/1.1703774. eprint: https://pubs.aip.org/aip/jmp/article-pdf/3/1/157/8158003/157_1_online.pdf.

[31] Freeman J. Dyson. "Statistical Theory of the Energy Levels of Complex Systems. III". In: *Journal of Mathematical Physics* 3.1 (Dec. 2004), pp. 166–175. ISSN: 0022-2488. DOI: 10.1063/1.1703775. eprint: https://pubs.aip.org/aip/jmp/article-pdf/3/1/166/8157965/166_1_online.pdf.

[32] Michel Gaudin. "Sur la loi limite de l'espacement des valeurs propres d'une matrice ale´atoire". In: *Nuclear Physics* 25 (1961), pp. 447–458. ISSN: 0029-5582. DOI: https://doi.org/10.1016/0029-5582(61)90176-6.

[33] O. Bohigas, M. J. Giannoni, and C. Schmit. "Characterization of Chaotic Quantum Spectra and Universality of Level Fluctuation Laws". In: *Phys. Rev. Lett.* 52 (1 Jan. 1984), pp. 1–4. DOI: 10.1103/PhysRevLett.52.1.

[34] Lea F. Santos and Marcos Rigol. "Onset of quantum chaos in one-dimensional bosonic and fermionic systems and its relation to thermalization". In: *Physical Review E* 81.3 (Mar. 2010). DOI: 10.1103/physreve.81.036206.

[35] Ranjan Modak and Subroto Mukerjee. "Finite size scaling in crossover among different random matrix ensembles in microscopic lattice models". In: *New Journal of Physics* 16.9 (Sept. 2014), p. 093016. DOI: 10.1088/1367-2630/16/9/093016.

[36] M. V. Berry and M. Tabor. "Level Clustering in the Regular Spectrum". In: *Proceedings of the Royal Society of London. Series A, Mathematical and Physical Sciences* 356.1686 (1977), pp. 375–394. ISSN: 00804630.

[37] Ahmed A. Elkamshishy and Chris H. Greene. "Observation of Wigner-Dyson level statistics in a classically integrable system". In: *Physical Review E* 103.6 (June 2021). DOI: 10.1103/physreve.103.062211.

[38] Y. Alhassid. "The statistical theory of quantum dots". In: *Rev. Mod. Phys.* 72 (4 Oct. 2000), pp. 895–968. DOI: 10.1103/RevModPhys.72.895.

[39] Subir Sachdev and Jinwu Ye. "Gapless spin-fluid ground state in a random quantum Heisenberg magnet". In: *Phys. Rev. Lett.* 70 (21 May 1993), pp. 3339–3342. DOI: 10.1103/PhysRevLett.70.3339.

[40] A. Kitaev. *A simple model of quantum holography.* KITP Program: Entanglement in Strongly-Correlated Quantum Matter, 2015.

[41] Julian Sonner and Manuel Vielma. "Eigenstate thermalization in the Sachdev-Ye-Kitaev model". In: *JHEP* 11 (2017), p. 149. DOI: 10.1007/JHEP11(2017)149. arXiv: 1707.08013 [hep-th].

[42] Ahmed Almheiri and Joseph Polchinski. *Models of AdS$_2$ Backreaction and Holography.* 2014. DOI: 10.48550/ARXIV.1402.6334.

[43] Kristan Jensen. "Chaos in AdS$_2$ Holography". In: *Physical Review Letters* 117.11 (Sept. 2016). DOI: 10.1103/physrevlett.117.111601.

[44] Julius Engelsöy, Thomas G. Mertens, and Herman Verlinde. "An investigation of AdS$_2$ backreaction and holography". In: *JHEP* 07 (2016), p. 139. DOI: 10.1007/JHEP07(2016)139. arXiv: 1606.03438 [hep-th].

[45] Subir Sachdev. "Holographic Metals and the Fractionalized Fermi Liquid". In: *Phys. Rev. Lett.* 105 (15 Oct. 2010), p. 151602. DOI: 10.1103/PhysRevLett.105.151602.

[46] Subir Sachdev. "Bekenstein-Hawking Entropy and Strange Metals". In: *Phys. Rev. X* 5 (4 Nov. 2015), p. 041025. DOI: 10.1103/PhysRevX.5.041025.

[47] Yingfei Gu et al. "Notes on the complex Sachdev-Ye-Kitaev model". In: *J. High Energy Phys.* 2020 (2020), p. 157. DOI: 10.1007/JHEP02(2020)157.

[48] Chenyuan Li, Subir Sachdev, and Darshan G. Joshi. "Superconductivity of non-Fermi liquids described by Sachdev-Ye-Kitaev models". In: *Physical Review Research* 5.1 (Jan. 2023). DOI: 10.1103/physrevresearch.5.013045.

[49] Pasquale Calabrese, Fabian H. L. Essler, and Maurizio Fagotti. "Quantum Quench in the Transverse-Field Ising Chain". In: *Physical Review Letters* 106.22 (June 2011). DOI: 10.1103/physrevlett.106.227203.

[50] Subir Sachdev. *Quantum Phase Transitions*. 2nd ed. Cambridge University Press, 2011. DOI: 10.1017/CBO9780511973765.

[51] Shenglong Xu and Brian Swingle. "Accessing scrambling using matrix product operators". In: *Nature Physics* 16.2 (Nov. 2019), pp. 199–204. DOI: 10.1038/s41567-019-0712-4.

[52] Ben Craps et al. "Lyapunov growth in quantum spin chains". In: *Physical Review B* 101.17 (May 2020). DOI: 10.1103/physrevb.101.174313.

[53] James R. Garrison and Tarun Grover. "Does a Single Eigenstate Encode the Full Hamiltonian?" In: *Physical Review X* 8.2 (Apr. 2018). DOI: 10.1103/physrevx.8.021026.

[54] J. Karthik, Auditya Sharma, and Arul Lakshminarayan. "Entanglement, avoided crossings, and quantum chaos in an Ising model with a tilted magnetic field". In: *Physical Review A* 75.2 (Feb. 2007). DOI: 10.1103/physreva.75.022304.

[55] Juan Maldacena and Douglas Stanford. "Remarks on the Sachdev-Ye-Kitaev model". In: *Phys. Rev. D* 94 (10 Nov. 2016), p. 106002. DOI: 10.1103/PhysRevD.94.106002.

[56] D A Trunin. "Pedagogical introduction to the Sachdev–Ye–Kitaev model and two-dimensional dilaton gravity". In: *Physics-Uspekhi* 64.3 (June 2021), pp. 219–252. DOI: 10.3367/ufne.2020.06.038805.

[57] Andreas Eberlein et al. "Quantum quench of the Sachdev-Ye-Kitaev model". In: *Phys. Rev. B* 96 (20 Nov. 2017), p. 205123. DOI: 10.1103/PhysRevB.96.205123.

[58] Irina Aref'eva et al. "Replica-nondiagonal solutions in the SYK model". In: *Journal of High Energy Physics* 2019.7 (July 2019). DOI: 10.1007/jhep07(2019)113.

[59] Antonio M. García-García et al. *Replica Symmetry Breaking and Phase Transitions in a PT Symmetric Sachdev-Ye-Kitaev Model*. 2021. DOI: 10.48550/ARXIV.2102.06630.

[60] Elliott Lieb, Theodore Schultz, and Daniel Mattis. "Two soluble models of an antiferromagnetic chain". In: *Annals of Physics* 16.3 (Dec. 1961), pp. 407–466. DOI: 10.1016/0003-4916(61)90115-4.

[61] M. C. Bañ uls, J. I. Cirac, and M. B. Hastings. "Strong and Weak Thermalization of Infinite Nonintegrable Quantum Systems". In: *Physical Review Letters* 106.5 (Feb. 2011). DOI: 10.1103/physrevlett.106.050405.

[62] Geoff Penington et al. "Replica wormholes and the black hole interior". In: (Nov. 2019). arXiv: 1911.11977 [hep-th].

[63] Geoffrey Penington. "Entanglement Wedge Reconstruction and the Information Paradox". In: *JHEP* 09 (2020), p. 002. DOI: 10.1007/JHEP09(2020)002. arXiv: 1905.08255 [hep-th].

[64] Ahmed Almheiri, Raghu Mahajan, and Juan Maldacena. "Islands outside the horizon". In: (2019). arXiv: 1910.11077 [hep-th].

[65] Ahmed Almheiri et al. "The Page curve of Hawking radiation from semiclassical geometry". In: *JHEP* 03 (2020), p. 149. DOI: 10.1007/JHEP03(2020)149.

[66] Gabor Sarosi. "AdS$_2$ holography and the SYK model". In: *Proceedings of XIII Modave Summer School in Mathematical Physics — PoS(Modave2017)*. Sissa Medialab, Mar. 2018. DOI: 10.22323/1.323.0001.

[67] Roman Jackiw. "Lower dimensional gravity". In: *Nuclear Physics B* 252 (1985), pp. 343–356. ISSN: 0550-3213. DOI: https://doi.org/10.1016/0550-3213(85)90448-1.

[68] Claudio Teitelboim. "Gravitation and hamiltonian structure in two spacetime dimensions". In: *Physics Letters B* 126.1 (1983), pp. 41–45. ISSN: 0370-2693. DOI: https://doi.org/10.1016/0370-2693(83)90012-6.

[69] Daniel Grumiller and Robert McNees. "Thermodynamics of black holes in two (and higher) dimensions". In: *Journal of High Energy Physics* 2007.04 (Apr. 2007), pp. 074–074. DOI: 10.1088/1126-6708/2007/04/074.

[70] Juan Maldacena, Douglas Stanford, and Zhenbin Yang. *Conformal symmetry and its breaking in two dimensional Nearly Anti-de-Sitter space*. 2016. arXiv: 1606.01857 [hep-th].

[71] N. V. Gnezdilov et al. "Ultrafast dynamics of cold Fermi gas after a local quench". In: *Phys. Rev. A* 107.3 (2023), p. L031301. DOI: 10.1103/PhysRevA.107.L031301. arXiv: 2108.12031 [cond-mat.quant-gas].

[72] V. Ohanesjan et al. "Energy dynamics, information and heat flow in quenched cooling and the crossover from quantum to classical thermodynamics". In: *arXiv preprint:2204.12411* (2022).

[73] Y. Cheipesh et al. "Quantum tunneling dynamics in a complex-valued Sachdev-Ye-Kitaev model quench-coupled to a cool bath". In: *Phys. Rev. B* 104.11 (2021), p. 115134. DOI: 10.1103/PhysRevB.104.115134. arXiv: 2011.05238 [cond-mat.str-el].

[74] C. W. J. Beenakker. "Electron-hole entanglement in the Fermi sea". In: *arXiv preprint:cond-mat/0508488* (2005).

[75] C. W. J. Beenakker et al. "Proposal for Production and Detection of Entangled Electron-Hole Pairs in a Degenerate Electron Gas". In: *Phys. Rev. Lett.* 91 (14 2003), p. 147901. DOI: 10.1103/PhysRevLett.91.147901.

[76]   Israel Klich. "Lower entropy bounds and particle number fluctuations in a Fermi sea". In: *J. Phys. A: Math. Gen.* 39 (2006), p. L85. DOI: 10.1088/0305-4470/39/4/102.

[77]   Israel Klich and Leonid Levitov. "Quantum Noise as an Entanglement Meter". In: *Phys. Rev. Lett.* 102 (10 2009), p. 100502. DOI: 10.1103/PhysRevLett.102.100502.

[78]   John Cardy. "Measuring Entanglement Using Quantum Quenches". In: *Phys. Rev. Lett.* 106 (15 2011), p. 150404. DOI: 10.1103/PhysRevLett.106.150404.

[79]   Dmitry A. Abanin and Eugene Demler. "Measuring Entanglement Entropy of a Generic Many-Body System with a Quantum Switch". In: *Phys. Rev. Lett.* 109 (2 2012), p. 020504. DOI: 10.1103/PhysRevLett.109.020504.

[80]   Rajibul Islam et al. "Measuring entanglement entropy in a quantum many-body system". In: *Nature* 528 (2015), p. 77. DOI: 10.1038/nature15750.

[81]   T. Sagawa. "Second Law-Like Inequalities with Quantum Relative Entropy: An Introduction". In: *Kinki University Series on Quantum Computing*. World Scientific, 2012, p. 125. DOI: 10.1142/9789814425193_0003.

[82]   R. Dorner et al. "Emergent Thermodynamics in a Quenched Quantum Many-Body System". In: *Phys. Rev. Lett.* 109 (16 2012), p. 160601. DOI: 10.1103/PhysRevLett.109.160601.

[83]   Michele Campisi and Rosario Fazio. "Dissipation, correlation and lags in heat engines". In: *J. Phys. A: Math. Theor.* 49 (2016), p. 345002. DOI: 10.1088/1751-8113/49/34/345002.

[84]   Takahiro Sagawa and Masahito Ueda. "Minimal Energy Cost for Thermodynamic Information Processing: Measurement and Information Erasure". In: *Phys. Rev. Lett.* 102 (25 2009), p. 250602. DOI: 10.1103/PhysRevLett.102.250602.

[85]   Wojciech H. Zurek. "Decoherence and the Transition from Quantum to Classical". In: *Physics Today* 44 (1991), p. 36. DOI: 10.1063/1.881293.

[86]   Maria Popovic, Mark T. Mitchison, and John Goold. "Thermodynamics of decoherence". In: *arXiv preprint:2107.14216* (2021).

[87]   Wojciech Hubert Zurek and Juan Pablo Paz. "Decoherence, chaos, and the second law". In: *Phys. Rev. Lett.* 72 (16 1994), p. 2508. DOI: 10.1103/PhysRevLett.72.2508.

[88]   Wojciech Hubert Zurek. "Decoherence, einselection, and the quantum origins of the classical". In: *Rev. Mod. Phys.* 75 (3 2003), p. 715. DOI: 10.1103/RevModPhys.75.715.

[89]   Davide Rossini et al. "Quantum Advantage in the Charging Process of Sachdev-Ye-Kitaev Batteries". In: *Phys. Rev. Lett.* 125 (23 Dec. 2020), p. 236402. DOI: 10.1103/PhysRevLett.125.236402.

[90]   Robert Alicki and Mark Fannes. "Entanglement boost for extractable work from ensembles of quantum batteries". In: *Phys. Rev. E* 87 (4 2013), p. 042123. DOI: 10.1103/PhysRevE.87.042123.

[91]   Karen V. Hovhannisyan et al. "Entanglement Generation is Not Necessary for Optimal Work Extraction". In: *Phys. Rev. Lett.* 111 (24 2013), p. 240401. DOI: 10.1103/PhysRevLett.111.240401.

[92]   Javier M. Magán. "Black holes as random particles: entanglement dynamics in infinite range and matrix models". In: *J. High Energ. Phys.* 2016 (Aug. 2016), p. 81. DOI: 10.1007/jhep08(2016)081.

[93]   Geoffrey Penington. "Entanglement wedge reconstruction and the information paradox". In: *J. High Energ. Phys.* 2020 (2020), p. 2. DOI: 10.1007/jhep09(2020)002.

[94]   Ahmed Almheiri et al. "The entropy of bulk quantum fields and the entanglement wedge of an evaporating black hole". In: *J. High Energy Phys.* 2019 (2019), p. 63. DOI: 10.1007/JHEP12(2019)063.

[95]   Ahmed Almheiri et al. "The Page curve of Hawking radiation from semiclassical geometry". In: *J. High Energ. Phys.* 2020 (Mar. 2020), p. 149. DOI: 10.1007/jhep03(2020)149.

[96]   V. Ohanesjan *et al. in preparation.*

[97]   John Goold et al. "The role of quantum information in thermodynamics—a topical review". In: *Journal of Physics A: Mathematical and Theoretical* 49.14 (Feb. 2016), p. 143001. ISSN: 1751-8121. DOI: 10.1088/1751-8113/49/14/143001.

[98]   Sebastian Deffner and Steve Campbell. *Quantum Thermodynamics: An introduction to the thermodynamics of quantum information.* 2019. arXiv: 1907.01596 [quant-ph].

[99]   Hong Zhe Chen et al. "Evaporating Black Holes Coupled to a Thermal Bath". In: (2020). arXiv: 2007.11658 [hep-th].

[100] Ancel Larzul, Steven J Thomson, and M Schiro. "Are fast scramblers good thermal baths?" In: (2022). arXiv: 2204.06434 [cond-mat].

[101] Ahmed Almheiri. "Holographic Quantum Error Correction and the Projected Black Hole Interior". In: (Oct. 2018). arXiv: 1810.02055 [hep-th].

[102] N. V. Gnezdilov et al. *Information to energy conversion in quantum composite systems at finite temperature.* 2021. arXiv: 2108.12031 [quant-ph].

[103] Berry Groisman, Sandu Popescu, and Andreas Winter. "Quantum, classical, and total amount of correlations in a quantum state". In: *Physical Review A* 72.3 (Sept. 2005). ISSN: 1094-1622. DOI: 10.1103/physreva.72.032317.

[104] Akram Touil and Sebastian Deffner. "Quantum scrambling and the growth of mutual information". In: *Quantum Science and Technology* 5.3 (May 2020), p. 035005. ISSN: 2058-9565. DOI: 10.1088/2058-9565/ab8ebb.

[105] Akram Touil and Sebastian Deffner. "Information Scrambling versus Decoherence—Two Competing Sinks for Entropy". In: *PRX Quantum* 2.1 (Jan. 2021). ISSN: 2691-3399. DOI: 10.1103/prxquantum.2.010306.

[106] Benjamin Doyon et al. "Non-equilibrium steady states in the Klein-Gordon theory". In: *J. Phys. A* 48.9 (2015), p. 095002. DOI: 10.1088/1751-8113/48/9/095002. arXiv: 1409.6660 [cond-mat.stat-mech].

[107] Denis Bernard and Benjamin Doyon. "Energy flow in non-equilibrium conformal field theory". In: *J. Phys. A* 45 (2012), p. 362001. DOI: 10.1088/1751-8113/45/36/362001. arXiv: 1202.0239 [cond-mat.str-el].

[108] Denis Bernard and Benjamin Doyon. "Non-Equilibrium Steady States in Conformal Field Theory". In: *Annales Henri Poincare* 16.1 (2015), pp. 113–161. DOI: 10.1007/s00023-014-0314-8. arXiv: 1302.3125 [math-ph].

[109] M. J. Bhaseen et al. "Far from equilibrium energy flow in quantum critical systems". In: *Nature Phys.* 11 (2015), p. 5. DOI: 10.1038/nphys3220. arXiv: 1311.3655 [hep-th].

[110] Andrea De Luca et al. "Nonequilibrium thermal transport in the quantum Ising chain". In: *Phys. Rev. B* 88.13 (2013), p. 134301. DOI: 10.1103/PhysRevB.88.134301. arXiv: 1305.4984 [cond-mat.str-el].

[111] Benjamin Doyon. "Lecture notes on Generalised Hydrodynamics". In: *SciPost Physics Lecture Notes* (Aug. 2020). ISSN: 2590-1990. DOI: 10.21468/scipostphyslectnotes.18.

[112] Márton Kormos. "Inhomogeneous quenches in the transverse field Ising chain: scaling and front dynamics". In: *SciPost Physics* 3.3 (Sept. 2017). DOI: 10.21468/scipostphys.3.3.020.

[113] Brian Swingle. "Unscrambling the physics of out-of-time-order correlators". In: *Nature Physics* 14.10 (Oct. 2018), pp. 988–990. DOI: 10.1038/s41567-018-0295-5.

[114] Vedika Khemani, Ashvin Vishwanath, and D. A. Huse. "Operator spreading and the emergence of dissipation in unitary dynamics with conservation laws". In: *Phys. Rev. X* 8.3 (2018), p. 031057. DOI: 10.1103/PhysRevX.8.031057. arXiv: 1710.09835 [cond-mat.stat-mech].

[115] Antonio M. García-García et al. "Quantum chaos transition in a two-site Sachdev-Ye-Kitaev model dual to an eternal traversable wormhole". In: *Physical Review D* 100.2 (July 2019). arXiv:1901.06031 [hep-th]. ISSN: 2470-0029. DOI: 10.1103/physrevd.100.026002.

[116] S. W Hawking. "Black hole explosions?" In: *Nature* 248 (1974), pp. 30–31. DOI: 10.1038/248030a0.

[117] S. W. Hawking. "Breakdown of predictability in gravitational collapse". In: *Phys. Rev. D* 14 (10 Nov. 1976), pp. 2460–2473. DOI: 10.1103/PhysRevD.14.2460.

[118] Don N. Page. "Information in black hole radiation". In: *Phys. Rev. Lett.* 71 (23 Dec. 1993), pp. 3743–3746. DOI: 10.1103/PhysRevLett.71.3743.

[119] D. I. Pikulin and M. Franz. "Black Hole on a Chip: Proposal for a Physical Realization of the Sachdev-Ye-Kitaev model in a Solid-State System". In: *Phys. Rev. X* 7 (3 July 2017), p. 031006. DOI: 10.1103/PhysRevX.7.031006.

[120] Aaron Chew, Andrew Essin, and Jason Alicea. "Approximating the Sachdev-Ye-Kitaev model with Majorana wires". In: *Phys. Rev. B* 96 (12 Sept. 2017), 121119(R). DOI: 10.1103/PhysRevB.96.121119.

[121] Ippei Danshita, Masanori Hanada, and Masaki Tezuka. "Creating and probing the Sachdev-Ye-Kitaev model with ultracold gases: Towards experimental studies of quantum gravity". In: *PTEP* 2017.8 (2017), p. 083I01. DOI: 10.1093/ptep/ptx108.

[122] Chenan Wei and Tigran A. Sedrakyan. "Optical lattice platform for the Sachdev-Ye-Kitaev model". In: *Phys. Rev. A* 103 (1 Jan. 2021), p. 013323. DOI: 10.1103/PhysRevA.103.013323.

[123] Anffany Chen et al. "Quantum Holography in a Graphene Flake with an Irregular Boundary". In: *Phys. Rev. Lett.* 121 (3 July 2018), p. 036403. DOI: 10.1103/PhysRevLett.121.036403.

[124]   L. García-Álvarez et al. "Digital Quantum Simulation of Minimal AdS/CFT". In: *Phys. Rev. Lett.* 119 (4 July 2017), p. 040501. DOI: 10.1103/PhysRevLett.119.040501.

[125]   Zhihuang Luo et al. "Quantum simulation of the non-fermi-liquid state of Sachdev-Ye-Kitaev model". In: *npj Quantum Information* 5 (June 2019), p. 53. DOI: 10.1038/s41534-019-0166-7.

[126]   Ryan Babbush, Dominic W. Berry, and Hartmut Neven. "Quantum simulation of the Sachdev-Ye-Kitaev model by asymmetric qubitization". In: *Phys. Rev. A* 99 (4 Apr. 2019), 040301(R). DOI: 10.1103/PhysRevA.99.040301.

[127]   N. V. Gnezdilov, J. A. Hutasoit, and C. W. J. Beenakker. "Low-high voltage duality in tunneling spectroscopy of the Sachdev-Ye-Kitaev model". In: *Phys. Rev. B* 98 (8 Aug. 2018), 081413(R). DOI: 10.1103/PhysRevB.98.081413.

[128]   Oguzhan Can, Emilian M. Nica, and Marcel Franz. "Charge transport in graphene-based mesoscopic realizations of Sachdev-Ye-Kitaev models". In: *Phys. Rev. B* 99 (4 Jan. 2019), p. 045419. DOI: 10.1103/PhysRevB.99.045419.

[129]   Alexander Altland, Dmitry Bagrets, and Alex Kamenev. "Sachdev-Ye-Kitaev Non-Fermi-Liquid Correlations in Nanoscopic Quantum Transport". In: *Phys. Rev. Lett.* 123 (22 Nov. 2019), p. 226801. DOI: 10.1103/PhysRevLett.123.226801.

[130]   Alexander Kruchkov et al. "Thermoelectric power of Sachdev-Ye-Kitaev islands: Probing Bekenstein-Hawking entropy in quantum matter experiments". In: *Phys. Rev. B* 101 (20 May 2020), p. 205148. DOI: 10.1103/PhysRevB.101.205148.

[131]   Andrei I. Pavlov and Mikhail N. Kiselev. "Quantum thermal transport in the charged Sachdev-Ye-Kitaev model: Thermoelectric Coulomb blockade". In: *Phys. Rev. B* 103 (20 May 2021), p. L201107. DOI: 10.1103/PhysRevB.103.L201107.

[132]   Dmitri V. Khveshchenko. "One SYK single electron transistor". In: *Lithuanian Journal of Physics* 60 (Aug. 2020), p. 3. DOI: 10.3952/physics.v60i3.4305.

[133]   Dmitri V. Khveshchenko. "Connecting the SYK Dots". In: *Condensed Matter* 5.2 (June 2020), p. 37. DOI: 10.3390/condmat5020037.

[134]   Alex Kamenev. "Course 3 Many-body theory of non-equilibrium systems". In: *Nanophysics: Coherence and Transport*. Ed. by H. Bouchiat et al. Vol. 81. Les Houches. Elsevier, 2005, pp. 177–246. DOI: https://doi.org/10.1016/S0924-8099(05)80045-9.

[135]   Ritabrata Bhattacharya, Dileep P. Jatkar, and Nilakash Sorokhaibam. "Quantum quenches and thermalization in SYK models". In: *J. High Energy Phys.* 2019.7 (July 2019), p. 66. DOI: 10.1007/JHEP07(2019)066.

[136]   Clemens Kuhlenkamp and Michael Knap. "Periodically Driven Sachdev-Ye-Kitaev Models". In: *Phys. Rev. Lett.* 124 (10 Mar. 2020), p. 106401. DOI: 10.1103/PhysRevLett.124.106401.

[137]   Arijit Haldar et al. "Quench, thermalization, and residual entropy across a non-Fermi liquid to Fermi liquid transition". In: *Phys. Rev. Research* 2 (1 Mar. 2020), p. 013307. DOI: 10.1103/PhysRevResearch.2.013307.

[138]   Xue-Yang Song, Chao-Ming Jian, and Leon Balents. "Strongly Correlated Metal Built from Sachdev-Ye-Kitaev Models". In: *Phys. Rev. Lett.* 119 (21 Nov. 2017), p. 216601. DOI: 10.1103/PhysRevLett.119.216601.

[139]   Milton Abramowitz and Irene Stegun. *Handbook of Mathematical Functions, With Formulas, Graphs, and Mathematical Tables,* New York: Dover Publications, Inc., 1964.

[140]   Yura Malitsky. "Golden ratio algorithms for variational inequalities". In: *Mathematical Programming* 184 (2020), pp. 383–410. DOI: `10.1007/s10107-019-01416-w`.

[141]   Y. Cheipesh et al. "Reentrant superconductivity in a quantum dot coupled to a Sachdev-Ye-Kitaev metal". In: *Phys. Rev. B* 100 (22 Dec. 2019), 220506(R). DOI: `10.1103/PhysRevB.100.220506`.

[142]   Olivier Parcollet et al. "Overscreened multichannel SU(N) Kondo model: Large-N solution and conformal field theory". In: *Phys. Rev. B* 58 (7 Aug. 1998), pp. 3794–3813. DOI: `10.1103/PhysRevB.58.3794`.

[143]   A. V. Lunkin, K. S. Tikhonov, and M. V. Feigel'man. "Sachdev-Ye-Kitaev Model with Quadratic Perturbations: The Route to a Non-Fermi Liquid". In: *Phys. Rev. Lett.* 121 (23 Dec. 2018), p. 236601. DOI: `10.1103/PhysRevLett.121.236601`.

[144]   Oguzhan Can and Marcel Franz. "Solvable model for quantum criticality between the Sachdev-Ye-Kitaev liquid and a disordered Fermi liquid". In: *Phys. Rev. B* 100 (4 July 2019), p. 045124. DOI: `10.1103/PhysRevB.100.045124`.

[145]   Debanjan Chowdhury et al. "Translationally Invariant Non-Fermi-Liquid Metals with Critical Fermi Surfaces: Solvable Models". In: *Phys. Rev. X* 8 (3 July 2018), p. 031024. DOI: `10.1103/PhysRevX.8.031024`.

[146]   Maria Tikhanovskaya et al. "Excitation spectra of quantum matter without quasiparticles. I. Sachdev-Ye-Kitaev models". In: *Phys. Rev. B* 103 (7 Feb. 2021), p. 075141. DOI: `10.1103/PhysRevB.103.075141`.

[147]   L. S. Levitov and G. B. Lesovik. "Charge distribution in quantum shot noise". In: *JETP Lett.* 58 (3 1993), p. 230.

[148]   Leonid S. Levitov, Hyunwoo Lee, and Gordey B. Lesovik. "Electron counting statistics and coherent states of electric current". In: *Journal of Mathematical Physics* 37.10 (1996), pp. 4845–4866. DOI: `10.1063/1.531672`.

[149]   C.M. Varma, Z. Nussinov, and Wim van Saarloos. "Singular or non-Fermi liquids". In: *Physics Reports* 361.5-6 (May 2002), pp. 267–417. DOI: `10.1016/s0370-1573(01)00060-6`.

Summary

Thermodynamics is one of the founding scientific pillars that has helped us better understand heat engines, biology, ecosystems, and even black holes. While it fundamentally describes large systems by examining the bulk behavior of their constituents, it is anchored in the statistical equivalence of equilibrium configurations of a formally infinite number of microscopic constituents. A question of its validity arises when one scales down to small quantum systems. Here, we have derived dynamic non-equilibrium relations that surprisingly resemble the classical thermodynamics laws, with a mix of quantum features that encode the dynamics of quantum information. Understanding the relation between post-quench dynamics of finite-size quantum systems and their initial thermodynamic state might have been a purely academic exercise fifteen years ago. But now, thanks to ultra-cold atomic quantum simulators and progress in quantum computers, the thermodynamics of finite-size quantum systems has practical implications too. The findings of this thesis contribute to understanding quantum many-body systems, particularly in the context of entanglement, non-equilibrium dynamics, thermalization, and charge transport.

Chapter 2 focuses on the out-of-equilibrium dynamics of two initially thermal and independent reservoirs of Fermi gas that are quench-coupled and, after a short time, decoupled again. Those quenches lead to an energy gain in both systems, regardless of the initial temperature imbalance, and the quenches' work is proportional to the mutual correlations of the systems, expressed through their von Neumann entropies. Based on this finding, in a follow-up paper, we showed that on the timescale of the Fermi time, the von Neumann entropies grow faster than the thermal transport between the systems. In the same work, we proved that the time-frame and temperature regime of this phenomenon are experimentally accessible in ultracold atoms, providing a platform for the measurement of quantum correlations.

Then, in Chapter 3, we studied the post-quench dynamics of two other classes of systems. Firstly, we analyzed the Sachdev-Ye-Kitaev (SYK) model, a toy system for strong quantum correlations, and proved that the same early-time energy increase appears for any temperature and system size, however, there is no thermal flux from the colder to the hotter system. Through the relative entropy, we were able to show that the initial thermal state is not immediately destroyed, which

refuted a previous claim that such a quench can heat a system with a colder bath. Then we studied a quench between two Mixed Field Isings (MFI) and demonstrated that the initial energy increase appears for all temperatures only when the systems are tuned to the quantum critical point, otherwise, we discovered a transition temperature above which the energy of the hotter system decreases right after the quench, re-establishing our classical intuition. Additionally, we have shown that in the thermodynamic limit, the energy increase persists only for highly entangled systems, like the SYK or MFI at the critical point, but is absent for generic quantum systems. This proves that the early-time quantum behavior does not contradict the late-time classical evaporation.

In Chapter 4, we analyzed the time evolution of the energies and how it relates to the before-quench state of the systems. By expanding the density matrix in a time series, we showed that when systems start from a thermal state, the early time evolution of the SYK is purely determined by the thermodynamics state. The situation is more complicated when the systems under consideration are Mixed Field Isings, whose energy evolution additionally depends on particular correlations within the individual systems. This provided an analytical explanation of the results presented in Chapter 3 and a better understanding of the appearance of a system-dependent transition temperature, above which the energy of the hotter MFI does not have a post-quench increase.

Chapter 5 turns the attention to charged SYK systems and explores the applicability of the same quench protocol in the experimental detection of a laboratory realization of an SYK. We found that the dynamics of the discharging process of the SYK quantum dot reveal a distinctive characteristic of the SYK non-Fermi liquid state. For example, when analyzing the quench-induced tunneling current between a charged SYK and a neutral reservoir, there is a temperature-dependent contribution to the current's half-life, which, at low temperatures, scales as T for the SYK and as T^2 for Fermi liquids. This provides an experimental feature for differentiating an SYK state from a conventional charged system. Additionally, we link this feature of the SYK current to the prominent observation of a linear in T resistivity of strange metals, which aligns with other reported results on conductivity in SYK chains.

Samenvatting

Thermodynamica is één van de fundamentele wetenschappelijke grondslagen die ons heeft geholpen om warmtemotoren, biologie, ecosystemen en zelfs zwarte gaten beter te begrijpen. Hoewel het fundamenteel macroscopische, i.e. grote, systemen beschrijft door het bulkgedrag van hun bestanddelen te onderzoeken, is het verankerd in de statistische gelijkwaardigheid van evenwichtsconfiguraties van een formeel oneindig aantal microscopische bestanddelen. De vraag van zijn geldigheid komt naar boven, wanneer men zich toespitst op kleine kwantumsystemen. In dit proefschrift hebben we dynamische niet-evenwichtsrelaties afgeleid voor zulk soort systemen die verrassend veel lijken op de klassieke wetten van de thermodynamica, met een mix van kwantumkenmerken die de dynamiek van kwantuminformatie coderen. Het begrijpen van de relatie tussen de post-quench-dynamics van kwantumsystemen met een eindige omvang en hun initiële thermodynamische toestand zou vijftien jaar geleden een puur academische exercitie kunnen zijn geweest. Maar dankzij ultrakoude atomaire kwantumsimulators en de vooruitgang op het gebied van kwantumcomputers heeft de thermodynamica van kwantumsystemen van eindige omvang nu ook praktische implicaties. De bevindingen van dit proefschrift dragen bij aan het begrip van kwantum-veeldeeltjessystemen, vooral in de context van verstrengeling, niet-evenwichtsdynamica, thermalisatie en ladingstransport.

Hoofdstuk 2 richt zich op de niet-evenwichtsdynamiek van twee aanvankelijk thermische en onafhankelijke reservoirs van Fermi-gassen die aan elkaar worden gekoppeld en na korte tijd weer worden ontkoppeld. Deze "quenches" leiden tot een energiewinst in beide systemen, ongeacht de aanvankelijke ongelijkheid van de temperatuur, en het werk verricht door de quench is evenredig aan de onderlinge correlaties van de systemen, uitgedrukt in hun Von Neumann-entropieën. Op basis van deze bevinding hebben we in een vervolgartikel aangetoond dat op de tijdschaal van de Fermi-tijd de von Neumann-entropieën sneller groeien dan het thermische transport tussen de systemen. In hetzelfde werk hebben we bewezen dat het tijdsbestek en het temperatuurregime van dit fenomeen experimenteel toegankelijk zijn in ultrakoude atomen, wat een platform biedt voor het meten van kwantumcorrelaties.

Vervolgens hebben we in hoofdstuk 3 de post-quench-dynamiek van twee andere klassen van systemen bestudeerd. Ten eerste hebben we het Sachdev-Ye-Kitaev

(SYK)-model geanalyseerd — een simpel systeem voor sterke kwantumcorrelaties — en bewezen dat dezelfde initiële energietoename optreedt voor elke temperatuur en systeemomvang, maar er is geen thermische flux van het koudere naar het hetere systeem. Door de relatieve entropie konden we aantonen dat de initiële thermische toestand niet onmiddellijk wordt vernietigd, wat een eerdere bewering weerlegde dat een dergelijke quench een systeem door middel van een kouder bad kan verwarmen. Vervolgens bestudeerden we een quench tussen twee Mixed Field Ising (MFI) modellen en toonden aan dat de initiële energietoename alleen voor alle temperaturen optreedt als de systemen zijn afgestemd op het kwantumkritische punt. Voor andere afstellingen ontdekten we een overgangstemperatuur waarboven de energie van de hetere temperaturen afneemt direct na de quench, waardoor onze klassieke intuïtie wordt hersteld. Bovendien hebben we aangetoond dat de energietoename binnen de thermodynamische limiet alleen aanhoudt voor sterk verstrengelde systemen, zoals de SYK of MFI op het kritieke punt, maar afwezig is voor generieke kwantumsystemen. Dit bewijst dat het kwantumgedrag in de eerste momenten niet in tegenspraak is met de klassieke koeling en verdamping op latere tijden.

In hoofdstuk 4 analyseerden we de tijdsevolutie van de energieën en hoe deze zich verhoudt tot de toestand vóór de quench van de systemen. Door de dichtheidsmatrix in een tijdreeks te expanderen, hebben we aangetoond dat wanneer systemen vanuit een thermische toestand beginnen, de vroege tijdsevolutie van de SYK puur wordt bepaald door de thermodynamische toestand. De situatie is ingewikkelder wanneer de onderzochte systemen Mixed Field Isings zijn, waarvan de energie-evolutie ook afhangt van bepaalde correlaties binnen de individuele systemen. Dit leverde een analytische verklaring op van de resultaten gepresenteerd in hoofdstuk 3 en een beter begrip van het optreden van een systeemafhankelijkheid transitietemperatuur, waarboven de energie van de hetere MFI geen toename post-quench meer kent.

Hoofdstuk 5 richt de aandacht op geladen SYK-systemen en onderzoekt de toepasbaarheid van hetzelfde quenchprotocol bij de experimentele detectie van een laboratoriumrealisatie van een SYK. We ontdekten dat de dynamiek van het ontladingsproces van de SYK-quantum dot een onderscheidend kenmerk van de niet-Fermi-vloeistof toestand van SYK onthult. Bij het analyseren van de door de quench geïnduceerde tunnelstroom tussen een geladen SYK en een neutraal reservoir is er bijvoorbeeld een temperatuurafhankelijke bijdrage aan de halfwaardetijd van de stroom, die bij lage temperaturen schaalt als T voor de SYK en als T^2 voor Fermi-vloeistoffen. Dit biedt een experimentele mogelijkheid om een SYK-toestand te onderscheiden van een conventioneel geladen systeem. Bovendien koppelen we dit kenmerk van de SYK-stroom aan de prominente observatie van een lineair in T-weerstand van vreemde metalen, wat overeenkomt met andere gerapporteerde resultaten over de geleidbaarheid in SYK-ketens.

Acknowledgements

Firstly I would like to thank my supervisors Koenraad Schalm and Jan Zaanen for their guidance and support during my Ph.D. journey. I am especially grateful for the freedom, they provided me with, to explore and work on topics that sometimes were not in the main focus of the group. However, my direct supervisor Koenraad Schalm was always willing to discuss and provide valuable insights on any topic of my interest. While at times this approach proved to be more challenging than I expected, it was worth it all along since, in my opinion, it was the basis for developing scientific independence and a hands-on attitude.

This thesis would not have been possible without my collaborators Yevheniia Cheipesh, Nikolay V. Gnezdilov, and Andrei I. Pavlov with whom I worked together on each topic covered in this thesis. We formed a group with diverse research backgrounds and interests, making everything more dynamic and interesting. I have enjoyed every moment we have worked together, our discussions and enthusiasm-driven debates. I deeply appreciate your contributions for I have learned so much from you all.

In the last year of my Ph.D. I re-connected with my mentor from the bachelor studies Irina Petreska, and, together with Trifce Sandev, we started working on mixing classical stochasticity and unitary evolution of quantum systems. Thank you for introducing me to this field, it came at a time when I was looking for new challenges and has been a source of inspiration ever since. In the same year, while learning and navigating stochastic waters, I met Benjamin Walter and each day of discussing or working together has been a delightful experience. My Ph.D. journey would have been even better if we had met at the last conference before the pandemic, rather than the first after, but I am glad our paths crossed. I am looking forward to working on all our envisioned projects.

Those years at Leiden would not have been enjoyable without my colleagues and friends Aleksandar Bukva, Floris Balm, Nicolas Chagnet, and Aravindh Shankar. With Aleksandar, we had conversations on everything from physics, and coding to cooking recipes as well as a shared interest in F1 and cycling. With Nicolas and Aravindh I could not only discuss some of our most tantalizing work problems but also have leisurely walks, deep-diving into the meaning of life, or simply a relaxing chit-chat. And then, I could not have wished for a better office mate than Floris. Our shared passion for natural sciences, politics, and the financial system

was a refreshing breeze during the heat storms of physics. Unfortunately, our office life was interrupted by the pandemic, but I am happy we are office-mates all over again for you have been my mentor and guide on Dutch society and there is still so much more I need to learn. Here, I want to thank NWO for funding my thesis, Leiden University for hosting me, the secretariat of the Lorentz Institute, and LION for all the help over the years. Also, I would like to thank the staff at the ALICE High-Performance Computing facility for allowing me to conduct most of the numerical studies.

Next, I want to express my gratitude to the professors from my undergraduate studies, especially Irina, Mimoza, Aleksandar, Lambe, and Danica. Thank you for always supporting me and providing me with a firm foundation which later made everything much easier. Besides receiving a good education, I found a kindred spirit there, my invaluable friend Enes, and I am so happy to have met you. I also want to thank Ludwik Dobrzynski first for coming to Macedonia and giving a lecture on the monumental efforts for building and running the LHC, then for supporting my dreams to go to CERN, introducing me to the joint HEP master program, and for being a true friend, especially during some of my most trying days in Paris.

I am extremely grateful to my parents, for supporting me throughout my education in Macedonia, and mostly for devoting their lives so that I and my brother could have a carefree childhood. This helped me stay focused and committed to studying and paving the road to where I am today. I want to thank my brother especially for unselfishly sharing pictures of my niece, a little bundle of joy that has always brought a smile to my face. While at family, I want to thank Vinzenz, who has been not only my best friend but also an international sibling. You have been around me not only to share the joy but to also lift me from the lowest points of my 8-year journey abroad. Thank you for believing in our friendship and never giving up on me.

In the end, all that has been achieved here is thanks to my love and steadfast companion Renata. Your love and unwavering support have been my anchor throughout this journey. You have been my sunshine through the gloomy Dutch days and a spring of joy even during the most difficult periods. There are no words to express how grateful I am to have you. Thank you for being on my side through all those years and founding our home in the Netherlands. Our journey, a mosaic of memories across diverse lands, now finds us side by side in this sunlit train carriage, the fields blurring past. I am filled with an exhilarating anticipation for the unwritten chapters of our shared future, a future as boundless and luminous as the love that binds us.

Curriculum Vitae

I was born, on 20$^{\text{th}}$ June 1991, and raised in Prilep, Republic of Macedonia. I had my secondary education at the local gymnasium "Mirče Acev" where I developed an interest in natural sciences.

After considering the idea of continuing my higher education in genetics and virology for a while, I decided to enroll in theoretical physics at the Ss. Cyril and Methodius University in Skopje, a decision I've enjoyed ever since. During my bachelor's studies, I worked on developing a Schlieren imaging setup, applications of the Hubbard model, and charge transport in molecular rotors. I also explored topics in strongly interacting electronic systems, for which in 2012 I attended a workshop at ICTP in Trieste, Italy, and later in particle physics which in 2013 led to my first international internship at CERN where I worked on an analysis of proton-proton collision data at the ALICE collaboration. Inspired by this internship, and my growing interest in the field, I decided to pursue a Master's degree in High-Energy Physics (HEP).

For this endeavor, I chose the joint program between École Polytechnique and ETH Zürich. During the first year, at École Polytechnique, I studied the foundations of theoretical and experimental HEP concluding it with a thesis on "Measurement of the Higgs boson width" in the CMS collaboration. For the second year of the master's program I moved to ETH Zürich where I focused on integrable systems, CFTs, holography, and string theory and graduated with a thesis on "Bootstrapping of meromorphic conformal field theories". During a gap year, after obtaining my Master's degree, I continued working on holographic theories and then took an internship at the Institute for Particle Physics and Astrophysics at ETH Zürich, where I worked on the observation of Higgs boson decay to bottom quarks with the CMS experiment at CERN.

Subsequently, I pursued my Ph.D. at Leiden University in the "Scanning New Horizons: Emergent Space-Time, Black Holes and Quantum Information" program. My research encompassed the thermalization of quantum systems, quantum information, transport in SYK chains, and holographic superconductors. Toward the end of my Ph.D., I became interested in the dynamics of quantum systems under stochastic resetting, leading to a research visit at SISSA in Trieste, Italy. Scientific results from my time at Leiden University have been presented at many national and international conferences.

List of Publications

- Floris Balm, Nicolas Chagnet, Sam Arend, Joost Aretz, Kevin Grosvenor, Martijn Janse, Ole Moors, Jonah Post, Vladimir Ohanesjan, David Rodriguez-Fernandez, Koenraad Schalm, Jan Zaanen, *T-linear resistivity, optical conductivity and Planckian transport for a holographic local quantum critical metal in a periodic potential*, Phys.Rev.B 108 (2023) 125145 [arXiv:2211.05492].

- V. Ohanesjan, Y. Cheipesh, N. V. Gnezdilov, A. I. Pavlov, K. Schalm, *Energy dynamics, information and heat flow in quenched cooling and the crossover from quantum to classical thermodynamics*, JHEP 05 (2023) 237 [arXiv:2204.12411].

- N. V. Gnezdilov, A. I. Pavlov, V. Ohanesjan, Y. Cheipesh, K. Schalm, *Ultrafast dynamics of cold Fermi gas after a local quench*, Phys. Rev. A 107, L031301 (2023) [arXiv:2108.12031].

- Y. Cheipesh, A. I. Pavlov, V. Ohanesjan, K. Schalm, N. V. Gnezdilov, *Quantum tunneling dynamics in a complex-valued Sachdev-Ye-Kitaev model quench-coupled to a cool bath*, Phys. Rev. B 104, 115134 (2021) [arXiv:2011.05238].

- Irina Petreska, Vladimir Ohanesjan, Ljupco Pejov, Ljupco Kocarev, *Tunneling of electrons via rotor-stator molecular interfaces: combined ab initio and model study*, Chem. Phys., 473 (2016) p. 32 [arXiv:1509.00848]